AGARD-AG-197

AGARD-AG-197

AGARD

ADVISORY GROUP FOR AEROSPACE RESEARCH & DEVELOPMENT

7 RUE ANCELLE 92200 NEUILLY SUR SEINE FRANCE

AGARDograph No. 197
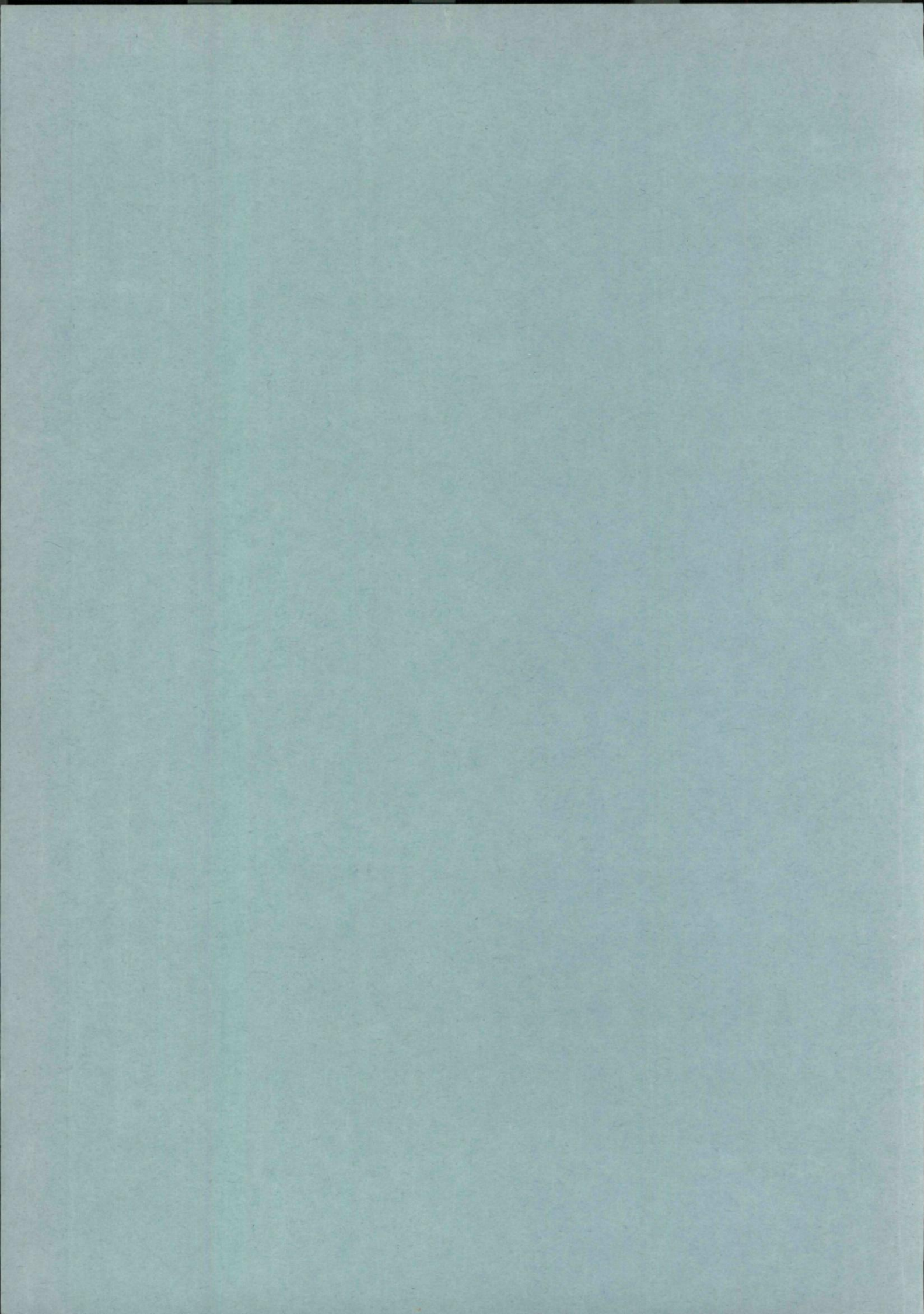
on

Hingeless Rotorcraft Flight Dynamics

by

K.H.Hohenemser

NORTH ATLANTIC TREATY ORGANIZATION

DISTRIBUTION AND AVAILABILITY
ON BACK COVER

NORTH ATLANTIC TREATY ORGANIZATION

ADVISORY GROUP FOR AEROSPACE RESEARCH AND DEVELOPMENT

(ORGANISATION DU TRAITE DE L'ATLANTIQUE NORD)

AGARDograph No.197

HINGELESS ROTORCRAFT FLIGHT DYNAMICS

by

Kurt H.Hohenemser

Washington University
St. Louis, Missouri, 63130, USA

Edited by

Robert A.Ormiston

Ames Directorate
U.S. Army Air Mobility R&D Laboratory
Moffett Field, Calif. 94035, USA

THE MISSION OF AGARD

The mission of AGARD is to bring together the leading personalities of the NATO nations in the fields of science and technology relating to aerospace for the following purposes:

— Exchanging of scientific and technical information;

— Continuously stimulating advances in the aerospace sciences relevant to strengthening the common defence posture;

— Improving the co-operation among member nations in aerospace research and development;

— Providing scientific and technical advice and assistance to the North Atlantic Military Committee in the field of aerospace research and development;

— Rendering scientific and technical assistance, as requested, to other NATO bodies and to member nations in connection with research and development problems in the aerospace field;

— Providing assistance to member nations for the purpose of increasing their scientific and technical potential;

— Recommending effective ways for the member nations to use their research and development capabilities for the common benefit of the NATO community.

The highest authority within AGARD is the National Delegates Board consisting of officially appointed senior representatives from each member nation. The mission of AGARD is carried out through the Panels which are composed of experts appointed by the National Delegates, the Consultant and Exchange Program and the Aerospace Applications Studies Program. The results of AGARD work are reported to the member nations and the NATO Authorities through the AGARD series of publications of which this is one.

Participation in AGARD activities is by invitation only and is normally limited to citizens of the NATO nations.

CONTENTS

PREFACE

During the last decade, hingeless rotorcraft have been the subject of substantial research, development, and testing, because of their potential for reduced maintenance, improved performance, and better flying qualities. Production of hingeless rotorcraft is now underway. Experience has shown that, compared to articulated rotors, hingeless rotors are more demanding with respect to the dynamic design. Structural integrity, good handling qualities, and flight stability depend on a proper assessment of the dynamics problems, much more so than for articulated rotorcraft.

This report reviews recent work on the flight dynamics of hingeless rotorcraft, with emphasis on concepts rather than on details. The usual division of aircraft dynamics into rigid body flight dynamics and structural dynamics that include vibrations and aeroelasticity, is not applicable for rotorcraft, especially hingeless rotorcraft. Elastic blade deformations greatly affect handling qualities and must be included in a discussion of hingeless rotorcraft flight dynamics. Here, a somewhat arbitrary line is drawn between flight dynamics and structural dynamics. Phenomena that involve blade torsional modes leading to potential classical flutter and phenomena that involve the higher blade bending modes and elastic fuselage modes essential for the vibration characteristics of the rotorcraft are relegated to structural dynamics. Phenomena that involve the lower blade flap and lag bending modes — including blade torsional elastic deflections, but excluding torsion dynamics — and the rigid-body modes are relegated to flight dynamics. This division assumes that blade torsional natural frequencies are several times greater than the rotor rotational frequency, which is true of current lifting rotors. According to the dividing line drawn here, air resonance phenomena and other low-frequency instabilities in flight belong to flight dynamics and are included here.

Although of great importance for the overall design, material selection and their properties are not considered here. Only lifting rotors are considered, omitting the special problems of hingeless tilting prop/rotor aircraft. Of the various feedback control systems, only those for the inner loop are considered since they can strongly couple with the elastic rotor modes. This survey report is not directed primarily to the dynamics specialist but rather to the rotorcraft design engineer who wishes to be introduced to the flight-dynamics problems of hingeless rotorcraft and to the methods for their solutions known to date.

Chapters 1 to 6 are almost purely descriptive with a few simple equations in chapter 4 that define several blade coupling parameters and, in chapter 6, that define several feedback parameters. Chapters 7 and 8, in addition to descriptive material, also contain mathematical formulations of the basic methods discussed. Most of the literature is cited in chapter 2, on the history of hingeless rotorcraft, in inverse chronological order within each section. The reference list has an appendix containing relevant recent publications not cited in the text.

SYMBOLS

Most symbols used are defined in the text. A few often recurring symbols are listed here.

a	airfoil lift slope
c	blade chord
C_M	$M/\pi R^3 \rho(\Omega R)^2$; hub moment coefficient in rotating reference system, positive down
I_b	blade flapping moment of inertia about rotor center or about equivalent flapping hinge where noted
N	blade number per rotor
P	dimensionless blade flapping frequency
R	rotor radius or hub rigidity parameter
α	angle of attack
β	blade flapping angle, defined as slope of line from rotor center to blade tip, positive up
$\beta_I = -a_1$	forward cyclic flapping
$\beta_{II} = -b_1$	left cyclic flapping
γ	$ac\rho R^4/I_b$, blade Lock number ($a = 5.6$), or glide-path angle
ζ	blade lead angle
θ	blade pitch angle, positive nose-up
$\theta_I = -\theta_s$	forward cyclic pitch
$\theta_{II} = \theta_c$	left cyclic pitch
ϵ	feedback system phase angle; also azimuth angle that defines mixed-flow region
λ	dimensionless inflow velocity, positive up; also real part of eigenvalue
μ	rotor advance ratio
ρ	air density
σ	$cN/\pi R$, rotor solidity ratio
ϕ	phase angle of control system
ψ	blade azimuth angle from aft position
Ω	angular speed of rotor
ω_β	blade flap natural frequency
ω_ζ	blade lead-lag natural frequency

SUMMARY

The state of hingeless rotorcraft research and development in the NATO countries as of 1973 is described. The scope of this report is limited to flight dynamics (as defined in the Preface) since most of the hingeless rotorcraft problems have occurred in this area. In the Introduction, the special place of the hingeless rotorcraft within the family of rotorcraft is considered. The chapter on the history of hingeless rotorcraft describes the hingeless rotor research and development of the various rotorcraft manufacturers and the hingeless rotor research at government laboratories and universities. A hierarchy of dynamic concepts from isolated blade dynamics to complete rotor/body dynamics is introduced. The effects of the basic rotor design parameters on flight dynamics are traced and certain hingeless rotorcraft problems are treated in some detail. A special chapter is devoted to the alleviation of hingeless rotor flight-dynamics problems by feedback control systems. Finally, analytical modeling techniques, mathematical analysis techniques, and model and flight testing techniques for hingeless rotorcraft are discussed.

1   INTRODUCTION

To view the various hingeless rotorcraft types within the entire family of rotorcraft, the rotors are first classified according to hinge arrangements and then according to flapwise and inplane bending stiffness. Some comments on the flight characteristics of different rotorcraft types conclude the Introduction.

1.1   Rotor Classification According to Hinge Arrangement

There are many different rotor blade hinge arrangements and many names for each arrangement. The hingeless rotor has been called rigid rotor, nonarticulated rotor, or semirigid rotor, the latter term having also been applied to the Bell teetering rotor. Actually, the hingeless rotor (as presently used) is not really hingeless, since only flapping and lead-lag hinges have been removed but not the feathering hinges. Truly hingeless rotors are presently being developed and these may be called bearingless rotors.

Again, for the floating or gimbaled hub configurations where the blades are all rigidly interconnected without individual flap or lead-lag hinges, but where the hub can tilt with respect to the rotor shaft either freely or subject to elastic restraints, there is a problem of definition. Such types have been called "semirigid" or "semihingeless," but a better term would be "hingeless floating." When there are two blades per rotor, this configuration is identical to the teetering rotor. Another rotor configuration widely used for tail rotors is one where flapping hinges are retained but lead-lag hinges are omitted. It seems logical to call this type semihingeless. Such an arrangement has also been used with a floating hub, as in the McDonnell rotor, which would then be termed "semihingeless floating." In many rotor configurations, the thrust bearings that absorb the blade centrifugal force are replaced by internal torsion packs or external straps. In this case, the feathering hinges contain only radial bearings. The preceding terminology will remain the same also for configurations where the metal bearings in any of the hinges are replaced by elastomeric bearings. The terminology used for the seven hinge arrangements is presented in table I.

TABLE I   HINGE ARRANGEMENTS

Term	Definition
Articulated	One flap, lead-lag, and feathering hinge per blade
Semihingeless	One flap and feathering hinge per blade
Semihingeless floating	Same as before with floating hub
Hingeless	One feathering hinge per blade
Hingeless floating	Same as before with floating hub
Teetering	Same as before with two blades per rotor
Bearingless	Truly hingeless

1.2   Rotor Classification According to Blade and Hub Flexibility

The effect of blade bending flexibility on articulated rotorcraft flight dynamics is noticeable but not substantial and an analysis that assumes the blades are rigid in bending is often adequate. However, this is not true for hingeless rotors. For hingeless rotor configurations, flapwise soft blades with flapwise natural frequencies (at normal rotor speed) of 1.05 to 1.15Ω are distinguished from flapwise stiff blades with such frequencies at 1.4Ω or more. As discussed later, the rotor derivatives of flapwise soft and flapwise stiff hingeless rotors are quite different.

The classification with respect to inplane blade bending stiffness of semihingeless or hingeless rotors is related to the problem of multiblade lead-lag dynamic instability, which is called (not very logically) ground or air resonance, depending on whether the instability occurs on the ground or in the air. Ground resonance has always been one of the main dynamic problems of rotorcraft. This type of dynamic instability occurs when a body vibration mode with horizontal rotor hub motion has a natural frequency equal to the rotor rotation frequency minus the blade lead-lag natural frequency, unless the body mode and the lead-lag blade mode are both sufficiently damped. Without aerodynamic forces on the blades, ground resonance cannot occur if the blade lead-lag natural frequency is higher than the rotor rotational frequency. Articulated blades cannot satisfy this condition and require friction or hydraulic dampers for the blade lead-lag motion in addition to adequate damping of those body modes for which frequency coalescence is possible. The most critical mode is usually the roll mode on the ground where the stiffness of the main landing gear determines the natural frequency of the body. The theory of ground resonance was originally developed by Coleman (ref. 1.1) and improved in reference 1.2.

For semihingeless or hingeless rotors, the blade lead-lag natural frequency can be raised above the normal rotor rotational frequency. In this case, ground resonance of the Coleman type (i.e., the blade aerodynamic forces are not considered) cannot occur. Neither the blade lead-lag motions nor the landing gear require dampers to prevent the instability on the ground. Such blades are considered "stiff inplane." Semihingeless or hingeless rotors designed with the blade lead-lag natural frequency below the normal rotor rotational frequency are called "soft inplane." Such blades have a crossover rotor speed at which the blade lead-lag natural frequency equals the rotor rotational frequency. Below this crossover rotor speed, ground resonance of the Coleman type cannot occur. Above this crossover frequency, the same precautions must be taken as for articulated blades. If the rotor rotational frequency minus the blade lead-lag natural frequency equals the frequency of a body mode having horizontal rotor motions, then both the blade lead-lag motion and the body motion must be sufficiently damped.

The Coleman analytical model for ground resonance, which neglects blade aerodynamic forces, is approximately valid for articulated rotors operating on the ground. For hingeless rotors on the ground and for any type of rotor in flight, aerodynamic effects

become important and must be included in a stability analysis. The difference between "soft inplane" and "stiff inplane" configurations is then not as straightforward as indicated by the Coleman analytical model. When aerodynamic coupling with flapping and feathering motions is included, a stiff inplane configuration is no guarantee against multiblade lead-lag instability. For a soft inplane configuration, these aerodynamic couplings can be used in such a way that, despite frequency coalescence, mechanical damping of the lead-lag blade motion and of the body mode on the ground may not be necessary.

All these phenomena are discussed in more detail later since they are intimately related to the flight-dynamic aspects of hingeless rotorcraft design. These introductory comments are intended to give the rationale for the adopted categorization of rotor systems and, at the same time, dispel the long-held notion that stiff inplane rotors are inherently more stable than soft inplane rotors. Both types have their special problems, and a careful flight dynamics analysis that goes far beyond the Coleman analytical model is needed.

In listing the 12 rotor types of table II, one must consider that stiff flapwise rotors occur only in hingeless rotors and are stiff inplane. The bearingless rotor with a flap-torsion flex beam is not listed. It could be designed either stiff inplane (ref. 1.3) or soft inplane (ref. 2.53). Since the truly hingeless rotor is still in the initial stages of development, it will not be discussed here.

TABLE II ROTOR TYPES

Rotor		Flown during	Manufacturer
Articulated		1920's	Cierva (Autogiro)
Semihingeless	soft inplane	1950's	Fairey (Rotodyne)
	stiff inplane		McDonnell (Convertaplane in cruising) and tail rotors
Semihingeless floating	soft inplane	–	–
	stiff inplane	1950's	McDonnell (Convertaplane before conversion)
	soft flapwise, soft inplane	1960's	Bolkow, Westland
Hingeless	soft flapwise, stiff inplane	1960's	Bell, Lockheed
	stiff flapwise, stiff inplane	1970's	Sikorsky (ABC)
Hingeless floating	soft inplane	1940's	Doman
	stiff inplane	1960's	Bell (Tilt prop/rotor)
Teetering	soft inplane	–	–
	stiff inplane	1940's	Bell, Hiller

Among the 12 rotor types listed in table II, only the 3 "hingeless" types are considered here. As shown later, there are essential dynamic differences between rotor types with the feathering hinges rigidly attached to the hub, and for which almost all bending deformations occur outboard of the feathering hinges in the blades proper, and rotor types for which part of the bending deflections occur inboard of the feathering hinges. The ratio of inplena/out-of-plane flexibility of the inboard flex elements does not change with blade pitch changes, while this ratio does vary with blade pitch setting for the flex elements outboard of the feathering hinges. Accordingly, the soft flapwise rotors are divided into subclasses with soft flapwise and stiff flapwise hubs. For stiff flapwise rotors, this difference does not occur since the hub must also be stiff flapwise. The gyro-controlled Lockheed rotor is unique. Thus six hingeless rotor types are indicated in table III; in all cases, the hub is stiff inplane.

TABLE III HINGELESS ROTOR TYPES

Blades	Hub	Manufacturer
Soft flapwise, soft inplane	Soft flapwise	Westland
Soft flapwise, soft inplane	Stiff flapwise	Bolkow, Vertol
Soft flapwise, stiff inplane	Soft flapwise	Bell
Soft flapwise, stiff inplane	Stiff flapwise	Bell
Soft flapwise, stiff inplane	Soft flapwise, gyro-controlled	Lockheed
Stiff flapwise, stiff inplane	Stiff flapwise	Sikorsky (ABC)

1.3 Comments on Differences in Flight Characteristics

The present discussion is limited to the effects of flapping configuration on flying qualities. There are four flapping configurations:

- F1 Hingeless floating (for two blades equivalent to teetering)
- F2 Articulated with flapping hinge offset
- F3 Hingeless soft flapwise
- F4 Hingeless stiff flapwise

In the sequence given, the hub momemt per unit cyclic pitch input is zero for F1, moderate for F2, substantial for F3, and large for F4. Configuration F1 uses only the moment of the rotor thrust vector with respect to the aircraft center of gravity to control pitch and roll. One advantage of this configuration is the ease with which the fuselage attitude can be trimmed in cruising flight where minimum drag fuselage attitude is important. The rotor attitude for a given speed is determined only by the parasite drag. The fuselage attitude can be changed by positioning the horizontal tail without causing hub moments or dynamic blade stresses. The hovering attitude of this configuration is sensitive to fore and aft c.g. shifts. The instability with angle of attack that increases with increasing forward speed and is typical of many rotorcraft, can easily be overcompensated by a small horizontal tail or by a nose-up fuselage trim moment which requires that the center of gravity be forward of the rotor thrust vector.

For configuration F1, the pitch and roll control power per unit cyclic pitch input depends on the g-load factor. Control power is reduced for pushovers or downward gusts and increased for pullups, coordinated turns, or upward gusts. Since at a zero g-load factor the control power is almost zero, a limit is imposed on maneuverability. If the hub tilting motions are elastically restrained, some control power is available even at a zero g-load factor. Pitch and roll damping depend on the g-load factor in the same way as the control power and are zero at zero g. For adequate control power and damping in normal flight, the rotor must be sufficiently above the fuselage that an adequate distance between rotor and aircraft c.g. is achieved.

Configuration F2, with offset flapping hinges, uses both the moment of the rotor thrust vector with respect to the aircraft c.g. and the hub tilting moment for pitch and roll control and damping. The hub moment contribution is typically 20 to 40% of the total rotor moment about the aircraft c.g. Control power and damping are not zero at a zero g-load factor. Fore and aft c.g. shifts have less effect on hovering attitude. However, both c.g. shifts and fuselage attitude trim cause alternating hub bending moments. Angle-of-attack instability at forward speed is more difficult to compensate. The rotor can be moved closer to the fuselage, which makes for a more compact configuration, but rotor/fuselage interference drag can become a problem.

Configuration F3 generates substantial blade root bending moments. The hub tilting moment and, to a lesser degree, the thrust moment with respect to the aircraft c.g., provide pitch and roll control as well as pitch and roll damping, which are now affected very little by the g-load factor. The c.g. can be shifted fore or aft with a relatively small effect on hovering attitude. The rotor can be placed closer to the fuselage. Because of the increased control power and pitch and roll damping, the time constants of the controls are much shorter than for articulated rotors. Step control inputs produce a constant angular rate response within a fraction of a second compared to 1 to 2 seconds for articulated rotorcraft. A disadvantage is that the fuselage attitude with respect to the rotor cannot be changed without producing high oscillatory moments in the blades and rotor hub and high horizontal tail loads. Changes in c.g. position have less influence on flight characteristics but produce oscillatory blade and hub moments and thus are limited by structural fatigue considerations. The angle-of-attack instability in forward flight is increased compared to articulated rotorcraft and must be compensated with a larger horizontal tail. If the tail incidence is incorrect, additional alternating blade and hub moments are generated. Substantial cross-control effects may exist, including roll with pitch control, pitch with roll control, and pitch with collective control. Pitch-roll cross-damping effects may also be substantial. Methods to alleviate these problems, such as blade structural coupling or control feedback, are discussed later.

In configuration F4, all the features listed for F3 are more pronounced. Since attitude differences between rotor and fuselage are practically impossible, large aircraft attitude changes between hovering and forward flight are unavoidable. A large horizontal tail is required to compensate the rotor angle-of-attack instability. Since the cross-control and cross-damping effects are also much greater than for F3, this configuration has been considered only for counterrotating rotors where some of the cross-control effects are compensated. However, the pitch with collective control change remains. One problem typical of configuration F4, and to a lesser extent F3, is the mismatch between the large cyclic pitch necessary for trim and the small cyclic pitch input required for maneuvering, which leads to longitudinal control oversensitivity that worsens in the upper flight-speed range.

A few comments will be made concerning high advance ratio operation when an auxiliary fixed wing and auxiliary propulsion are used. Because the rotor is unloaded by the fixed wing, configuration F1 requires airplane-type controls at high forward speeds. Rotor attitude can be adjusted independently of the fuselage and wing to obtain low rotor dynamic loads. Configuration F2 loses control power with increasing fixed-wing lift sharing and needs a large hinge offset if airplane-type controls are not provided. Configuration F3 does not require airplane-type controls even for low rotor lift. However, maneuvering with the rotor controls produces considerable oscillatory blade and hub loads. Also, reducing the rotor speed to relieve blade tip Mach number reduces control power. If counterrotating rotors are used for configuration F4, high rotor lift can be retained at high advance ratio so that a fixed wing is not required. However, auxiliary propulsion is still needed to reach high advance ratios. With auxiliary propulsion, large attitude changes between hovering and forward flight can be alleviated.

2 HISTORY OF HINGELESS ROTORCRAFT

The history of hingeless rotorcraft is first presented within the general history of rotorcraft, covering all types listed in table II. A brief history of the hingeless types is then given in the order of table III, followed by a section on hingeless rotor research outside the aircraft industry. The history of the U.S. rotorcraft development up to 1955 is summarized in reference 2.1. The first rotorcraft to reach substantial forward velocities was built in the early 1920's by Cierva. It had an autorotating lifting rotor. Cierva first tried a semihingeless rotor, probably soft inplane, but this was not satisfactory. From what is now known, this was a difficult configuration. The blades had very low lead-lag damping and, because of the flapping hinges, there was no way to obtain effective aerodynamic body damping at zero thrust. The semihingeless, soft inplane configuration was later used by Fairey in the tip-jet-driven Rotodyne, which experienced ground resonance problems. The hingeless floating, soft inplane configuration is dynamically similar to the semihingeless type and it is also deficient in aerodynamic body damping. It was developed in the 1940's and 1950's by Doman, who also experienced problems with both ground and air resonance.

Beginning with the semihingeless, soft inplane rotor, there are three methods by which the design can be improved with respect to ground resonance. Cierva's solution was to adopt the damped lead-lag hinge. The Cierva C-8 was introduced in 1928 from England to the U.S. by Pitcairn, and fully articulated blades with lag hinge dampers have been widely used ever since. A second method, later used in the McDonnell and Bell convertaplanes and in many tail rotors, is to stiffen the blades in the chordwise direction so that they are stiff inplane, which prevents ground resonance. The third method is to retain the soft inplane blades but omit the flapping hinges. This hingeless rotor configuration was adopted by Westland in England and by Bolkow in Germany in the 1960's although not specifically to alleviate ground resonance. As mentioned before, the Coleman ground resonance analysis is conservative for hingeless rotorcraft since aerodynamic effects are important even when the rotor is operated on the ground. Experience has shown that soft inplane, hingeless rotorcraft can be designed without mechanical blade damping if frequency positioning and aerodynamic coupling effects are properly used. Otherwise, they require only relatively small blade damping devices that can be of the elastomeric type.

The stiff inplane blade was used not only in conjunction with flapping hinges, as in the McDonnell and Bell convertaplanes and in many tail rotors, but was also adopted for hingeless rotorcraft developed by Bell and Lockheed in the 1960's. Although the Coleman-type instability is not possible with these rotors, multiblade lead-lag instabilities involving aerodynamic blade forces did occur. The original McDonnell design as tested in dynamic models had such an instability even without coupling with a body mode. The instability was removed for the full-scale aircraft before flight testing by reversing pitch-lag coupling in the sense of pitch-up with lag (ref. 2.2). The Lockheed design also had a variety of lead-lag instabilities involving coupled flapwise, feathering, and body motions (ref. 2.50). The instabilities were discovered in flight testing. The original Bell hingeless floating prop/rotor design was also subject to lead-lag instability and had to be modified (ref. 2.30). Historically, it appears that the stiff inplane configurations were more troublesome with respect to instabilities than the soft inplane hingeless configurations, despite the fact that these configurations are free of the Coleman-type instability.

The hingeless rotorcraft listed in table III are not the first to be flown. Before Cierva, many helicopter experiments were conducted with hingeless rotors, for example, those by Bréguet, Dorand, and others. In the 1930's, after Cierva introduced the articulated rotor, Wilford developed the cyclic-pitch-controlled, hingeless gyroplane and contributed to the development of the cyclic and collective pitch controlled hingeless coaxial helicopter built by Rieseler. (This was an early predecessor of the stiff flapwise Sikorsky ABC helicopter.)

Of the 10 configurations in table II that have flown, only two have been widely produced: the articulated rotor developed in the 1920's and the teetering rotor developed in the 1940's. These two configurations have been continuously improved since their inception

to obtain better performance, better flying qualities, lower maintenance, and lower vibration levels. Nevertheless, with historical perspective, it is surprising how little planned development work went into lifting rotors compared to engines or fixed-wing airframes. Tests with dynamically similar Mach or Froude scaled rotor models were nonexistent for most prototypes or inadequate in their parameter variations. Essential analytical tools to support lifting rotor design have only recently been developed. For this reason, after more than 50 years of rotorcraft technological development, it is not known which of the various rotor configurations is best for a certain task and how to optimize the rotor not only with respect to performance but also with respect to flying qualities, weight, maintenance, vibrations, and life-cycle cost. The hingeless rotorcraft have begun to compete with the articulated and the teetering configurations; possibly this competition will involve a much closer look at the lifting rotor development problem as a whole.

2.1 Westland Hingeless Rotorcraft

Westland Aircraft Limited in Yeovil, Somerset, U.K., began the development of the Westland W.G. 13, subsequently named the Lynx, in 1967. The soft flapwise, soft inplane, soft flapwise hub configuration was selected mainly for its simplicity and ease of maintenance. For flying qualities, an effort was made to depart as little as possible from the characteristics of the offset hinge articulated rotor. The rotor design goals were to minimize the hub moment per unit cyclic pitch input. For hingeless blades, torsional deflections from combined flap and lead-lag bending are an important factor (treated in more detail later). The Westland design philosophy was to minimize this bending torsion coupling as much as possible.

The Lynx rotor head (fig. 2.1) has tapered inboard titanium flex beams of elliptical cross section, conventional feathering hinges with needle roller bearings and tension-torsion bars to transmit centrifugal loads, and a circular outboard titanium flex element. The flat hub with the four flex beams and feathering hinge housings is made from a single titanium forging. Outboard of the feathering hinge, the inplane and out-of-plane stiffnesses are approximately equal because of the circular flex element. This feature together with a relatively high blade torsional and control stiffness alleviates structural feathering feedback. The blade inplane natural frequency at
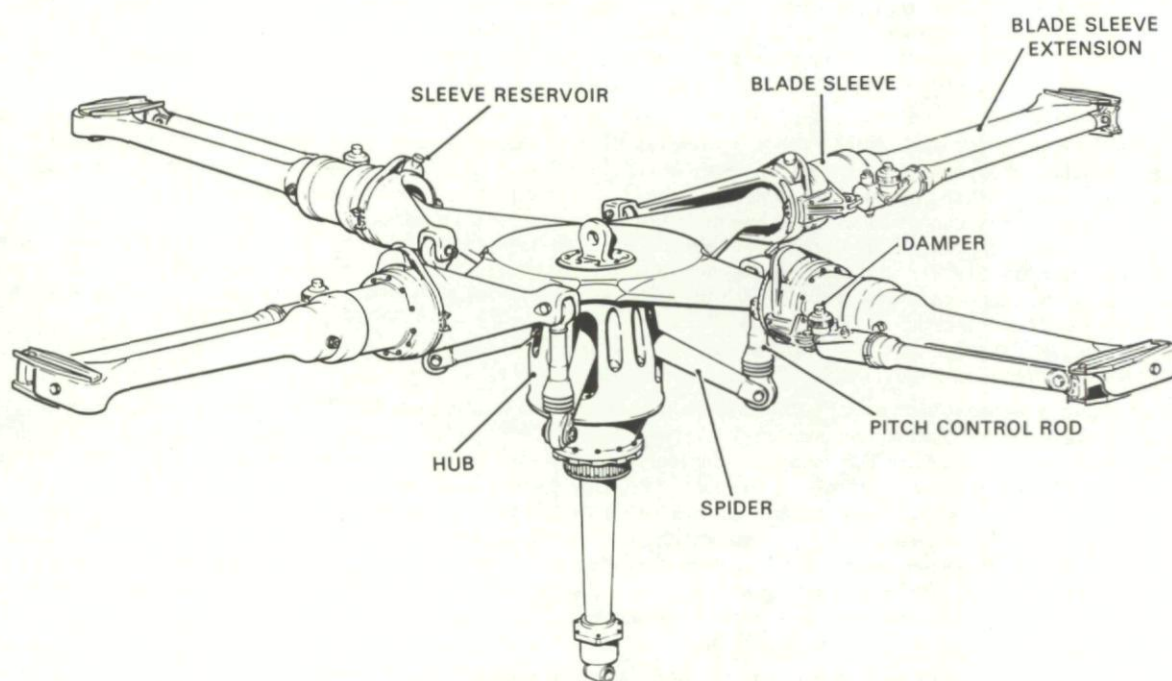

Fig. 2.1   Rotorhead and blade attachment of Westland W.G. 13 Lynx helicopter.

normal rotor speed is 0.64Ω, the crossover rotor speed is about 0.45Ω, and the blade out-of-plane natural frequency is 1.09Ω. The lag dampers provided may produce more damping than necessary. The blade Lock number is 8.2. The Lynx variants have gross weights from 8300 to 9500 lb and are powered by two Rolls Royce BS 360 engines that have a maximum contingency rating of 900 shp. The four-bladed rotor is 42 ft in diameter with 15.5-inch blade chord. The cruising speed depends on the gross weight of the variant and ranges from 140 knots at 9500 lb to 160 knots at 8300 lb. As of mid-1973, 600 flight hours have been accumulated, about 200 flight hours on one flight-test aircraft. Production delivery is planned for mid-1975.

To improve high-speed flying qualities, a vertical acceleration feedback into collective pitch is provided, which is independent of the automatic stabilization equipment (ASE), and is considered an integral part of the basic flight controls. The dynamic stability analytical effort concentrated on the problem of avoiding ground and air resonance since the soft inplane configuration is vulnerable in this respect. No dynamic models were used in the development. However, a Scout helicopter was modified to carry a 32.3-ft hingeless rotor that was dynamically similar except for lower blade torsional frequency. The Scout first flew in August 1970, and had accumulated about 40 flight hours when flight testing of the Lynx began in March 1971. Both the Scout and the Lynx are equipped with blade lead-lag dampers. Apparently no major flight dynamics problems have been encountered. Pilots were able to adapt quite well to the higher control sensitivity compared to articulated rotorcraft; the small amount of control cross-coupling proved to be unobtrusive. Development of the ASE has led to acceptable aircraft handling characteristics in turbulence.

In publications and sales brochures, the rotor system is called "semirigid" — not a very good characterization of the system since, according to table III, it is the most flexible of all hingeless rotors. The term "semirigid" apparently stems from the earlier usage of the word "rigid rotor" applied to the Lockheed, Bolkow, and Bell types, which are nearly as flexible as the Westland rotor, at least in flap bending. According to table III, the Westland hingeless rotor has a "soft flapwise hub" while the Bolkow hingeless rotor has a "stiff flapwise hub." Publications on the development of the Westland hingeless rotorcraft are listed as references 2.3 to 2.8.

2.2 Bolkow/Vertol Hingeless Rotorcraft

Bolkow GmbH in Ottobrunn, F.R. Germany, began its fiberglass hingeless blade development in 1961. After whirl stand and wind-tunnel testing, the development of the BO-105 began in 1964. Almost all bending flexibility was allocated to the blades. The rotor

head (fig. 2.2) is a titanium forging that includes integral housings for the feathering bearings. Tension-torsion straps carry the centrifugal load. The blades are tuned to provide a flap-bending natural frequency of about 1.12Ω and a lag-bending frequency of about $.65\Omega$. The low inplane natural frequency is achieved by a relatively large trailing-edge cutout at the blade root. The BO-105 helicopter has a skid gear and no blade lead-lag dampers. Because of the relatively high damping of the fiberglass blades with fibers wrapped around a
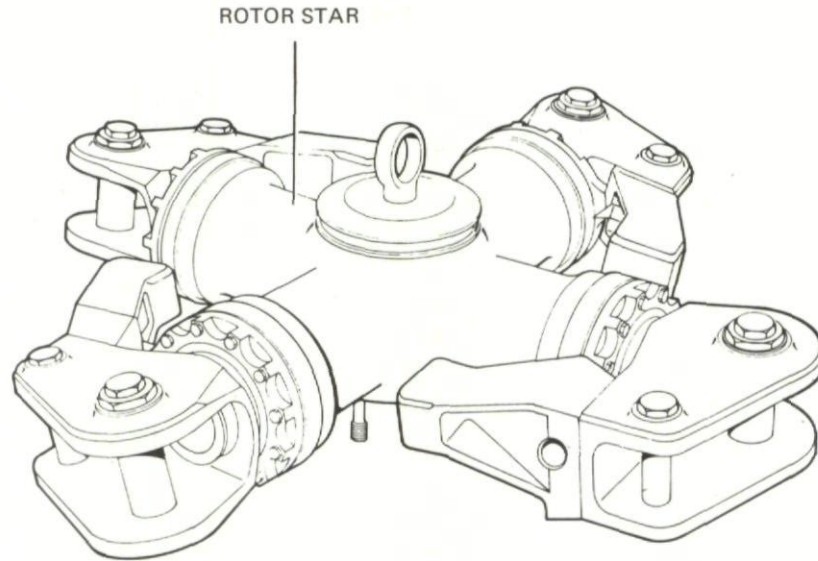
ROTOR STAR

Fig. 2.2   Rotorhead and blade attachment of MBB BO-105 helicopter.

single retention bolt, freedom from ground and air resonance is achieved with a precone angle of 2.5° and a chordwise c.g. of 24.5%. Lead-lag damping is increased or decreased when the blade coning angle is respectively greater or less than the precone angle.

The BO-105 helicopter with a maximum gross weight of 5070 lb, is powered by two Allison 250-C20 turbines each having a maximum rating of 400 hp. The four-bladed rotor is 32.2 ft in diameter with 10.6-in. blade chord. The blade Lock number referred to the virtual flapping hinge is 7.9. As of mid-1973, 20,000 flight hours have been accumulated on 101 aircraft with a maximum of 1200 flight hours on one aircraft. The cruising speed at sea level is 125 knots. A dive speed of 170 knots has been reached. The maximum load factor at 100 knots was 2.4 based on a gross weight of 5070 lb. Production began in January 1971.

According to a license and cooperation agreement with Sud Aviation, a three-bladed, 33-ft-diam rotor of the Bolkow type was installed on an Alouette II and was extensively flight tested beginning in early 1966. Flight testing of the BO-105 helicopter began somewhat later in February 1967. The Sud Aviation tests with the Bolkow three-bladed hingeless rotor were continued with the more modern SA-340, which began flight tests with the Bolkow rotor system in April 1967. The flap-bending frequency was 1.15Ω and the precone angle was increased from 2° to 4°. Ground resonance was observed at low collective pitch settings. Other problems were also encountered, including a reversal of the maneuvering stick force gradient and high blade loads in autorotation at reduced rotor speed. These problems were solved in part by modifications (ref. 2.17). However, for the follow-up production version of the SA 341 Gazelle, the hingeless rotor design was abandoned and an articulated rotor was used. The blade lead-lag natural frequency was unusually high because elastomeric lead-lag dampers were used. Through mergers, the original Sud Aviation is now Aerospatiale Helicoptéres and the original Bolkow GmbH is now Messerschmitt-Bolkow-Blohm GmbH (MBB).

In earlier publications on the Bolkow rotor, this type was called "rigid rotor." Later the term "hingeless rotor" was used. According to table III, this type is a stiff hub hingeless rotor versus the soft hub rotors developed by Lockheed, Bell, and Westland. Boeing-Vertol has adopted the stiff hub rotor type for its Model 179 UTTAS helicopter presently in development. Publications on the Bolkow/Vertol hingeless rotorcraft development are listed as references 2.10 to 2.23. The flight mechanical effects of the hingeless rotor are emphasized, in particular the use of the potential structural coupling inherent in the stiff flapwise hub hingeless rotor design to avoid ground and air resonance and to obtain good handling qualities despite the substantial angle-of-attack instability of the hingeless rotor at high forward speed. In addition to the work related to the Model 179 UTTAS helicopter, Boeing-Vertol also performed substantial design, analysis, and experimental studies toward a tilt prop/rotorcraft with the stiff hub type of rotor. Full-scale tests of this rotor were conducted in the Ames 40-by-80-ft Wind Tunnel. References 2.14 and 2.21 pertain to this work; reference 2.9 is a useful review of VTOL dynamics.

2.3   Bell Hingeless Rotorcraft

Bell Helicopter Company, Fort Worth, Texas, began experimenting with hingeless rotors in the late 1950's. A Model 47 J was first modified to replace the teetering rotor with a three-bladed hingeless rotor, 33 ft in diameter, which had flap-bending flexures between the hub and feathering hinges. The flexures were subsequently removed and the diameter of the rotor was reduced to 31.6 ft, resulting in a "stiff inplane, stiff hub" configuration. This rotorcraft was flight tested by NASA in 1962, and Huston and Tapscott reported (ref. 2.34) substantially increased control power and damping. Although the test rotor was fabricated from standard teetering rotor components, the flight loads remained within the design fatigue loads. About 50 flight hours were logged on the various three-bladed hingeless rotor configurations of the Model 47 and XH-13H. In 1962, Bell built a larger three-bladed hingeless rotor (42 ft in diameter) from standard UH-1B hub components and modified 21-in. chord blades. This rotor had flap-bending flex elements between hub and feathering hinges and falls in the category "stiff inplane, soft flapwise hub." The modified UH-1B helicopter was flown to 151 knots. The same rotor was fitted in 1963 to a commercial Model 204B fuselage, and blade root cuffs were added to reduce rotor power.

In 1964, a four-bladed hingeless rotor, 44 ft in diameter, again featuring the soft flapwise hub, was fitted to the commercial Model 204B helicopter and flown to 150 knots in a slight dive. In 1965, this rotor was evaluated on the Army-Bell high-performance compound vehicle with fixed wing and auxiliary jet propulsion. The vehicle was flown to 196 knots but exhibited a high 4/rev vibration level at that speed. In 1966, the diameter of the four-bladed rotor was extended by an inboard nonfeathering housing to increase the lifting capability of the rotor. Both 10° twist and 6° twist blades were available. A flight speed of 130 knots was achieved. Hovering maneuvers gave the critical loads in the mast, limiting the offset c.g. capability. In 1968, the same rotor was installed on the

T-55 powered Model 583 test vehicle and flown to 147 knots at 9,000 lb and to 138 knots at 12,000 lb gross weight. The standard Bell electronic stability and control augmentation system (SCAS) was also found to work well with the hingeless rotor by reducing gust response and improving phugoid-mode stability. In 1969, an improved version of the four-bladed, 44-ft-diam rotor with 6° twist and thin blade tips was installed on the high-performance compound helicopter and used in the High Mach Number/High Advance Ratio Flight-Test Program. Flight speeds up to 220 knots were achieved with the hingeless rotor and a teetering rotor was tested to 274 knots. Maneuvers of 1.8 g were performed with the teetering rotor at 226 knots and maneuvers of 2.3 g were performed with the hingeless rotor at 200 knots. About 70 flight hours were accumulated on the various four-bladed hingeless rotor configurations up to 1969.

In 1969/71, a four-bladed hingeless rotor, 48.3 ft in diameter, was designed and built. It featured a forged titanium rotor hub with integral flexures, stainless steel blades, and automatic electrical scissors folding of the two blade pairs for ground storage. This rotor had flown for 127 flight hours as of July 1, 1973, reaching speeds of 150 knots. The gross weight of the test vehicle is 14,000 lb, and it is powered by a T-55-L7B/-7C engine of 2250-hp normal rated power. The blades have 21-in. chord and 9° twist. The mast is installed with 3° forward and 2° left tilt. Flight-test results with this latest Bell soft flapwise hub, stiff inplane Model 609 rotor are reported in reference 2.24. Other publications related to the Bell hingeless rotor developments are references 2.25 to 2.36. Figure 2.3 shows the rotor hub and blade attachment of the Model 609 rotor system. The blade flap frequency at normal rotor speed is 1.05Ω, the first blade inplane frequency for cyclic modes is 1.4Ω, and the blade Lock number is 5.5.
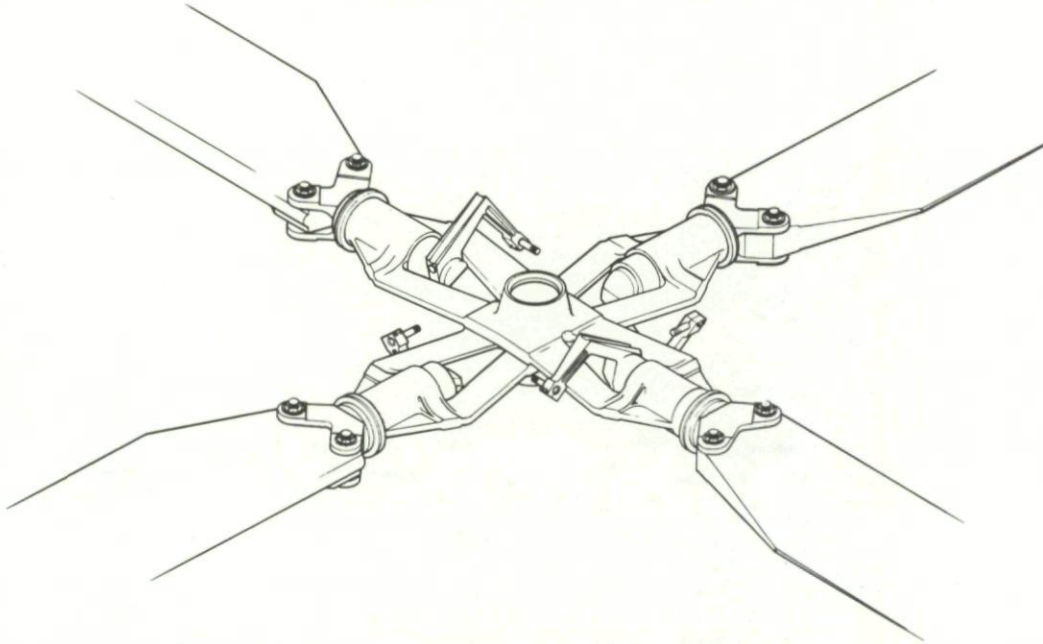

Fig. 2.3   Rotorhead and blade attachment of Bell Model 609 rotor.

2.4   Lockheed Hingeless Rotorcraft

Lockheed-California Company, Burbank, California, began the development of hingeless rotorcraft in the late 1950's with Model CL-475, which was flown with two- and four-bladed wooden rotors and a three-bladed metal rotor. All research vehicles and prototypes featured a mechanical cyclic pitch feedback system — usually referred to as the Lockheed gyro-control system. A more descriptive term would be "floating gyro-swashplate control." The swashplate acts as a gyroscope of substantial inertia and is floating in tilt under the influence of restraining springs, dampers, pilot-imposed spring moments, gyro inertial moments, and blade feedback moments. In all but the latest configuration (called "Advanced Mechanical Control System" or AMCS), the entire blade feathering moments were transmitted to the floating gyro-swashplate. The largest portion of the feathering moment was normally proportional to the blade flapping moment because the blades were swept forward outboard of the feathering hinge. However, the feedback signal was "corrupted" by the blade pitching moments, which could become large in partial blade stall conditions, and by lead-lag moments, which (because of flap-bending deflections outboard of the feathering hinge) could produce a substantial and not always beneficial feedback into the cyclic controls. In the AMCS, irreversible actuators between the floating gyro-swashplate and the blade cyclic pitch control were used to prevent the blade feathering moments from acting on the floating gyro-swashplate. The forward sweep of the blades was eliminated and the blade root flap bending deflections were transmitted by separate linkage and springs to the gyro-swashplate so that blade flapping feedback would not be corrupted by lead-lag and blade feathering moments. Figure 2.4 is a schematic of the AMCS (taken from ref. 2.37). The rotor head and blade attachment of the AH-56A AMCS are shown in figure 2.5.

After Model CL-475 was flight tested, the development of a larger research helicopter, the XH-51A, began in 1962. It had a three-bladed, 35-ft-diam rotor, retractable skids, and was powered by a P&W PT6 500-hp turboshaft engine. Its design gross weight was 3500 lb. It reached 152 knots and 2.4 g load factor in the three-bladed version, and 172 knots and 2.5 g load factor in a four-bladed version. The latter version was then tested as a compound helicopter with an additional wing and a J-60 jet engine for auxiliary propulsion. It reached 263 knots — with an advance ratio of 0.72 — and a high-speed load factor from 0 to 2.89 at the design gross weight of 4500 lb. Derivatives of the XH-51A include:

1.   The XH-51N with provisions for varying the control gyro inertia and control spring rate for NASA flight research.

2.   A "matched stiffness blade root flexure" version, where the feathering bearings were replaced by torsional flexures with equal inplane and flapping stiffness. Air resonance occurred below 89% normal rotor speed and the inplane stresses at normal rotor speed were higher than for the stiff inplane rotor. Consequently, this configuration was abandoned. The Westland Lynx helicopter, although somewhat similar dynamically, avoided these problems since it had a much higher blade feathering natural frequency in the absence of the floating gyro-swashplate and since it had lead-lag dampers.

3.   The commercial Model L-286 of which two were built and certified by the FAA. One, used as a corporate aircraft, has accumulated over 1500 flight hours.
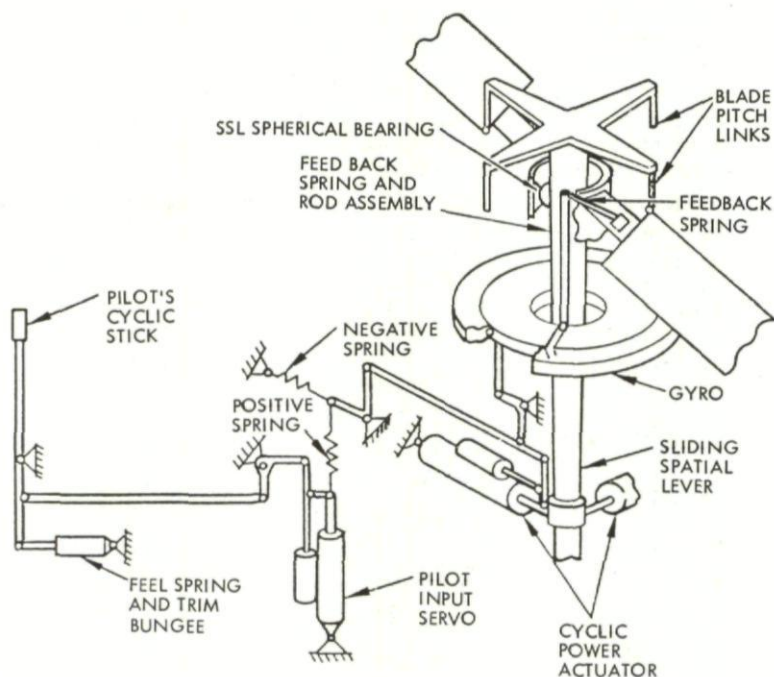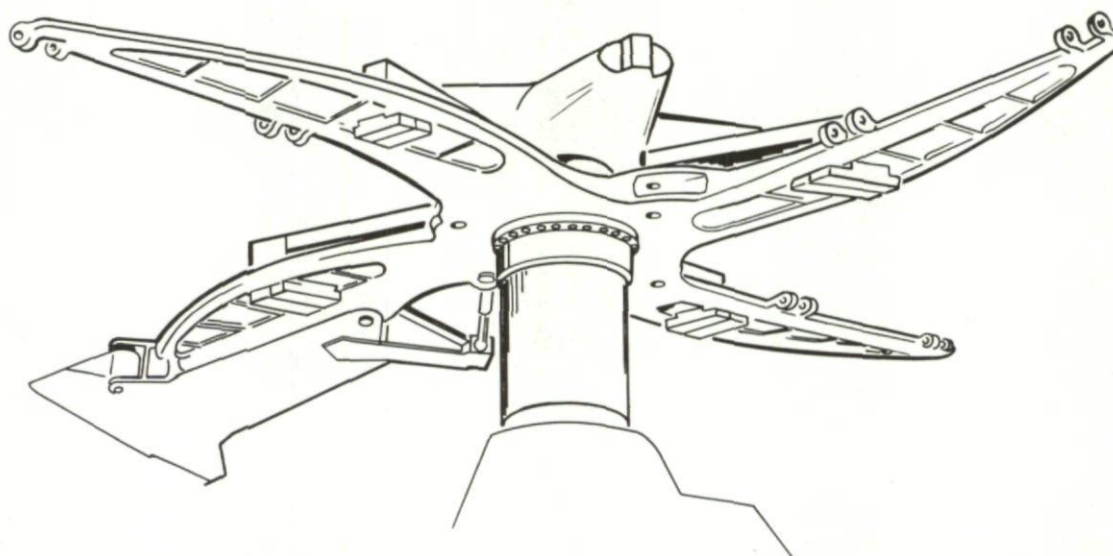
Fig. 2.4 Lockheed AMCS gyro-control system.

Fig. 2.5 Rotorhead of the AH-56A/AMCS

The development of the AH-56A Cheyenne compound helicopter began in late 1965. The first flight was in September 1967. During the flight-test development, the design gross weight increased from 17,000 to 18,300 lb, the diameter of the four-bladed rotor increased from 50.4 to 51.2 ft, the fixed wing area increased from 130 to 195 ft², and the rating of the single GE T-64 engine increased from 3425 to 3925 hp. Blade forward sweep and droop angles were increased. The direction of antitorque rotor rotation was changed to clockwise from the left side of the aircraft. The last change was to replace the feathering feedback gyro control system with the flapping feedback system or AMCS (described before). The blade Lock number in this configuration is 6.4. In 1972 and early 1973, the AH-56A/AMCS was flown to 220 KTAS and to load factors from 0.2 to +2.6 g at 150 to 180 KEAS without reaching limits on speed, load factor, loads, vibration, or controllability. No SAS was used for the flight tests.

Publications related to the Lockheed hingeless rotorcraft developments are references 2.37 to 2.62. The first quantitative though approximate analysis of the floating gyro-swashplate system was given in reference 2.59. A significant contribution to the problem of ground and air resonance of soft inplane hingeless rotors was made in reference 2.54. The question of replacing the floating gyro-swashplate with a more conventional electromechanical control system is analyzed in reference 2.44. A new dynamic problem of reactionless blade mode stability was analyzed in reference 2.38. In addition to the work related to the hingeless rotorcraft prototypes, Lockheed, in cooperation with USAAMRDL, Ames Directorate, conducted several wind-tunnel tests with hingeless rotor models to determine derivatives and frequency response data for the basic rotor and for the rotor with flapping feedback (refs. 2.43, 2.45, 2.46, and 2.48). Full-scale hingeless rotor tests were conducted in cooperation with NASA Ames (refs. 2.42, 2.49 and 2.60).

2.5 Sikorsky ABC Hingeless Rotorcraft

Sikorsky Aircraft in Stratford, Connecticut, began the research and development of the Advancing Blade Concept (ABC) coaxial hingeless rotor system in 1968. The blades are stiff flapwise, stiff inplane with a stiff hub, and the blade natural frequencies both flapwise and inplane are about 1.5Ω. In a coaxial configuration, each rotor can be operated with a nonzero rolling moment since the

two opposite rolling moments of the two rotors can be balanced. Thus the advancing blade can produce a larger flap-bending moment than the retreating blade. In single-rotor configurations, whether articulated or hingeless, the advancing blade lift must be kept sufficiently low that, despite the low lift of the retreating blade, the rolling moment is balanced. This requirement limits the total thrust severely with increasing rotor advance ratio. For coaxial rigid rotors, these limitations can be overcome if structural constraints are not violated. Theory and tests have shown that at the same blade tip Mach number at a flight speed of 180 knots, the hingeless coaxial rotor can have a ratio of aerodynamic blade lift coefficient over solidity twice the average for the single rotor (C_L/σ = 0.18 vs. 0.09). This fact, together with the compactness of the configuration, was the main stimulus for the development of the ABC hingeless rotorcraft.

After preliminary design and analytical studies, a full-scale 40-ft-diam rotor system was built for testing in the Ames 40-by-80-Foot Wind Tunnel. An important development item was the tapered titanium blade spar. In 1970, the rotor system was first whirl-tested and then wind-tunnel tested to 180 knots, to an advance ratio of 0.91, and to 23,000 lb of lift for 62 hours. In 1973, a 1/5 Froude scale model was tested on the Princeton Dynamic Model Track at velocities equivalent to 38 knots. Two demonstrator rotorcraft with 35-ft-diam rotors and about 10,000-lb gross weight are being readied for flight tests as of mid-1973. The blade Lock number referred to a virtual flapping hinge is 6.5. Publications on the Sikorsky ABC hingeless rotor development are references 2.63 to 2.67. Figure 2.6 is a sketch of the ABC rotor system.
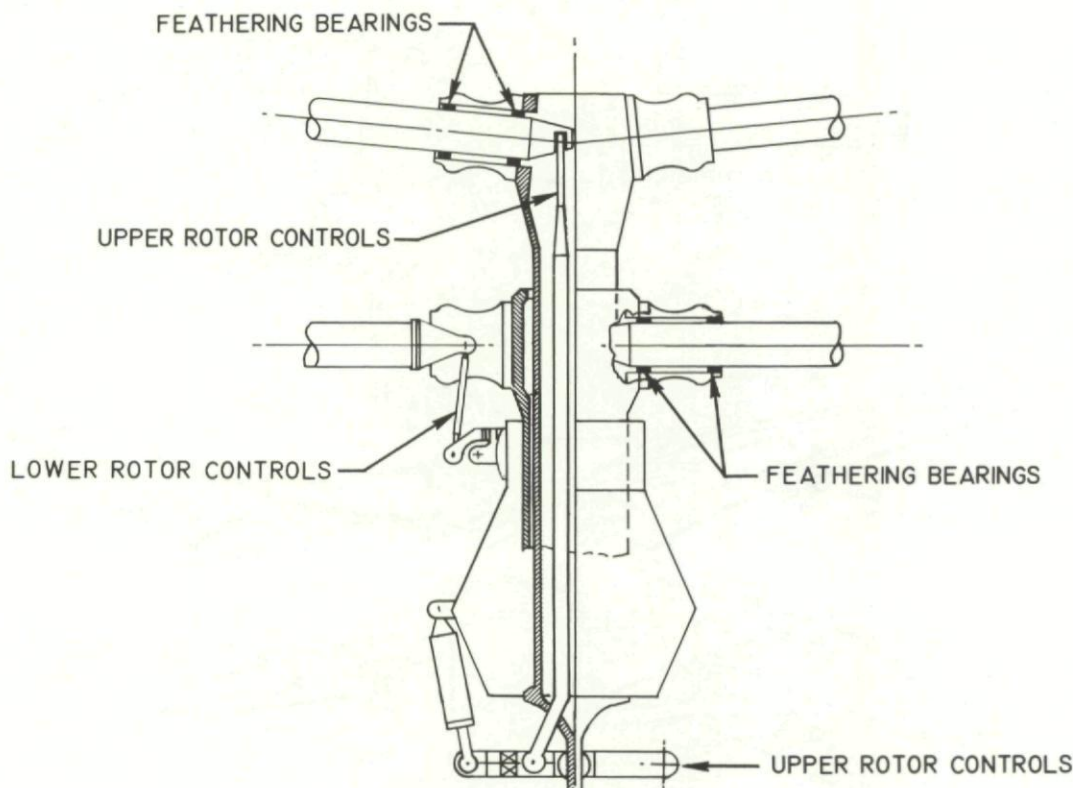

Fig. 2.6 Sikorsky ABC rotor system.

2.6 Hingeless Rotor Research Outside the Aircraft Industry

Since the advent of modern hingeless rotorcraft in the late 1950's, hingeless rotor research has also been conducted at government research laboratories and at universities. Some of the NASA Langley contributions in flight and model testing and in evaluating hingeless rotors have already been mentioned (refs. 2.31 to 2.34). Contributions of NASA Ames in full-scale hingeless rotor testing have also been mentioned (refs. 2.42, 2.49 and 2.60). Concurrent with the hingeless rotor development at Westland, RAE Farnborough conducted theoretical and experimental research on hingeless rotors (refs. 2.68 to 2.70). During the last few years, USAAMRDL, Ames Directorate, has initiated a vigorous hingeless rotor research program. The extensive model test program in cooperation with Lockheed was mentioned previously (refs. 2.43, 2.45, 2.46 and 2.48). The problem of single cantilever blade dynamics, including both elastic and inertial coupling between flap-bending, lag-bending, and torsion and the aerodynamic loads, has been systematically attacked, and correlations with test results have been achieved (refs. 2.71 to 2.76).

Usually, university research is not directed toward such a specific subject as hingeless rotor technology. Exceptions are the MIT work on single cantilever blades (refs. 2.77 and 2.78), the Princeton University work on hingeless rotor control theory (refs. 2.79 and 2.80), the University of Delaware work again on single cantilever blades (ref. 2.81), the Washington University work on hingeless rotor dynamics including unsteady rotor wake effects, random gust responses, and tilting moment feedback effects (refs. 2.82 to 2.88), and the City University, London, work (refs. 2.89 and 2.90). A number of hingeless rotor models were tested on the Princeton Dynamic Model Track (refs. 2.63 and 2.91).

3 CLASSIFICATION OF HINGELESS ROTORCRAFT FLIGHT DYNAMICS

As mentioned in the Preface, those phenomena that involve the coupling of the rigid-body modes with the lower-frequency blade flap and lead-lag bending modes are considered within the field of flight dynamics, whereby blade torsion is considered to be elastic deflection but not a separate mode. One way to treat all problems of flight dynamics is with the help of a single global analytical model that includes all kinematic, structural, aerodynamic, and control dynamic aspects. Research on several global models has been conducted for many years, for example the Lockheed Rexor model and the Bell C81 model. Such global models require the integration of a large number of non-linear differential equations and provide time histories of the rotorcraft system after a disturbance from trim.

Establishing a trim condition and the subsequent time history require a substantial computer effort. Because of the large number of terms and parameters involved in a global analytical model, it is usually possible to adapt the model to an observed phenomenon and

thus to gradually improve the validity of the model. Because of the numerous approximations involved, an a priori substantiation of a global model is a dubious enterprise. However, in the course of time, such a global model becomes a depository of past hardware experience and increases in value. Even under the best of circumstances, after the credibility of a global analytical model has been reasonably well established, such a model, when used in its complete form, is not a very good design tool. It limits the visibility of the effects of the separate parameters, and the usual restraints on computer time and costs prevent systematic studies of parameter variations.

For this reason, the use of several much simpler and specialized working analytical models becomes important. They usually represent linear approximations and describe only certain aspects of flight dynamics. The complete global models — at least in their present state of development — should not be used directly as a design tool but rather should be used to determine the limitations of the much simpler working models. Suboptions of Rexor and C-81 are available which permit locking out certain degrees of freedom, thereby reverting to simpler working models. From the point of view of a single global analytical model, there would be no reason for a classification of hingeless rotorcraft flight dynamics. However, if simplified models are used, there is a hierarchy of dynamics concepts, beginning with isolated blade dynamics, each of which can give valuable insights into certain aspects of hingeless rotor flight dynamics.

3.1 Isolated Blade Dynamics

According to the dynamic concept of the isolated blade, the root attachment of the blade is assumed to be uniformly rotating with the rotor angular speed, without horizontal or vertical motions and without angular roll or pitching motions. There is no coupling between the individual blades. For steady flight, the motions of all blades are assumed to be the same if time is counted from the instant when a blade is located aft at zero azimuth angle. Summing the forces and moments transferred by each blade to the hub yields the effect of the rotor on the body in steady flight. This concept can be extended slightly if one also assumes a steady angular roll or pitch rate of the rotor to determine the rotor forces and moments on the hub for these conditions. Many phenomena of flight dynamics can be treated with the concept of the isolated blade. This is true of some types of instability; see, for example, the extensive work by Niebanck and associates (ref. 3.1), which applies a normal mode analysis (ref. 3.2) for isolated blades to problems of classical flutter, stall flutter, torsional divergence, and flapping and flap-lag instabilities. Most problems of articulated rotorcraft flight dynamics can be solved by use of the dynamics of isolated blades (ref. 3.3). An exception is the problem of ground resonance of the Coleman type.

In hingeless rotor flight dynamics, a wide field can be covered by considering only the isolated blade. The simplest type of blade modeling is a rigid straight blade elastically hinged at the rotor center. A reasonable approximation is often obtained if only the flapping hinge is retained and if the blade is assumed to be rigid inplane and in torsion. Reference 2.55 develops this blade model with linear quasisteady aerodynamics, but with reversed-flow effects. At low lift and high advance ratio, the analytical results compare reasonably well with wind-tunnel tests, not only for steady-state conditions but also for frequency responses (refs. 2.43, 2.46, and 2.48). Flapping instability limits can also be obtained with this blade model, though they are unconservative (see ref. 2.82). The rigid blade model has been extended to include elastic torsion in reference 2.52. Elastic torsion becomes important at high advance ratio with large regions of reversed flow. When inplane modes are considered in the low advance ratio region, the straight blade approximation can again be used with appropriate locations of elastically restrained flapping and lead-lag hinges. As the blade pitch setting is increased, chordwise and flapwise modes become elastically coupled and are no longer normal modes. For soft inplane blades, this elastic coupling is of little concern. For stiff inplane blades, the elastic coupling can either stabilize or destabilize the lead-lag motion, depending on the flexibility of the hub. These coupling effects are discussed in detail later.

The blade torsional mode including control system flexibility has also been approximated by a rigid blade with a torsion flexure at the root. Usually, the torsional natural frequency is several times the rotor rotational frequency and blade torsional inertia can therefore be neglected for low-frequency phenomena important in flight dynamics. Structural or kinematic coupling can change the blade pitch with flapping (δ_3 coupling) or change the pitch with lag (a_1 coupling), both of which are very important in flight dynamics (discussed in detail later). When proceeding from the approximate rigid blade with spring-restrained hinges for flapping, lead-lag, and pitching motions to the actual blade with radially distributed flexibility, the problem becomes exceedingly complex. It has been treated without elastic flap-lag coupling and without elastic torsion in reference 2.77 and with these elastic effects in reference 2.72. Without droop, sweep, torque offset, control flexibility, and kinematic couplings of any kind and for uniform blades, it was found (ref. 2.72) that, in hover and without precone angles, all practical configurations were stable. A positive precone angle was destabilizing except for matched stiffness configurations.

3.2 Isolated Hub Multiblade Dynamics

The next step in the study of dynamic concepts is to analyze interblade coupling. The hub is assumed to again remain fixed with respect to both horizontal and vertical linear motions and to angular pitching and rolling motions of the aircraft. Interblade coupling can occur because (1) control flexibility allows pitching moments from one blade to affect the control position for the other blades and (2) in rotor feedback systems, for example, rotor coning is fed into the collective control or rotor tilting is fed into the cyclic control. The coupled blade equations in the rotating reference system can be solved for natural modes and natural frequencies or for the response to control or gust inputs. For N blades, N coupled rotor modes are obtained for each isolated blade mode. This type of analysis was performed in references 2.59 and 2.86.

Another more desirable method uses multiblade coordinates defined in the stationary reference system. This approach is more efficient computationally and provides results that are easier to interpret. Coleman (ref. 1.2) introduced this concept in his analysis of ground resonance, and distinguished between progressing and regressing multiblade inplane modes. The resultant blade center of gravity rotates with respect to the rotor either in the direction of rotation (progressing mode) or opposite the direction of rotation (regressing mode). Without aerodynamic forces, only the latter multiblade inplane mode can become unstable. Another analysis of this type using progressing and regressing multiblade flapping modes is given in reference 2.21. Collective modes are added in reference 2.15. A full complement of multiblade flapping modes was used in reference 2.85. In addition to the progressing and regressing tilting modes, the coning mode (where all blades move in the same direction simultaneously), the differential coning or reactionless flapping modes for rotors with four, six, or more blades, and the progressing and regressing warping modes were included.

Any rotor with three or more blades has a coning mode, a progressing tilting mode, and a regressing tilting mode. A four-bladed rotor has, in addition, a reactionless flapping mode — blades 1 and 3 move up while blades 2 and 4 move down. A five-bladed rotor has instead a progressing warping mode and a regressing warping mode which are also reactionless. These multiblade modes become aerodynamically coupled in forward flight. For inplane blade motions, in addition to the progressing and regressing modes of reference 1.2, there is also the collective or drive train mode where all blades move simultaneously in lead-lag and, for four-bladed rotors, the reactionless or scissors mode where subsequent blades move in opposite directions. The stability of this mode was analyzed in reference 2.38. For rotors with more than four blades, there are inplane equivalents to the progressing and regressing warping modes.

In hover, the isolated blade analysis can be used with little modification to determine the stability of some of the multiblade modes. However, the proper blade root boundary conditions must be used. For example, a collective flap-lag coupled mode analysis

must include shaft torsional flexibility and engine and transmission rotational inertia. For the reactionless coupled flap-lag mode, the isolated blade root conditions are appropriate. If there is little coupling between blades, progressing and regressing tilting and coupled inplane modes may be approximately represented by the isolated blade analysis. Interblade coupling destabilizes some isolated blade modes while it stabilizes others. Coupling for tilting feedback is treated later.

3.3 Body Dynamics with Rotor Derivatives

Rotorcraft linear flight dynamics can be formulated mathematically in the same way as is customary for linear airplane flight dynamics. A body-fixed reference system is used. The longitudinal axis through the aircraft center of gravity is either aligned with the principal inertia axis of the body, whereby the off-diagonal terms of the inertia tensor are zero, or the longitudinal axis is aligned with the direction of flight, which allows wind-tunnel data to be used directly. Often these two axes are sufficiently close to each other that their difference can be neglected. The nonlinear equations of motion can be linearized about a suitable trim condition. The aerodynamic forces and moments are represented by a 6×6 matrix of derivatives with respect to the three linear and three angular velocity increments. The rotor contributions to these 36 derivatives can be computed with the isolated blade analysis if interblade coupling is neglected. If interblade coupling is included, the derivatives can be obtained with an isolated hub type of analysis by determining the hub forces and moments per unit linear and angular velocity increment from trim. The rotor derivatives can also be determined from wind-tunnel tests by measuring the effects of pitch and yaw attitude increments from trim and the effects of steady pitch, yaw, and roll rates. In the latter case, the rotor derivatives include not only the effects of aerodynamic forces and moments but also gyroscopic reactions. Rotor mass, rotor pitch, and roll and yaw inertia are added to those of the body. This is equivalent to assuming that the changes in rotor attitude relative to the body are small compared to changes in the body attitude.

The validity of the rotor derivative concept depends on the frequency separation between the flight dynamic modes — phugoid, short-period pitching mode, dutch roll mode — and the lowest multiblade rotor modes such as the regressing tilting mode or regressing inplane mode. For articulated rotors, this frequency separation is not large and there is considerable coupling between some flight dynamic modes and the rotor regressing flapping mode (see ref. 3.4, which is based on the analysis of ref. 3.5). If there is a gust input, the rotor derivative concept requires that the entire rotor disk become simultaneously embedded in the gust. As shown in reference 2.28, this assumption leads to a substantial overestimation of the gust response compared to an analysis that includes the effects of gradual penetration of the rotor disk into a gust region.

So far as hingeless rotors are concerned, reference 2.44 states that the derivative approach was inadequate for a flight dynamics analysis of the Lockheed AH-56A helicopter and gave the impression of greater aircraft stability. Only long-period modes such as the phugoid can be approximated by the derivative analysis since their frequency is widely separated from that of the lowest rotor mode, which is the regressing flapping mode. For stiff flapwise blades, the frequency of the regressing flapping mode is 0.4Ω or higher and coupling with the body modes is less important. The derivative approach should be adequate for all flight dynamics modes, although air resonance may remain a problem.

3.4 Flapping Rotor-Body Dynamics

Next in the study of flight dynamics concepts is to add to the six body degrees of freedom the rotor flapping degrees of freedom. In terms of the multiblade rotor modes discussed previously, these are the coning mode, the regressing mode, and the progressing tilting mode. Thus a nine-degree-of-freedom flight dynamics system is obtained. Control flexibility, kinematic or structural feedback between blade flapping and blade pitch, the feedback of blade flapping into the control system, or conventional SAS can be included. In comparison with the rotor derivative concept, substantial differences in short-period flight dynamics are obtained. As for the isolated hub (hub fixed) dynamics, the stability of some rotor modes is also affected by the coupling with the body.

There is good evidence that the nine-degree-of-freedom flight dynamics model is adequate for most purposes, both for articulated and hingeless rotorcraft. Reference 2.44 compares this nine-degree-of-freedom with a 13-degree-of-freedom analytical model including inplane dynamics. The addition of the inplane modes had little effect on the flight dynamics as determined for various feedbacks from body motions and from rotor tilting. Also the stability of the inplane modes was little affected by the variations in flapping dynamics caused by the feedback systems. The studies of reference 2.44 extended from hover to flight speeds above 200 knots. Similar observations were made for hover in reference 2.88.

3.5 Complete Rotor-Body Dynamics

Since inplane mode instabilities are potential problems for hingeless rotors, careful analysis is needed for both stiff inplane and soft inplane types. The obvious first step is to ensure that the isolated blade shows good margins with respect to these instabilities. Since interblade coupling and coupling with body modes can reduce some of these margins — while increasing others — a complete rotor-body analysis is required to prevent ground or air resonance in hingeless rotorcraft. The results of such an analysis for hover are described in reference 2.15. Here 18 degrees of freedom were used, 5 for the rigid body motions except yaw, 4 for rotor pylon and tail boom flexibility, and 6 for the blades in flapping and in lead-lag. This analysis is extended to include a torsional degree of freedom and forward flight conditions in reference 2.10. Rotor dynamics are described by the progressing, regressing, and collective flapping and inplane modes. Kinematic or structural coupling of blade flapping and lead-lag motions with blade feathering are included without a separate consideration of the feathering degrees of freedom. The collective lead-lag mode, which is a drive train mode, is neglected.

The linear analysis of reference 2.15 (outlined in Sec. 7.1) is useful not only for verifying air resonance stability but can also be used, with some modification, for other problems of flight dynamics. It is practical for this purpose to use a body-fixed reference system rather than an inertial reference system as in reference 2.15. In its linear form, such a model is not much more complex than the nine-degree-of-freedom analytical model discussed previously. As stated in reference 2.37, such a model was very flexible and efficient for the solution of all flight-dynamics problems. In a hybrid computer, nonlinear control systems can be evaluated and real-time pilot-in-loop simulator studies can be performed. If reactionless mode instability is suspected as a potential problem, the scissor inplane mode and the differential coning mode for a four-bladed rotor must be included (ref. 2.38). For all flight dynamics models discussed, linear perturbations from trim were studied. Such linear models can be generated from a nonlinear "master" model that may also have additional degrees of freedom for feathering, for higher blade flapping modes, or for pylon or other fuselage elastic modes, and that is also suitable for certain structural dynamics problems. The evolution of linear perturbation models from a nonlinear master model is described in reference 2.37.

4 BASIC ROTOR DESIGN PARAMETERS THAT AFFECT FLIGHT DYNAMICS

Before special hingeless rotorcraft problems are discussed, it is useful to consider some of the basic rotor design parameters and their effects on flight dynamic characteristics. Only the simplest flight dynamic concepts — isolated blade or isolated hub dynamics — are used to outline trends. Valid quantitative data can be expected only from the more complex treatments of rotor/body dynamics.

4.1 Number of Blades per Rotor

To date, hingeless rotors have had only three or four blades. Flying qualities are not directly affected by the number of blades per rotor; neither is the usual regressing-mode type of ground or air resonance influenced by the number of blades per se. For a given total blade area and rotor radius, the higher number of rotor blades results in more slender blades with higher aspect ratio which will be more flexible in bending, thereby indirectly affecting flying qualities.

For interblade coupling, the number of blades has a direct effect on potential multiblade instabilities. A four-bladed rotor has *reactionless modes both inplane (scissors mode) and flapwise (differential coning mode). The stability of the scissors mode has caused* some concern for the Lockheed hingeless four-bladed rotor (ref. 2.38). A three-bladed hingeless rotor cannot have reactionless modes. Flapping instability at high advance ratio is also strongly affected by blade number (ref. 2.85). For example (see fig. 8.2, later), a three-bladed rotor with tilting moment feedback has a lower stability margin than a four-bladed rotor with identical blades.

4.2 Fundamental Blade Flap Frequency

In section 1.2, hingeless rotors were classified as soft flapwise when the fundamental blade flap frequency was 1.05 to 1.15Ω and as stiff flapwise if this frequency was 1.4Ω or more. In section 1.3, some handling qualities differences were noted between the hingeless floating or teetering rotor, the articulated rotor with flapping hinge offset, the hingeless soft flapwise, and the hingeless stiff flapwise rotors. The stiffer the blades are flapwise the more the attitude of the rotor is frozen with respect to the fuselage and the larger are the fuselage attitude changes between hovering and cruising flight, unless auxiliary propulsion is used. Increased flapwise blade stiffness increases angle-of-attack instability and the horizontal tail must be larger to compensate. Increased flapwise blade stiffness also increases the effects of control cross-coupling and damping cross-coupling. Finally, increased flapwise blade stiffness increases the mismatch between longitudinal cyclic pitch required for trim and that required for transient maneuvering, unless auxiliary propulsion and a fixed wing are used, both of which reduce the longitudinal cyclic pitch requirements for trimmed forward flight.

The main advantages of hingeless rotors — reduced maintenance, fewer hub parts, and improved control response — can be realized with soft flapwise blades, and the trends of many flight dynamic characteristics are unfavorable with increasing blade flap bending stiffness. Therefore, it appears that the design goal should be to reduce the flapwise stiffness (or the fundamental blade flap frequency) to the minimum value consistent with the structural requirements of adequate margins for the most severe trim, gust, and maneuver conditions. An interesting comparison provided by Bell Helicopter Company shows that, for the earlier Bell hingeless rotors, the flexure fatigue stress endurance limit was reached for a flapping angle of $1.5°$ to $2°$, while the latest Model 609 Flexbeam rotor has an allowable flapping angle of $4°$ — about the same as for the Lockheed AH-56A helicopter.

Soft flapwise blades are not suitable for transfering large moments to the hub as is required for the Sikorsky advancing blade concept (ABC) coaxial helicopter. Some of the disadvantages of flapwise stiff blades are avoided in a coaxial configuration. Other disadvantages remain and are discussed later.

4.3 Fundamental Blade Lead-Lag Frequency

In section 1.2, a hingeless rotor is classified as soft inplane or stiff inplane if the blade edgewise natural frequency is below or above the rotational frequency, respectively. If the rotor is soft inplane, special precautions must be taken against the Coleman type of ground resonance; if the rotor is stiff inplane, this type of dynamic instability is not possible. However, other types of inplane mode instability that result from coupling with flapping and feathering and with the body modes are possible both for soft inplane and stiff inplane rotors.

The blade inplane mode is at best only weakly damped, and substantial resonant amplification results from excitation by a forcing frequency near the natural frequency. The first design consideration is therefore to avoid a near coincidence of an operational rotor rotational frequency with the fundamental blade lead-lag frequency. This design requirement is difficult for a helicopter whose rotor speed in cruise is reduced to obtain high forward speed with low blade tip Mach number. The McDonnell XV-1 convertaplane operated in cruise with about half the hovering rotor speed. It had stiff inplane blades that passed through the 2/rev inplane resonance during transition to reduced rotor rpm in cruising flight. This was feasible, although high transient inplane moments occurred. Passing at a high advance ratio through the 1/rev inplane resonance of a soft inplane rotor would probably be impractical, although it might be possible with lag dampers. The soft inplane configuration is therefore more suitable for helicopters with a normal range of rotor speeds but less suitable for compound helicopters that reduce rotor rpm in cruise.

The inplane blade natural frequency must be selected carefully. For soft inplane blades, if it is too high, resonant response from 1/rev excitation becomes a problem and the range of operational rotor speeds becomes impractically narrow. If it is too low, the inplane blade damping required to avoid ground or air resonance increases rapidly, as shown for the BO-105 in Fig. 4.1 (obtained by cross-plotting Fig. 15 of ref. 2.11). For a pure helicopter without a fixed wing and auxiliary propulsion, a reasonable compromise
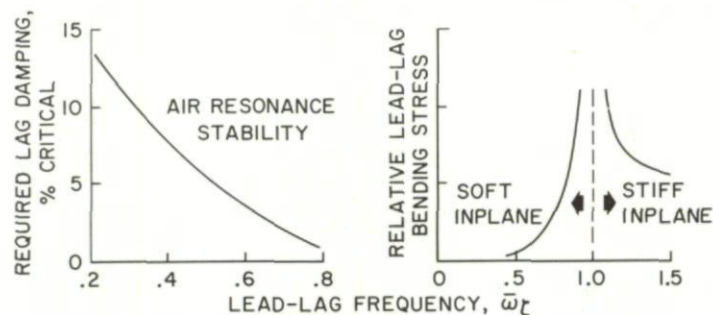

Fig. 4.1   Effect of lead-lag frequency on air resonance stability and on blade stress.

between the two conflicting trends is an inplane natural frequency of 0.65 to 0.70Ω at normal operating rotor speed. The edgewise blade natural frequency for stiff inplane rotors must also be selected to avoid near resonance operation. The inplane natural frequency usually decreases with increasing blade pitch angle (Fig. 4.2), so the natural frequency of a stiff inplane rotor should not be too low. Another limitation concerns the regressing inplane mode frequency $\omega_\zeta - \Omega$, which should be sufficiently high to avoid the possibility of pilot-induced oscillations. An inplane natural frequency from 1.4 to 1.5Ω at normal rotor speed and zero pitch setting appears to be a reasonable choice.
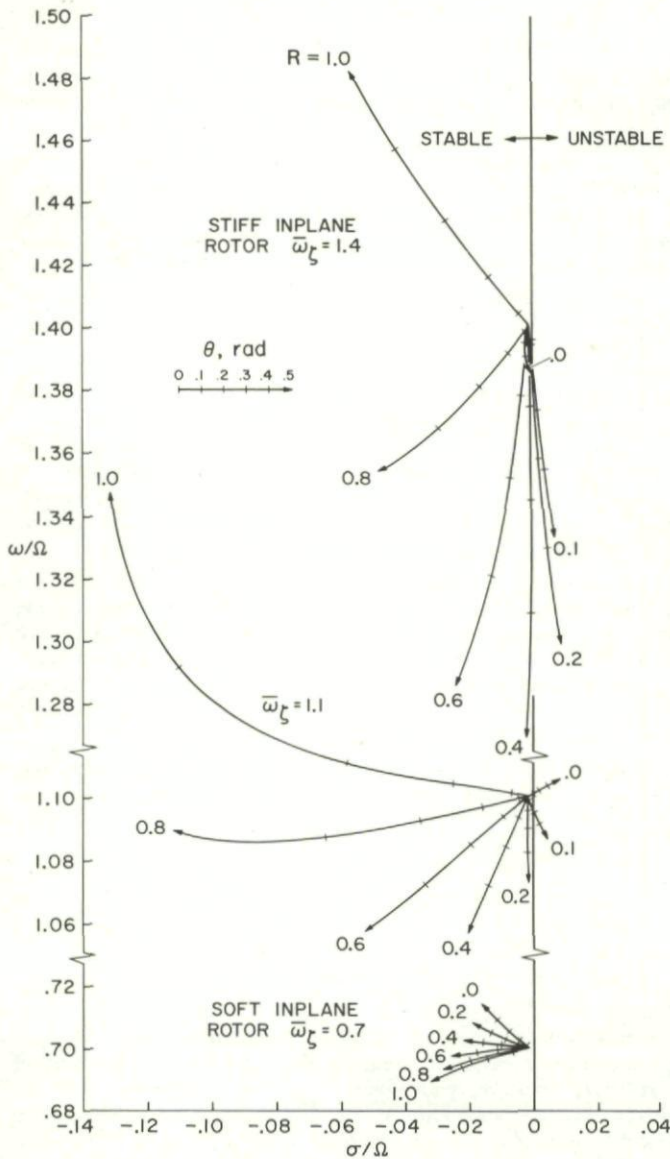
Fig. 4.2 Effect of blade pitch angle on blade inplane frequency and damping for various hub rigidities R.

4.4 Hub Flexibility

As mentioned previously, the Westland, Bell, and Lockheed hingeless rotor design, provide part of the flap-bending flexibility in the hub. These configurations are "soft flapwise hub" as opposed to the Bolkow and Vertol "stiff flapwise hub" configurations. The motivation for the "soft flapwise hub" in the stiff inplane Bell and Lockheed rotors is to combine high inplane and torsional stiffness with low out-of-plane stiffness. The flex beam inboard of the feathering hinge does not soften the blade torsionally and alleviates the reduction in inplane blade natural frequency that usually occurs with increasing pitch setting. The inboard flex beam also provides a means to control structural pitch-flap and pitch-lag couplings which can have an important effect on flight dynamics (as discussed later).

For a soft inplane rotor, the reduction in inplane frequency with pitch setting is of lesser concern, and all of the flexibility can be outboard of the feathering hinge, although at a penalty in blade torsional stiffness. The motivation for the "soft flapwise hub" in the soft inplane Westland rotor was the need for an effectively matched stiffness blade design. The blade root flex element has the same stiffness inplane and out of plane, and the flapping softness must be achieved by the inboard flex beams that are integral with the hub. This configuration also provides higher blade torsional stiffness.

As shown in references 2.74 and 2.76, the soft hub in combination with stiff inplane blades can destabilize the lead-lag motion. For an isolated rigid blade with root flexures, various combinations of hub and blade stiffnesses may be characterized by a parameter R defined as

$$R = \frac{\omega_\zeta^2 R_\beta - \omega_\beta^2 R_\zeta}{\omega_\zeta^2 - \omega_\beta^2} \qquad (4.1)$$

The terms ω_ζ and ω_β are the nonrotating blade inplane and flap natural frequencies at zero pitch and R_β and R_ζ are the ratios of total stiffness over blade stiffness in flapping and lead-lag, respectively, at zero pitch setting. A rigid hub with all the flexibility in the blade (Bolkow/Vertol rotor) corresponds to R = 1. A soft hub with a rigid blade, with all the flexibility in the hub, corresponds to R = 0. Combinations of a soft hub and flexible blades (as in the Westland, Bell and Lockheed hingeless rotors) are characterized by values of R between 0 and 1.

Figure 4.2 (taken from ref. 2.74) gives the frequency and damping $(-\sigma/\Omega)$ of the lead-lag mode for various R values. For soft inplane blades, an increase in pitch setting always increases the damping for any value of R. For stiff inplane blades this is true only for R > 0.4. The natural frequency of stiff inplane blades decreases with increasing pitch except for very high R values. Figure 4.2 is valid (for blades rigid in torsion) for a Lock number of 5 and for a flapping frequency of 1.15Ω in hover. Low values of R in combination with stiff inplane blades require special attention. The results in figure 4.2 show how a simple dynamic model can lead to important insights. The model should not be used quantitatively since too many simplifications are involved, such as rigid blades, quasisteady linear aerodynamics, zero advance ratio, absence of pitch-flap and pitch-lead coupling, etc. Nevertheless, it shows that, for soft inplane blades, the value of R is of little concern, while for stiff inplane blades low values of R require special attention.

4.5 Pitch-Lead Coupling

Pitch-lead coupling is a very important design parameter for both articulated and hingeless rotors. Pitch-lead coupling occurs for articulated rotors if the rotating pitch links are not perpendicular to the plane through the pitch horn and feathering axis. For hingeless blades, the inplane mode is usually coupled with the flapping mode and may involve some feathering motion as well. In particular, there is an elastic coupling from preflap setting which can best be visualized by assuming a rigid blade with root flexures. General relations are now introduced which are also applicable to elastic pitch-flap coupling (discussed later). Figure 4.3 (taken from ref. 2.10) shows four elastically restrained equivalent hinges used in the MBB flight dynamics analysis in conjunction with a rigid blade. This model is useful in a discussion of pitch-lead and pitch-flap coupling. The lowest dash-dot line in figure 4.3 is perpendicular to the rotor shaft and represents the hub plane. The feathering axis is elevated with respect to the hub plane by the precone angle β_k. The blade axis is elevated further with respect to the feathering axis by the flapping angle β and is displaced from the feathering axis by lag angle ζ. Contrary to the sign of ζ in figure 4.3, ζ is positive for lead. In addition to the feathering, flapping, and lead-lag hinge — all elastically restrained — figure 4.3 shows a blade torsion hinge that is ignored here. Also, the feathering, flapping and lead-lag axes are assumed to intersect at one point.

The total lead angle, $\zeta+\zeta_p$, consists of an elastic portion ζ and a prelead ζ_p. The elastic lead moment transferred to the hub is proportional to ζ:

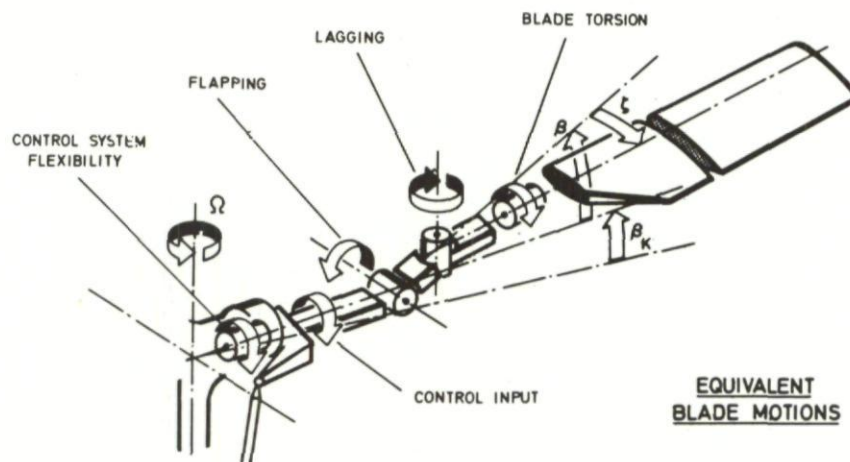$$M_\zeta = C_\zeta \zeta \qquad (4.2)$$

Fig. 4.3 Representation of elastic blade by a rigid blade with four elastically restrained hinges.

while ζ_p represents a prelead angle that exists for zero lead moment (ζ_p is an important design parameter — also called the forward sweep angle). Similarly, the blade axis is elevated with respect to the feathering axis by $\beta + \beta_p$. The elastic flap moment M_β transferred to the hub is proportional to β:

$$M_\beta = C_\beta \beta \tag{4.3}$$

while β_p represents a preflap angle that exists for zero flap moment (β_p is an important design parameter — also called the negative droop angle).

If the components of the elastic moments M_β and M_ζ are taken with respect to the feathering axis and if small angles are assumed, the feathering moment, positive for the direction of increasing pitch angle θ, is:

$$M_\theta = C_\theta \theta = M_\beta(\zeta + \zeta_p) - M_\zeta(\beta + \beta_p) \tag{4.4}$$

Inserting Eqs. (4.2) and (4.3) into Eq. (4.4) yields:

$$C_\theta \theta = \beta\zeta(C_\beta - C_\zeta) + \beta\zeta_p C_\beta - \zeta\beta_p C_\zeta \tag{4.5}$$

If β is constant and if Eq. (4.5) is differentiated with respect to ζ, one obtains the elastic pitch-lead ratio:

$$\theta_\zeta = [\beta(C_\beta - C_\zeta) - \beta_p C_\zeta]/C_\theta \tag{4.6}$$

If ζ is constant and if Eq. (4.5) is differentiated with respect to β, one obtains the elastic pitch-flap ratio:

$$\theta_\beta = [\zeta(C_\beta - C_\zeta) + \zeta_p C_\beta]/C_\theta \tag{4.7}$$

Equation (4.7) is used in the following section. For matched stiffness rotors with $C_\beta = C_\zeta$, the first terms in Eqs. (4.6) and (4.7) are zero and constant pitch-lead and pitch-flap ratios are obtained, depending only on the prelead and preflap angles. For other rotors, usually $C_\zeta \gg C_\beta$ so that C_β can be neglected vs. C_ζ.

For blades with low chordwise frequency, the aerodynamic lead-lag damping from pitch-lead coupling is approximately

$$\eta_\zeta = -\beta\theta_\zeta\gamma/8(\omega_\zeta/\Omega) \tag{4.8}$$

an expression first established in somewhat different form in reference 4.1. It shows that such a rotor requires negative pitch-lead coupling (for positive β) to obtain aerodynamic damping of the lead-lag motion. Without matched stiffnesses and for $C_\zeta \gg C_\beta$, Eq. (4.6) yields

$$\theta_\zeta = -(\beta + \beta_p)C_\zeta/C_\theta \tag{4.9}$$

So far as the elastic pitch-lead coupling is concerned, it does not matter which part of the total flapping angle with respect to the feathering axis is elastic and which part is preflap. This has an important consequence if precone of the feathering axis is used. Precone angle has been used to relieve the blade root of the flapping moment from normal lift. However, precone angle reduces $\beta + \beta_p$, and if the precone angle is made larger than the natural coning angle, $\beta + \beta_p$ becomes negative and the lead-lag motion becomes unstable. The use of excessive precone in the Aerospatiale hingeless rotor experiments was the suspected reason for some of the difficulties experienced. From equation (4.9), it is clear that precone angle should be used with caution for a soft inplane rotor. The blade root flap bending moment can be relieved also by preflap which, unlike precone, does not affect the stability of the lead-lag motion as much. However, preflap relieves only the blade root bending moment, but not the moment on the feathering bearings.

Without prelead or preflap, Eq. (4.5) can be written in the form

$$\theta/\beta\zeta = (C_\beta - C_\zeta)/C_\theta \tag{4.10}$$

For the BO-105 soft inplane hingeless rotor helicopter, the right-hand side of Eq. (4.10) has the value −0.1/deg (ref. 2.10) so the pitch-lead coupling ratio for $\beta = 2°$ would be −0.2. For stiff inplane blades, C_ζ is much larger and higher absolute values of the elastic pitch-lead coupling ratio occur, unless the control stiffness C_θ is increased with C_ζ. The preceding equations should not be used quantitatively. They are intended to illustrate very general trends for soft inplane hingeless rotors. A more accurate treatment of the effects of pitch-lead coupling for hover, also based on the concept of rigid blades with root flexures, is given in references 2.74 and 2.76. Figure 4.4 (taken from these references) shows, for a Lock number of 5 and a flapping frequency of 1.15Ω, stability limits in terms of pitch angle vs. pitch-lead coupling ratio θ_ζ. The right-hand side refers to a soft inplane rotor with $\omega_\zeta = 0.7\Omega$. The parameter R defined in Eq. (4.1) has little influence. Positive pitch-lead coupling at positive β is destabilizing, as indicated by Eq. (4.8). The left-hand side refers to a stiff inplane rotor with $\omega_\zeta = 1.4\Omega$. Without elastic flap-lag coupling and R = 0, negative pitch-lead coupling is destabilizing, as would occur for a soft hub and a stiff blade. However, for larger values of R, positive pitch-lead coupling becomes
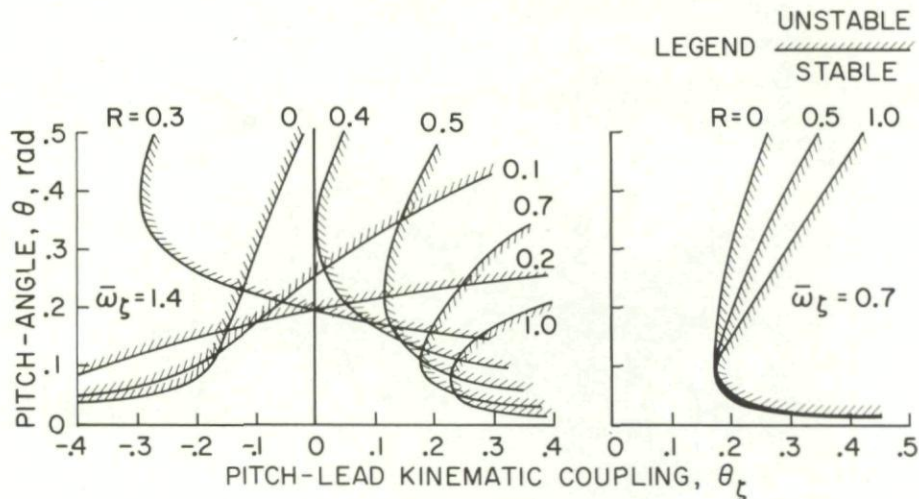
Fig. 4.4   Stability boundaries of pitch setting versus pitch-lead coupling in hover.

destabilizing and, for R = 0.2, instability at high pitch setting cannot be avoided, regardless of the pitch-lead coupling ratio. For the stiff inplane rotor, a clear trend of the effects of pitch-lead coupling cannot be established. Within the limitations of the analysis, Fig. 4.4 shows that it is probably easier to avoid isolated lead-lag motion instability for a soft inplane blade rather than a stiff inplane blade since, in the soft inplane case, hub flexibility has little effect and a negative pitch-lead coupling is always stabilizing.

4.6   Pitch-Flap Coupling

Pitch-flap coupling is an important parameter for both articulated and hingeless rotors. For articulated rotors, it occurs if the attachment point between the rotating pitch link and the pitch horn is not on the flapping axis. The pitch-flap coupling ratio is given by

$$\theta_\beta = -\tan \delta_3 \qquad (4.11)$$

For hingeless rotors, this coupling can occur if the feathering axis participates in the flapping motion, that is, for soft flapwise hub configurations. Because the hub can be highly flexible, this pitch-flap coupling ratio can be substantial. For stiff hub configurations, an elastic pitch-flap coupling can exist if the flapping mode shape involves some feathering motion. In addition to this pitch-flap coupling, there is an elastic pitch-flap coupling for a rigid blade with root flexures as expressed by Eq. (4.7). For a matched stiffness blade, $C_\beta = C_\zeta$, a negative pitch-flap coupling (which is usually desirable) is obtained by prelag $-\zeta_p$. For other rotors and for $C_\zeta \gg C_\beta$,

$$\theta_\beta = -\zeta \, C_\zeta/C_\theta + \zeta_p \, C_\beta/C_\theta \qquad (4.12)$$

If ζ and ζ_p are of the same order of magnitude, the second term is smaller than the first one. For a desirable negative pitch-flap coupling, an elastic lead angle is needed which can be obtained with a prelag larger than the natural lag from the driving torque. Reference 2.11 shows that, for the BO-105 helicopter, 2.5° prelag would increase the equivalent δ_3 angle from about −5° to +10°. The −5° without prelag results from the elastic lag from the driving torque which, according to equation (4.12), produces positive pitch with up flapping.

The effects of negative pitch-flap coupling on the flying qualities of hingeless rotorcraft are numerous. Control and gust sensitivity are reduced. The angle-of-attack instability is diminished. The control and damping cross-coupling is changed. For the BO-105 helicopter flying at 100 knots, even such a small change as 15° in equivalent δ_3 angle reduces (according to refs. 2.10 and 2.11) the angle-of-attack instability by 40% and increases the time to double amplitude for the phugoid mode from 5.5 to 8.5 seconds.

Pitch-flap coupling also influences the blade lead-lag motion stability. For a stiff inplane hingeless floating proprotor in axial flight, reference 2.30 shows that negative pitch-flap coupling is destabilizing and positive pitch-flap coupling is stabilizing. Because of the large pitch setting required in proprotor flight, the inplane blade frequency is greatly reduced and nearly coincides with the flap frequency. Changing the pitch-flap coupling from negative to positive removes the frequency coalescence and stabilizes the blade lead-lag motion. A lead-lag blade instability (ref. 2.50) of the stiff inplane Lockheed AH-56A helicopter that occurred in high-speed forward flight (denoted "half-P-hop") was eliminated in part by changing from a positive pitch-flap coupling ratio of 0.22 to about zero coupling. But for the AH-56A reactionless mode lead-lag instability, reference 2.38 indicates that changing from zero to a negative pitch-flap ratio of −0.38 was destabilizing. For stiff inplane rotors, it appears desirable to limit negative pitch-flap coupling ratios to values that will not result in near-frequency coalescence between inplane and out-of-plane blade modes.

Note that pitch-lead coupling mainly affects the damping of the blade lead-lag motion and is thus important for ground and air resonance. Once such instabilities are avoided, the effect of pitch-lead coupling on the flying qualities is usually not substantial. In contrast, pitch-flap coupling always affects the flying qualities significantly.

In addition to the pitch-lead and pitch-flap couplings, there are numerous other coupling terms between pitch, flap, and lead-lag displacements, the effects of which have not yet been delineated. For example, figure 4.3 indicates that a change in feathering angle produces a change in flapping angle because of $\zeta + \zeta_p$ and a change in lead angle because of $\beta + \beta_p$. A pitch/rate-of-lead coupling also exists since a change in centrifugal force tends to twist the blade in proportion to its pitch angle. The more elaborate types of analysis include most of these terms, but their effects have not been isolated and studied in detail.

4.7   Chordwise Blade Balance

It has long been recognized that chordwise blade balance in conjunction with control flexibility is an important parameter in rotorcraft flight dynamics (ref. 4.2). The main parameter that influences elastic blade torsion or elastic feathering is the offset between the aerodynamic center of the blade and its center of gravity. If the chordwise position of the blade center of gravity is ahead of the aerodynamic center, an elastic feathering feedback is introduced which tends to alleviate aerodynamic disturbances. For example, an increase in the rotor angle of attack normally increases the lift on the advancing blade and decreases the lift on the retreating blade, resulting in an aft tilt of the tip path plane. The reaction to the lift increase is seen mainly in the inertial forces centered in the blade chordwise center of gravity. Thus the advancing blade, because of control flexibility, is elastically feathered with the leading edge down and the retreating blade is feathered with the leading edge up, which introduces an elastic forward cyclic pitch that alleviates the aft tilt

of the tip path plane. This process is the same for both articulated and hingeless rotors. However, because of the flap bending stiffness of the hingeless blade, the hub moment from the elastic feathering is much greater.

An aft cyclic control input has the same effect on the blades as an increase in rotor angle of attack. The elastic feathering opposes the control input and thus reduces the control power. If the rotorcraft experiences a pitch-up rate, the advancing blade is subjected to a down gyroscopic moment and the retreating blade, to an up gyroscopic moment. The reaction is indicated by the increased lift of the advancing blade and the reduced lift of the retreating blade. An elastic forward cyclic pitch that results increases the damping derivative of the rotor. Thus the main effects of center-of-gravity position forward of the aerodynamic center are to reduce control power (which is ample anyway in a hingelss rotorcraft), to increase pitch and roll damping, to reduce angle-of-attack instability, and to reduce gust sensitivity — all favorable effects obtainable with small weight penalty. According to reference 2.13 a 3% forward shift of the center-of-gravity of the BO-105 blade would reduce the rotor angle-of-attack instability by 30% at 100 knots and would increase the time to double amplitude of the phugoid mode from 6 to 40 seconds. The BO-105 blade and control system is relatively soft with a blade torsional frequency ratio of $\omega_\theta/\Omega = 3.4$. For blades that are torsionally stiffer (such as those of the Westland Lynx hingeless helicopter), the effects of elastic cyclic pitch feedback are smaller.

In the discussion of feedback systems in a subsequent chapter, the kind of feedback produced by chordwise overbalance is classified as proportional tilting feedback with a phase angle near zero. This type of feedback destabilizes the flapping motion and should be used with caution at high advance ratio. In addition to tilting feedback, chordwise overbalance also provides an elastic negative pitch-cone coupling that is beneficial for all aspects of flight dynamics.

For soft flapwise blades, the lift is transferred to the hub mainly via centrifugal forces centered in the chordwise c.g.; for stiff flapwise blades, this transfer is mainly elastic and centered in the shear axis of the blade cross section. For stiff flapwise blades, the location of the shear axis is more important than that of the chordwise c.g.

5 SPECIAL PROBLEMS OF HINGELESS ROTORCRAFT

The special flight dynamics problems of hingeless rotorcraft refer to basic configurations without control feedback. The use of control feedback to improve hingeless rotor flight dynamics is treated later. The phenomena discussed here were mentioned in connection with the classification of flight dynamics and with the discussion of basic rotor design parameters. Those previous comments are now discussed further.

5.1 Blade Lead-Lag Motion Instability

The problem of blade lead-lag motion instability, both for soft and stiff inplane rotors, has probably attracted more attention than any other hingeless rotor problem. According to the definition in the Preface, this problem belongs to flight dynamics because of the low frequency of the air resonance mode. Potentially unstable blade lead-lag modes have been observed either as regressing modes with a body frequency of $\Omega - \omega_\zeta$ or $\omega_\zeta - \Omega$ for soft or stiff inplane blades, respectively, or as the reactionless scissors mode for four-bladed rotors. In addition, the Lockheed AH-56A helicopter with the original feathering feedback system with floating gyroswashplate experienced a so-called 1P $\times$ 2P blade flap-lag instability (ref. 2.50). The instability range was centered at an intermediate rotor angular speed for which the blade inplane natural frequency ratio ω_ζ/Ω was 2.0. Tilting the rotor is equivalent to 1/rev flapping and results in large 2/rev Coriolis inplane blade moments in the absence of lead-lag hinges. These moments are in resonance with the inplane natural frequency when $\Omega = \omega_\zeta/2$. Because of the feedback of the inplane moments into the floating gyroswashplate, the 2/rev inplane oscillations were actually self-excited and dynamically unstable. In the latest (AMCS) control system, feathering feedback into the floating gyroswashplate has been replaced by pure flapping feedback, and the 1P $\times$ 2P mode cannot be self-excited. Experience with this phenomenon, however, should show the need for caution when stiff inplane rotors are operated at angular speeds near $\Omega = \omega_\zeta/2$ with the rotor tilted.

To avoid inplane blade stability problems, the first requirement is to provide the lead-lag motion of the isolated blade with adequate damping at all operational flight conditions. For stiff inplane blades, mechanical damping is difficult to provide because of the small deflections. For soft inplane blades, mechanical dampers of the elastomeric type are quite effective. Aerodynamic damping depends on numerous paramters. Figure 4.2 shows the effect of hub flexibility in terms of the parameter R defined in Eq. (4.1). Figure 4.4 shows the combined effect of the parameter R and the pitch-lead coupling ratio θ_ζ on the stability boundary in hover. For soft inplane rotors, a negative pitch-lead coupling ratio increases the lead-lag damping. For stiff inplane rotors, there is no clear trend with pitch-lead coupling. For the Lockheed stiff inplane rotor with a soft hub, positive pitch-lead coupling is stabilizing (ref. 2.38). For the AMCS version, the pitch-lead coupling in the first lead-lag bending mode is 0.36 and there is an additional positive pitch-lead coupling from a 2° negative preflap setting or droop (evident in Eq. 4.6). Since positive pitch-lead coupling is stabilizing for the Lockheed stiff inplane rotor, equation (4.6) shows that increasing lift, associated with increasing β, is destabilizing, which agrees with the experience described in reference 2.38. This is opposite the soft inplane rotor characteristics where negative pitch-lead coupling is stabilizing and where equation (4.9) shows that increasing lift, associated with increasing $\beta+\beta_p$, yields a more favorable pitch-lead coupling.

The effect of negative pitch-flap coupling on the lead-lag damping of the stiff inplane Lockheed rotor is unfavorable (ref. 2.38). It was mentioned previously that negative pitch-flap coupling, which is very desirable for all handling characteristics, should probably be used with caution in stiff inplane rotors to prevent the flapwise and chordwise blade frequencies from becoming too close. Although no corresponding studies are available for soft inplane blades, such limitations should not exist since in this case negative pitch-flap coupling increases the difference between blade flap and lead-lag natural frequencies.

Very little is known about the damping of the isolated blade lead-lag mode in forward flight. Reference 2.10 shows that the change in damping of the isolated blade inplane mode and of the coupled blade-inplane body mode of the BO-105 helicopter is slight between 0 and 110 knots. The first mode has a damping ratio of about 0.03 at the ω_ζ frequency and the second mode has a damping ratio of 0.08 at the $\Omega-\omega_\zeta$ frequency. On the other hand, Lockheed experience with the so-called "half-P-hop" mode near the $\omega_\zeta-\Omega$ body frequency indicates that the damping diminishes at high speed. Since the inplane mode was strongly coupled with vertical body motions (because of a soft collective control system and positive pitch-flap coupling), the instability may have been atypical of stiff inplane rotors. The stability limit was moved from 180 to 250 knots by increasing the collective control stiffness by 70%, removing the positive pitch-flap coupling, increasing the blade prelead angle (forward sweep) by 60%, and adding collective control system dampers.

In contrast to the "half-P-hop" instability at high forward speed, the reactionless mode instability subsequently encountered (ref. 2.38) appears to be of more general significance. This instability occurred at low speed and high lift and probably could have been approximately predicted from an isolated blade analysis since coupling with body modes was not involved. This instability appears to have resulted from the increased adverse pitch-lead coupling due to the large coning angle at the high rotor lift condition. In terms of the hub stiffness parameter R, the Lockheed rotor apparently has a rather soft hub associated with a low value of R and figure 4.4 shows that positive pitch-lead coupling would be stabilizing. According to Eq. (4.6) this can be provided by negative preflap (droop) but may become overcompensated by a high β at high lift. For rotors with higher R values, figure 4.4 shows that negative pitch-lead coupling is stabilizing and this is improved at high lift conditions. Note that results in figure 4.4 were obtained without distributed blade

bending flexibility and represent only general trends. Blade stall also has a large effect on blade inplane stability. For soft inplane blades, references 2.10 and 2.71 show that blade stall causes a deterioration in damping of the coupled flap-lag blade mode. For the BO-105 helicopter, aerodynamic damping of this mode goes to zero at 18° pitch setting in hover.

Despite the fact that stiff inplane rotors cannot have ground resonance of the Coleman type, these rotors are more demanding of the dynamic design than soft inplane rotors. A careful isolated blade analysis including all elastic coupling effects is necessary for all operating conditions to assure adequate aerodynamic damping of the lead-lag mode since mechanical damping is impractical. Negative pitch-flap coupling, otherwise very desirable to alleviate hingeless rotorcraft flying qualities problems, should be provided with caution to avoid near coalescence of blade flapping and inplane natural frequencies. The soft inplane rotor is somewhat less demanding of the dynamic design since some general rules are applicable. For example, negative pitch-lead coupling is nearly always beneficial, preconing of the feathering axis is detrimental except for matched stiffness rotors, and additional lead-lag damping can be obtained readily by simple mechanical elastomeric dampers. Special attention must be given to stall conditions.

After adequate damping of the isolated blade lead-lag mode is assured, the stability of the coupled rotor/body modes must be examined. The critical regions are those near frequency coalescence of the regressing inplane mode with a body mode. Since the regressing inplane mode for both soft inplane and stiff inplane rotors has a frequency of 0.3 to 0.4Ω, frequency coalescence can be expected with the short-period rolling mode, which is also in this frequency range for soft flapwise rotorcraft. The short-period pitching mode is usually much lower — near 0.1Ω. Pylon or empennage modes are usually much higher, but they must be checked for possible frequency coalescence with the regressing inplane mode. Figure 5.1 (taken from ref. 2.15) shows the natural frequencies of the short-period roll mode, short-period pitch mode, and the coupled inplane regressing mode as a function of rotor speed for the BO-105 helicopter. Frequency coalescence of the roll mode and inplane regressing mode falls in the normal operating rotor speed range typical of soft flapwise rotorcraft. All three modes are adequately damped with a damping ratio of 0.5 for the roll mode, 0.8 for the pitch mode, and 0.07 for the coupled regressing inplane mode.
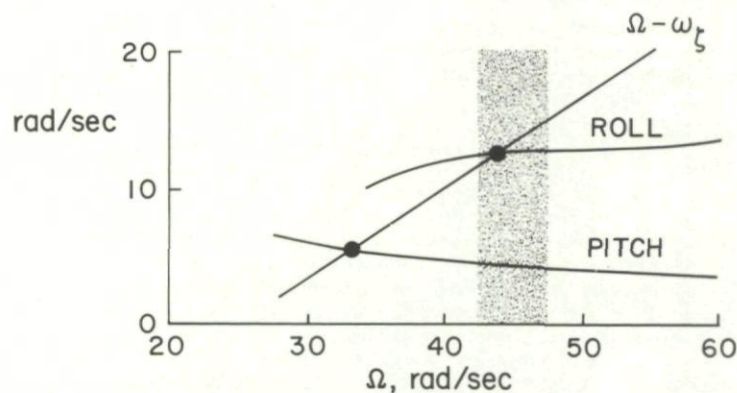

Fig. 5.1   Frequency of short-period roll mode, short-period pitch mode, and coupled inplane regressing mode versus rotor speed for BO-105 helicopter.

An interesting study (ref. 2.15) shows that without aerodynamics the frequencies of the three modes remain approximately unchanged from figure 5.1. However, the roll mode would become unstable in the operating rotor speed range, while the regressing mode — because of the assumed mechanical blade damping — would remain stable. The analysis depends critically on the value of the assumed blade inplane structural damping ratio, which was 2% in this case. With zero structural damping, the coupled regressing mode, even if all aerodynamic terms are included, becomes unstable at the lower end of the operational rotor speed range. For the soft inplane rotorcraft, some inplane damping must be provided either aerodynamically or by special elastomeric dampers if the blades have inadequate structural damping.

5.2   Rotor Angle-of-Attack Instability

In addition to blade lead-lag instabilities, the rotor angle-of-attack instability of hingeless rotors has also been a major concern. Figure 5.2 compares the hub moment derivative with rotor angle of attack in the unstalled region for an articulated rotor with 2% hinge offset and a hingeless rotor with a flapping frequency of 1.15Ω. For stiffer blades, the increase in angle-of-attack instability would be still more pronounced. To minimize angle-of-attack instability, it is therefore desirable to keep the flap-bending stiffness of the blades, particularly in the root section, as low as possible, consistent with structural considerations. This has been done with several hingeless rotorcraft that have elastic blade flap frequencies of 1.05 to 1.12Ω. Although a negative pitch-flap coupling increases the flap frequency, it reduces the rotor angle-of-attack instability and should be included since it also alleviates vertical gust sensitivity. As mentioned before, the pitch-flap coupling ratio of the Lockheed AH-56A helicopter was changed from +0.22 to 0 and then to −0.38 despite an unfavorable though acceptable effect of this change on the damping of the blade lead-lag mode, and despite the rotor feedback control system that alleviates most of the rotor angle-of-attack instability.
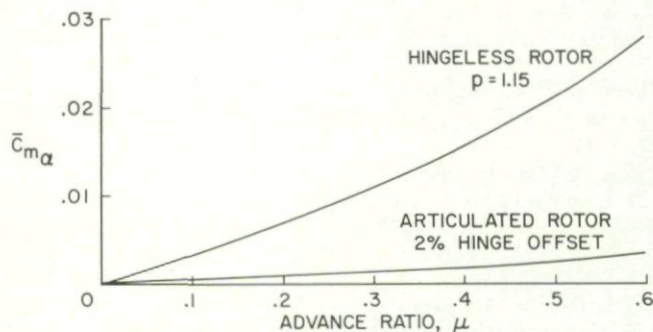

Fig. 5.2   Rotor pitching moment with hub angle-of-attack derivative versus advance ratio.

Another means of reducing angle-of-attack instability is chordwise overbalance (discussed in Sec. 4.7). To be effective, the control system must be relatively soft. This can introduce other problems in the reversed-flow region at high advance ratio, such as blade flutter or blade torsional divergence, quite apart from the blade weight penalty. Any rotor angle-of-attack instability that remains after all design efforts to minimize it must be compensated either by a sufficiently large horizontal tail surface or by a control feedback system. The latter solution is discussed in the next chapter. A relatively large tail surface, though it can be effective in removing or reversing the rotor angle-of-attack instability, must be adjusted carefully to avoid large oscillatory blade flap-bending moments. The tail surface must also be used to compensate in part the large speed stability derivative of hingeless rotors, which, according to figure 5.9, can destabilize

the phugoid mode. Because of the rotor downwash effects on the horizontal tail and on the fuselage, the design for acceptable longitudinal flight dynamics should be supported by model testing that includes the rotor.

Considerable angle-of-attack instability and pitch divergence tendency will be tolerated by pilots so long as control power and control sensitivity are sufficient. For example, hingeless rotor helicopters have been flown when the time to double amplitude of a pitch disturbance was 1.5 seconds (ref. 2.20). However, care must be taken to ensure that adequate control margins beyond trim are available for all possible flight attitudes. In the presence of angle-of-attack instability, an increasing pitch-up attitude requires increasing forward control for trim. Once a pitch-up attitude is reached which requires full-forward control for trim, any further pitch-up disturbance cannot be controlled and will lead to a temporary uncontrollable divergence until collective pitch or flight speed is reduced. For helicopters with angle-of-attack instability, a trim analysis is desirable not only for steady flight conditions but also for possible transient conditions to ensure that control margins adequate for recovery are available.

5.3 Control Problems

Recommended V/STOL handling qualities are discussed in references 5.1, 5.2, and 5.4. U.S. military requirements for V/STOL flying qualities are given in reference 5.3 and flying qualities requirements for U.S. Army helicopters are given in reference 5.5. None of these documents considers the special flying qualities of hingeless rotorcraft. The first four references attempt to combine requirements for rotorcraft with V/STOL type airplane flying qualities — a difficult enterprise. Even basic terms such as control power and control sensitivity are used with entirely different meanings in the various documents. The fact is that very little data are available on basic hingeless rotorcraft flying qualities. All of the extensive Lockheed experience was gained with a hingeless rotor with an integrated control feedback system that features a floating gyroswashplate. The basic characteristics without the feedback system are computed in reference 2.44 but are not substantiated by flight tests. The longitudinal stability and control characteristics of the Bolkow BO-105 helicopter are well documented, but few other comparable data are available. The discussion of the control and stability qualities of hingeless rotorcraft is therefore incomplete.

Hingeless rotor control is of the rate command type (refs. 5.1 and 5.2) in contrast to the attitude command type for longitudinal airplane controls. The time constant, that is, the time to reach 63% of the asymptotic pitch or roll rate, is a fraction of a second compared to several seconds for articulated rotorcraft. *Total control power* is defined as the *angular acceleration* for the *maximum* step pitch or roll control input, in agreement with references 5.1 and 5.2. *Specific control* power is termed the *angular acceleration* for a *unit* step control input. This quantity is called "control sensitivity" in references 5.1 and 5.2 and merely "control power" in other references. Actually, a fraction of a second is required to develop the control power even if a step control input is assumed. This time delay, almost imperceptible to the pilot, can usually be ignored. Reference 5.2 recommends a time constant for the acceleration buildup after a step control input of less than 0.2 second. However, a rotor designer can do very little to substantially influence this time constant.

Control sensitivity is defined as the asymptotic pitch or roll rate per unit step control input. In reference 5.6, stick deflections of 14 to 20 deg/sec/in. are recommended for armed helicopters; these values are accepted as valid at least for roll control, despite considerably lower requirements given in reference 5.5. For articulated rotors, the time constants for the build-up of the pitch or roll rate given in reference 5.5 can hardly be achieved without SAS. For hingeless rotors, these time constants ($I_y{}^{\cdot 3}/8$ and $I_y{}^{\cdot 3}/15$ in pitch for visual and instrument flight, respectively) can be achieved easily and are usually less. From this point of view, SAS for hingeless rotorcraft is not necessary.

While there are no inherent difficulties with specific control power and with the time constant for the pitch or roll rate buildup, the total installed control power depends on the trim requirements. Figure 5.3 (taken from ref. 2.20) shows longitudinal and lateral cyclic pitch required for trim for the BO-105 helicopter. Forward cyclic pitch of more than 6° and lateral cyclic pitch up to 2° are *required for trim.* These values are about the same as required for an articulated rotor. Since the specific control power is much larger than for articulated rotors, the total control power is also very much larger. In flight, this large control power is balanced by a large pitch and roll damping. On the ground this balance is not available and the pilot must use only small control excursions. Thus the hingeless rotor does have a problem of high control sensitivity on the ground. This is significant for autorotational landings. The experience with numerous autorotational landings with the Westland Lynx and the Bolkow BO-105 has shown that this type of landing can nevertheless be performed satisfactorily. The high control sensitivity on ground contact is also important for slope or ship deck
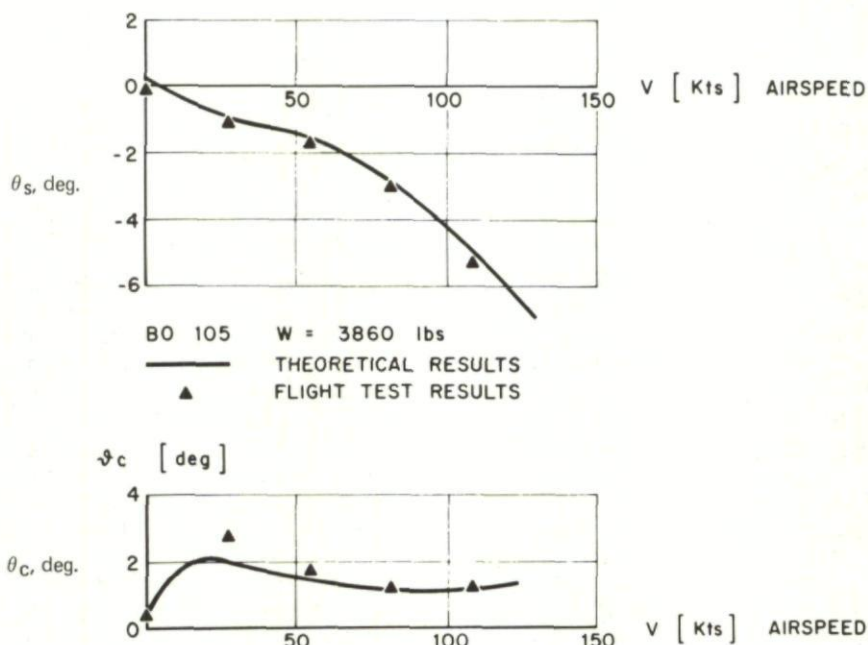

Fig. 5.3 Cyclic trim requirements for BO-105 helicopter.

landings and takeoffs and for taxiing. Slope landings up to 12° (left, right, and nose-up slope) have been carried out with the Lynx as well as operation from two ships, without significant handling problems or blade stresses. Taxiing trials of the naval version of the Lynx have also been completed without abnormal problems.

For longitudinal control requirements in maneuvers, figure 5.4 (taken from ref. 2.11) shows the BO-105 longitudinal control required to attain load factors from 1.0 to 2.2 g at 110 knots. The original blades with a NACA 0012 airfoil were predicted to give a control reversal at 1.6 g. The newer NACA 23012 cambered airfoil postpones partial blade stall and avoids control reversal. However, the stick deflection per g is very small — only a fraction of an inch per g. While this is also not atypical for articulated rotors, hingeless rotors are usually characterized by small stick deflections per g-load and control reversal in the high-speed flight regime with partial retreating blade stall. Associated with this are handling difficulties at high speed in turbulence which are also not atypical of articulated rotorcraft without SAS.

LONGITUDINAL STICK POSITION

BO 105
GW = 2050 kp = 4500 lbs
TAS = 110 Kts
H = 5000 ft

● ▲   FLIGHT TEST
─ ─ ─ ANALYSIS

100 % D_β ≅ 12 in. STICK TRAVEL
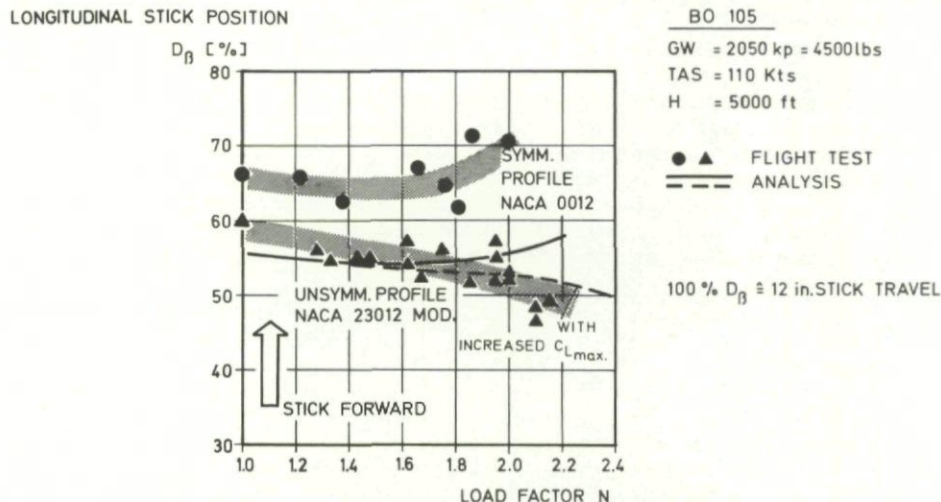
Fig. 5.4 Longitudinal control position versus load factor for BO-105 helicopter.
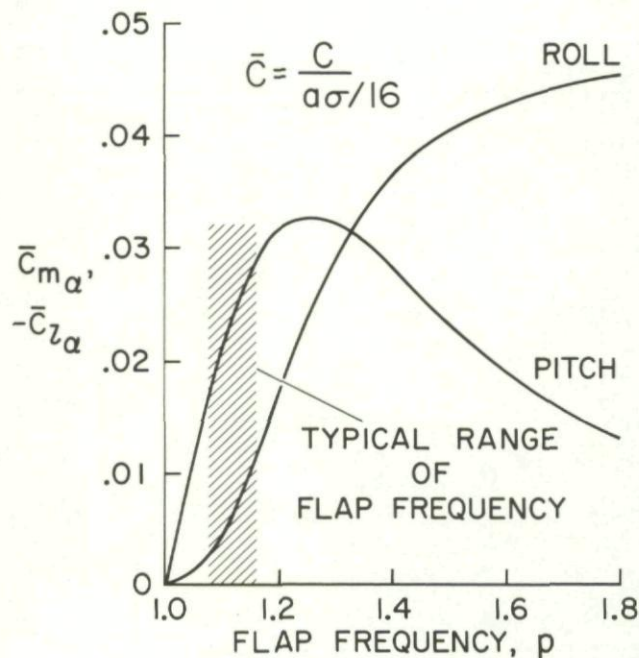
Fig. 5.5 Rotor pitch and roll moment with hub angle-of-attack derivative versus flap frequency, $\mu = 0.6$, $\gamma = 5$.

Another problem is that of control cross-coupling. Three types of cross-coupling must be alleviated by proper design methods. First, there are direct control cross-coupling effects where a longitudinal control input also produces a rolling moment, and a lateral control input also produces a pitching moment. Second, changes in angle of attack produce both pitching and rolling moments. Third, pitch rate produces not only pitch damping but also a rolling moment, and roll rate produces not only roll damping but also a pitching moment. All three types of cross-coupling depend on blade flapping frequency and advance ratio. Figure 5.5 shows the second type of coupling at an advance ratio of 0.6 as a function of blade flapping frequency. For the soft flapwise rotor (1.05 to 1.15Ω flap frequency), the coupling is moderate but becomes large for the stiff flapwise rotor (≥ 1.4Ω flap frequency). The two major design parameters that can alleviate all three types of cross-coupling are control phase angle and negative pitch-flap coupling.

Figures 5.6 and 5.7 (taken from ref. 2.79) give the trend of pitch and roll cross-coupling with increasing blade flap. frequency in hover. Figure 5.6 shows the hub rolling and pitching moment coefficients per unit lateral cyclic pitch. The circle represents the upper limit of soft flapwise blades (P = 1.17 for $\gamma = 6$), and the square represents a stiff flapwise blade (P = 1.33 for $\gamma = 6$); C_ℓ is the right rolling moment coefficient and C_m is the nose-up pitching moment coefficient. A right cyclic pitch control input assumed in figure 5.6 provides a right rolling moment and nose-up pitching moment. A nose-up cyclic pitch control input would produce a nose-up pitching moment and a left-rolling moment. To compensate this coupling, soft flapwise rotors require 10° to 20° control phase shift so that an aft motion of the stick provides aft plus right cyclic pitch. This is achieved by shifting the swashplate axes for longitudinal and for lateral cyclic control in the direction of rotor rotation by an amount equal to the control phase angle. If negative pitch-flap coupling is used, this control phase shift must be larger. For stiff flapwise blades, the control phase shift must be 45° and more.

Figure 5.7 shows hub rolling and pitching moment coefficient per unit pitching angular velocity, again for $\gamma = 6$. (Circles and squares have the same meaning as before.) For P = 1.17, there is moderate cross-coupling in the sense that a nose-down pitching velocity produces a right rolling moment. In a turn, the angle of attack of the rotor will increase with an associated roll hub moment to the left, which will partially compensate for the damping cross-coupling. If a portion of the damping cross-coupling effect is uncompensated, the same lateral control input will be required in both left and right coordinated turns, since both types of turns involve a nose-up pitch rate. This asymmetry for left and right turns is well known in many helicopters and can be alleviated by negative pitch-flap coupling.

The cross-coupling effects change with forward flight, so that a compromise control phasing between hover and cruising flight must be selected. The compromise becomes more difficult as the blade flapwise stiffness increases. With increasing advance ratio,
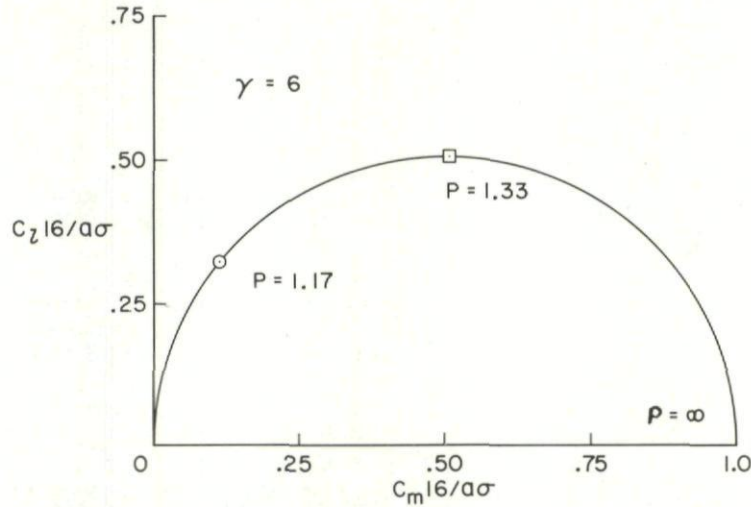
Fig. 5.6   Hub moment response to unit lateral cyclic control in hover (cross-control coupling).

collective pitch changes increase the pitching and rolling moments which also are more pronounced for stiffer flapwise blades. As for dynamic cross-coupling effects, figure 5.8 (taken from ref 2.20) shows (for hover) the combined cross-control and cross-damping effects after a pitch control input. These results were computed for the BO-105 helicopter. It is seen that, with a control phase angle of 75° (15° shift compared to the usual 90° phase angle arrangement for hinged rotors), the cross-coupling effects on attitude are quite small up to 4 seconds after the control step input. In forward flight, the cross-coupling becomes larger. Note that in computing the control power of hingeless rotors the asymmetric downwash effectively reduces the control power (ref. 5.7). The asymmetric downwash effect can be approximated by reducing the Lock number of the blade (as shown in refs. 2.79 and 2.80). This and other methods are compared with experimental hingeless rotor response measurements in reference 2.75.

Thus, for soft flapwise rotors, the various cross-coupling effects require special design consideration, but at low advance ratio they do not present a serious problem.

5.4 Dynamic Stability Problems

Dynamic stability problems of hingeless rotorcraft are mainly caused by the larger angle-of-attack instability compared to articulated rotorcraft. This may result in unstable phugoid oscillations or a pitch divergence at high flight speeds. As mentioned previously, the derivative approach for dynamic stability analysis cannot be used for those modes that couple appreciably with the rotor modes. The rotor coning mode with a frequency $\omega_\beta > \Omega$ and the rotor advancing flapping mode with frequency $\Omega + \omega_\beta$ are affected very little by coupling with the body and can be predicted with a fixed hub analysis. However, the rotor regressing flapping mode with frequency $\omega_\beta - \Omega$ couples with at least some of the body modes and also with the other rotor modes; therefore, the rotor flapping modes must be included for a valid analysis of rotorcraft flight dynamics.

First consider the phugoid mode, as determined from the derivative approach, since the effect of the rotor flapping modes on the phugoid can be neglected. The three derivatives that determine the phugoid characteristics are the pitch damping derivative M_q, angle-of-attack derivative M_α (which is proportional to the vertical damping M_w), and the speed derivative M_u. For positive pitch damping, M_q is negative; for positive angle-of-attack stability, M_α is negative; and for positive speed stability, M_u is positive. Figure 5.9 (taken from an unpublished note by Mr. Livingston of Bell Helicopter Co.) shows the stable phugoid range in terms of M_u − M_α boundaries for a hingeless helicopter with rather soft flapwise blades flying at 160 knots. Below the lower line, the divergence is static; above the upper line, the divergence is oscillatory. A certain amount of angle-of-attack instability can be tolerated if the speed stability is positive and not too large. In forward flight, the speed stability is determined mainly by the horizontal tail incidence, which must be adjusted carefully to obtain a stable phugoid mode.

Reference 2.11 shows phugoid characteristics obtained with the derivative approach for the BO-105 helicopter, where the period is 15 seconds at 100 knots and the time to double amplitude is 6 seconds. With various rotor modifications, the unstable phugoid can be made nearly stable. Reference 2.44 presents the dynamic stability results of an analysis with three rotor flapping modes (called a 9 X 9 model) for the Lockheed AH-56A without the control feedback system. The longitudinal and lateral-directional motions are coupled because of the regressing rotor flapping mode. The inplane regressing mode with a frequency of about 0.6Ω was found to have a negligible effect on the flight stability.

With the regressing rotor flapping mode, there are five eigenvalues for longitudinal motion and five for lateral-directional motion instead of the usual four. No mode shapes are given in
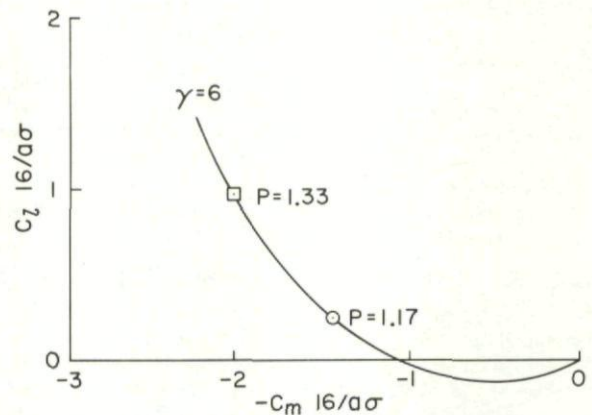

Fig. 5.7   Hub moment response to unit pitch-up angular velocity in hover (cross-damping coupling).
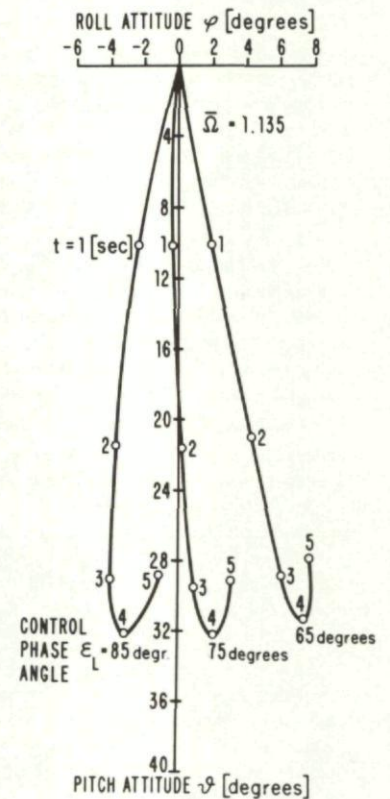

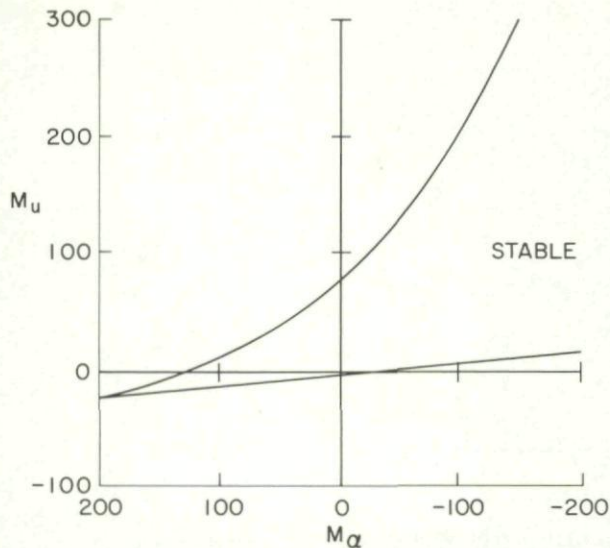Fig. 5.8   Attitudes following a unit pitch control input for the BO-105 helicopter.

Fig. 5.9 Phugoid stability boundaries of a soft flapwise
hingeless helicopter at flight speed of
160 knots

reference 2.44 so the degree of modal coupling is not known. Longitudinally, two complex conjugate eigenvalues correspond to a stable phugoid which, between 50 and 150 knots, has a period of 22 seconds and a damping ratio of 0.5, and a stable short-period pitch mode with a period of 1.5 seconds and a damping ratio of 0.9. (The regressing rotor flapping mode with fixed hub has a period of about 2 seconds.) Furthermore, the pitch divergence is small at 50 knots but its time to double amplitude is 3 seconds at 150 knots. Laterally, the regressing rotor flapping mode couples with the roll convergence to produce a stable short-period roll mode with a period of 1 second and a damping ratio of 0.5. In addition, there was a weakly damped dutch roll mode with a period of 4 seconds and a damping ratio of 0.2 and a spiral mode with a real eigenvalue near zero. Why the AH-56A without control feedback has a stable phugoid and a pitch divergence while the BO-105 has an unstable phugoid is not clear. From figure 5.9, a stable phugoid in the presence of angle-of-attack instability is possible only for a narrow range of speed stability M_u.

From reference 2.44, it appears that the AH-56A helicopter can be flown up to 150 knots without a control feedback system. The aircraft with a time to double amplitude of 3 seconds for the pitch-up divergence at 150 knots would probably not be harder to handle than current articulated rotorcraft without SAS at that speed. Only in the upper speed range from 150 to 220 knots, where the time to double amplitude for the pitch divergence goes to 1.5 seconds and less, would it be questionable whether the pilot, after failure of the SAS, could reduce the speed to an acceptable level without risking an upset. Because of the crisp control response, high-speed flight without SAS may be feasible for such a short period of time. Unfortunately, this basic question was not resolved. Note that, because of the large unloading of rotor lift to the fixed wing in the high-speed flight regime, the angle-of-attack instability of the AH-56A helicopter is considerably less than for a comparable wingless helicopter because partial blade stall substantially aggravates rotor angle-of-attack instability. An aft position for the wing was also used to provide improved angle-of-attack stability.

5.5 Winged and Compound Hingeless Rotorcraft

It is by now well understood that the cruise speed of the pure helicopter is limited to about 150 knots. Even this speed can be obtained only with penalties in hover performance and with a deterioration of handling qualities because of partial retreating blade stall effects in maneuvering. This deterioration may be somewhat greater for hingeless rotorcraft than for articulated rotorcraft. One way to overcome the speed limitation of pure helicopters is to unload the rotor in high-speed flight by a fixed wing. Although a fixed wing clearly improves the maneuvering capability at high speed, it involves considerable penalties in weight, hover download, climb performance, and autorotational performance. The forward tilt of the unloaded rotor is greater than that of the fully loaded rotor. To achieve the desired lift sharing between rotor and wing, the fuselage attitude with respect to rotor attitude must be properly adjusted. As mentioned previously, such an adjustment is more difficult for hingeless rotors because of the large hub moments involved. It is likely that the design problems of a hingeless winged rotorcraft are greater than for an articulated winged rotorcraft.

For a compound helicopter where auxiliary propulsion is provided in addition to a fixed wing, high-speed flight can be achieved with the fuselage and rotor attitude approximately horizontal. In this case, the hingeless rotor is not at a disadvantage with respect to the articulated rotor. Several compound hingeless rotorcraft have been flown: the Lockheed XH-51A compound helicopter (ref. 2.56), the Bell UH-1 compound helicopter with four-bladed hingeless rotor (ref. 2.26), and the Lockheed AH-56A helicopter (refs. 2.50 and 2.39). The first two compound rotorcraft had auxiliary jet engines, the latter had a tail-mounted pusher propeller. The XH-51A compound reached a flight speed of 263 knots, the UH-1 hingeless rotor compound reached 220 knots, and the AH-56A AMCS was flight tested to 210 knots. All three compound hingeless rotorcraft had stiff inplane blades.

Two main interrelated questions should be answered for a compound helicopter: Should the rotor speed be substantially reduced in cruise, and should conventional airplane-type controls be provided for cruise? The McDonnell XV-1 compound used airplane-type controls in cruise and the rotor autorotated at 50% normal rotor speed with a constant rotor angle of attack controlled by a rotor speed governor. In cruising flight, the rotor had very little effect on handling qualities since it was articulated and carried only 10 to 15% of the total lift. The penalties for true airplane-type handling qualities in cruising flight were the weight and additional complexity of airplane-type controls and the necessity for a 30-second transition period between the two flight modes (ref. 5.8). This solution would probably be impractical for a hingeless rotor since substantial hub moments would have to be overcome by the airplane-type controls.

As demonstrated by the three flight-tested hingeless compound helicopters mentioned previously, rotor controls of soft flapwise hingeless rotors can be adequate in high-speed flight with the rotor unloaded. Some difficulties were experienced with the Bell UH-1 hingeless compound because of inadequate longitudinal control power to overcome the angle-of-attack stability from the two horizontal tails. This difficulty is typical and indicates that compensating for the rotor angle-of-attack instability with horizontal tails is not a good solution. The rotor angle-of-attack instability should be minimized by optimizing the rotor design parameters rather than resorting to a large horizontal tail. For the Lockheed compound rotorcraft, this was accomplished by the control feedback system with floating gyroswashplate, so the problem of inadequate control power at high speed was not encountered. The Bell UH-1 compound needed conventional airplane-type controls for the flight tests with a teetering rotor. These controls were retained for the tests with the four-bladed hingeless rotor, but only the ailerons were actually used.

Whether the cruise speed of the rotor can be substantially reduced without a loss in rotor control effectiveness remains to be determined. Modern turbine powerplants are quite flexible with respect to operational speed. For stiff inplane hingeless rotors, the 2/rev inplane resonance is a barrier to reduced rotor speed. For soft inplane hingeless rotors, the 1/rev inplane resonance is an even more formidable barrier to reduced rotor speed. To provide adequate rotor control moments at reduced rotor speed is also a structural problem since the centrifugal relief of the flap bending moments at the blade root is reduced. Tests with the Bell UH-1 compound have shown that, with thin blade tips, an advancing blade Mach number of 0.94 can be reached without excessive blade and control loads. If a somewhat reduced rotor speed in cruise of about 600 ft/sec blade tip speed is assumed, a cruise speed of 250 knots (advance ratio of 0.7) appears feasible for a well designed hingeless compound helicopter using only rotor controls throughout the flight speed range.

5.6 Coaxial Hingeless Rotorcraft

Although several coaxial rotorcraft have been developed, this configuration — at least in the West — has never reached production. When articulated or soft flapwise rotors are used, the separation between the two coaxial rotors must be quite large. A compact coaxial configuration is possible only with stiff flapwise hingeless rotors. In addition to its compactness, this configuration also offers the possibility of substantially increasing the lift capability of the rotor system at high speed (as explained in Sec. 2.5). Figure 5.10 (taken from ref. 2.65) compares the achievable lift coefficients versus rotor advance ratio of articulated rotors and the Sikorsky ABC (advancing blade concept) rotor system. At an advance ratio of 0.6, the ABC rotor system can carry twice the lift of an articulated rotor, with a slightly better lift/drag ratio (neglecting shaft and hub drag). The coaxial stiff flapwise hingeless rotorcraft is an alternative solution to the winged helicopter. With auxiliary propulsion, it is an alternative solution to the compound helicopter. Although aerodynamically more efficient (except for the higher hub and shaft drag), the question is whether the coaxial hingeless rotorcraft is competitive with the winged or compound helicopter because of the greater weight, complexity, and the flight dynamics problems inherent in the coaxial system.
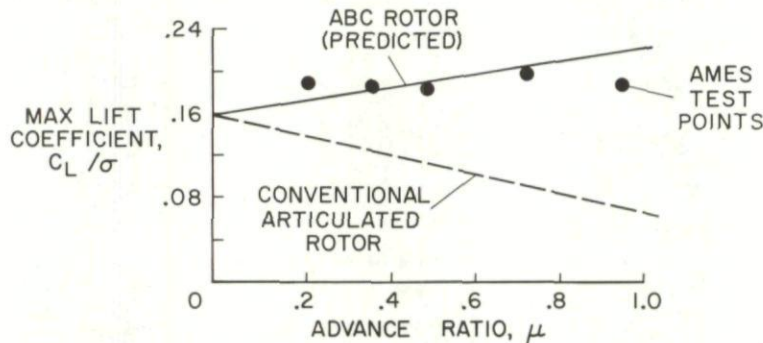
Fig. 5.10 Maximum aerodynamic blade loading for a single rotor and for a stiff flapwise
coaxial rotor system.

Because of the high flapwise and edgewise blade natural frequencies, the regressing modes may not substantially couple with the flight dynamics modes. The derivative approach to flight dynamics discussed in section 3.3 may be adequate in this case. The most outstanding characteristics of the stiff flapwise hingeless rotor are the large specific control power, the large angle-of-attack instability, and the large cross-coupling effects. Figures 5.6 and 5.7 show how specific control power, control cross-coupling, damping, and cross-damping in hover increase with flapwise blade stiffness. Figure 5.5 shows the hub moment derivatives with angle of attack without stall effects versus blade flap frequency for an advance ratio of 0.6. The angle-of-attack instability at a flap frequency of 1.5Ω is not much greater than at 1.12Ω, but the associated rolling moment is substantially higher than the pitching moment. For coaxial rotors, the rolling moments cancel but the shaft moments will increase and the clearance between the rotors will be reduced. The rolling moment due to angle of attack is produced by the large increase in lift on the advancing blade (negative $C_{\ell a}$). In trimmed flight, the advancing blade, in keeping with the ABC concept, is more highly loaded than the retreating blade so the tip-path planes are tilted toward each other — a tilt that increases with increasing rotor angle of attack.

A prelead of $-1.5°$ is used for the ABC rotors, the elastic blade axis is at 25% chord, and the blade center of gravity is at 25% chord for the outer quarter of the blade and at 29% inboard. Because of the high blade bending stiffness, much of the aerodynamic blade force is reacted elastically without producing a torsional moment. The reduction in rotor clearance resulting from gyroscopic action is cancelled in part by a suitable coupling between cyclic pitch controls. Precone is used to relieve blade root bending stresses. Because of the nearly matched stiffness design and the high blade bending stiffness, the precone sould have little effect on pitch-lead coupling, unless the control system is unusually soft. When the 40-ft rotors were operated in the Ames 40-by-80-foot Wind Tunnel over a wide range of conditions, no dynamic instabilities of any kind were encountered (ref. 2.66). Since there is no substantial pitch-flap coupling and no blade mass overbalance that might relieve the angle-of-attack instability, a large horizontal tail is required. At higher flight speeds, the calculated rotor derivatives are in good agreement with those measured for the full-scale rotors in the 40-by-80-foot Wind Tunnel (ref. 2.65). At low speeds, there are substantial discrepancies between the calculated derivatives and those measured with a 1/5-scale Froude model in the Princeton Dynamic Model Track (ref. 2.63).

From the model data available thus far, the main flight dynamics problems appear to be:

(a) A large angle-of-attack instability, not alleviated by structural or other pitch-flap coupling effects, requiring a large horizontal tail. Even at 38 knots and including tail effects, this instability is substantial, requiring $1.4°$ forward cyclic pitch to compensate a $10°$ pitch-up attitude.

(b) A mismatch between large longitudinal cyclic pitch required for trim and small maneuvering cyclic pitch values. At 38 knots, a $20°$ level flight flare requires $9°$ forward cyclic pitch for trim.

(c) A large pitching response from collective pitch input.

(d) A reduction in yaw control power from differential collective pitch during low-speed descent conditions. This type of yaw control is replaced at higher speed by rudder control.

(e) Large changes in aircraft attitude between hover and high-speed flight since the rotor tip path plane attitude with respect to the fuselage is almost constant.

Some of these problems can be solved or alleviated by a rotor feedback system, as shown in the following section. Other problems are inherent in the stiff flapwise coaxial rotor configuration.

6 FEEDBACK SYSTEMS FOR HINGELESS ROTORCRAFT

Whether hingeless rotorcraft require control feedback systems and if so, of what type, depends on the design and the operational envelope. For moderate speeds, low blade flapwise stiffness, structural pitch-flap coupling, and adequate horizontal tail size, feedback systems are unnecessary. For hingeless rotorcraft with higher speed capabilities, the increased gust sensitivity and increased angle-of-attack instability become increasingly more difficult to counteract without a feedback control system. The present discussion is limited to inner-loop feedback systems designed to improve helicopter handling characteristics. The design philosophy has been to improve control dynamics by use of feedback systems without changing the basic pitch or roll rate command type of control response in contrast to the pitch attitude command type for airplanes. Electronic or fluidic feedback systems are presently considered less

reliable than the basic mechanical controls, and failure of the feedback systems should not degrade flying qualities to a point where pilot effort becomes excessive. When "fly-by-wire" systems are accepted, the feedback loops become integral components of the control systems and the requirement of flight worthiness with failed feedback loops will no longer be justified. Then a type of control system entirely different from the "natural" unaugmented helicopter controls can be selected. TAGS is an example of such a fly-by-wire system with integral feedback loops, whereby the sidearm controller commands altitude rate, heading rate, lateral and forward velocities (ref. 6.1). It has also been suggested (ref. 6.2) that an onboard Kalman filter/controller be used which would allow all state variables to be fed back into the controls while only a few variables are actually being measured.

Since helicopter fly-by-wire technology is still in the experimental stage, only feedback systems are examined here which retain the natural pitch or roll rate command but improve the response characteristics of the helicopter. Among these systems, a distinction must be made between the integrated feedback systems designed to be operative at all times and the auxiliary feedback systems that permit operation with only the basic controls. Articulated and teetering rotorcraft presently have auxiliary feedback systems, so that flights can be made with or without the stability augmentation system (SAS). The control authority is limited to about 25% to ensure that a "hardover" signal will not endanger the aircraft. If the SAS malfunctions, the servos are often automatically centered and locked.

Without SAS, the helicopter usually has marginal handling qualities in the upper flight-speed regime. With a dual SAS that indicates a failure of one system, the pilot can avoid flight regimes with marginal unaugmented handling qualities so that, if a second system fails, he can revert without risk to the basic controls. Many such articulated rotorcraft are in operation. From the discussion in section 5.4, it appears that the same principle could most likely be applied to some hingeless rotorcraft types. The Lockheed design philosophy was different and led to an integrated mechanical feedback system (previously noted). The latest form, the AMCS, is discussed in more detail in section 6.1. In subsequent sections, lagged and proportional rotor tilting moment feedback, coning and normal acceleration feedback, and conventional hingeless rotor stability augmentation are treated.

6.1 Lockheed Gyro-Controlled Rotor

The system in its latest AMCS form can best be described as a full authority attitude gyro positioned in space by the pitch or roll rate command of the pilot. Figure 6.1 (taken from ref. 2.39) (except for the dashed feedback loop explained later) is a simplified block
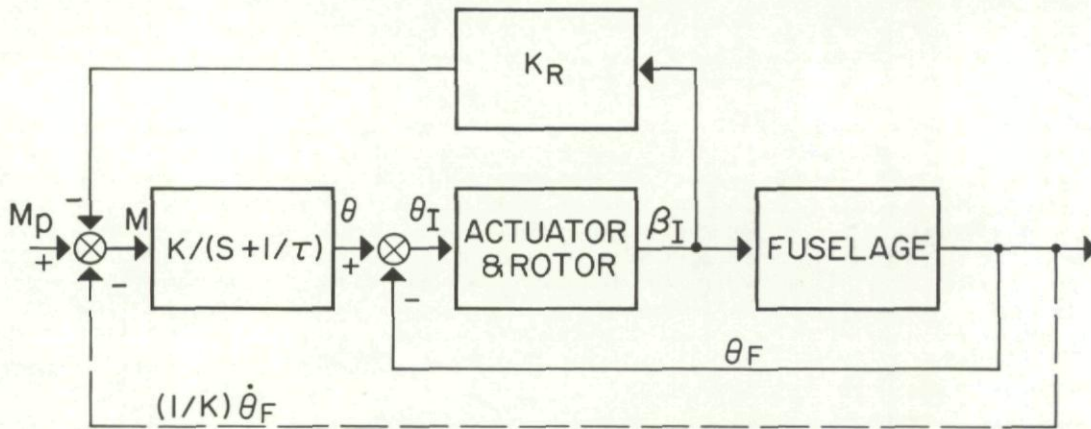

Fig. 6.1 Simplified block diagram for Lockheed AMCS.

diagram of the system for one axis. The pilot input moment M_p combines with the feedback moment from cyclic flapping $K_R \beta_I$ to produce the input moment to the floating gyroswashplate M:

$$M = M_p - K_R \beta_I \tag{6.1}$$

where K_R is the rotor feedback gain. The gyro acts as a first-order system with a lag τ. Its space-referenced attitude is given by

$$\theta = \frac{K}{s + (1/\tau)} M \tag{6.2}$$

The small term $1/\tau$ originates from the asymptotic alignment mechanism between gyroswashplate and fuselage, which can consist of either damping of the rotating gimbal axes or weak non-rotating centering springs. The difference between the gyroswashplate attitude and fuselage attitude is proportional to the cyclic pitch input θ_I as indicated in figure 6.1 by the fuselage feedback loop and where K_F is about 0.7.

$$\theta_I = K_F(\theta - \theta_F) \tag{6.3}$$

The cyclic pitch input θ_I is modulated by actuator and rotor dynamics to obtain the cyclic flapping β_I. For low-frequency response, one can set β_I proportional to θ_I:

$$\beta_I = A\theta_I \tag{6.4}$$

Cyclic flapping β_I is fed back as a gyroswashplate moment (eq. 6.1) and also produces (via fuselage dynamics) the fuselage attitude change θ_F. θ_F is subtracted from the gyro attitude, (eq. 6.3) so that the fuselage follows the attitude of the gyro which, in turn, is positioned by the pilot with the help of an attitude rate command (eq. 6.2). For zero fuselage aerodynamic damping, the asymptotic pitch or roll rate per unit stick deflection — that is, the control sensitivity — is determined only by the gyro dynamics and is independent of rotor dynamics. Because the aerodynamic damping of the fuselage increases with increasing flight speed, the control sensitivity decreases with flight speed since the pilot moment M_p must overcome both the gyro moment M and the feedback moment from cyclic flapping $K_R \beta_I$, which asymptotically is proportional to the fuselage damping moment. Within the validity of equation (6.4), the rotor has no influence on stability and control characteristics and these are exclusively determined by gyro and fuselage dynamics. This statement refers to the hub tilting moments that are the main source of hingeless rotorcraft attitude instability. Since rotor lift and drag forces contribute to handling qualities, they must be determined.

The rotor characteristics are also of no consequence with respect to the effects of gusts on the pitch or roll attitude since the rotor gust moments are alleviated by the gyroswashplate, at least for the lower frequency range. Since the gyroswashplate acts as a low-pass filter, the higher-frequency components of the gust spectrum are not alleviated. An analysis of the higher-frequency response requires

the use of rotor dynamics instead of equation (6.4). However, the low-frequency behavior is well represented by this equation. A necessary addition to the floating gyroswashplate system is a negative spring system applied to the swashplate to partially compensate the positive springs through which the pilot inputs are transferred to the swashplate. Without these negative springs, the gyro lag τ would be undesirable.

The effect of rotor characteristics can be eliminated not only with respect to the low-frequency dynamic control responses but also with respect to trim, which depends only on τ and the body trim moments. Trim values for the AH-56 AMCS are less than 1 inch of stick deflection between 0 and 200 knots, both for lateral and longitudinal control. Stick sensitivities in pitch decrease from 9°/sec/in. to 6°/sec/in. between 0 and 200 knots and are constant at 13°/sec/in. in roll. In wind-up turns, even at 200 knots, the stick deflection is only 1 in./g. There was no stick gradient reversal even up to the highest level tested — 2 g. The pitch-roll cross-coupling is zero.

No values for frequency and damping of the various flight dynamics modes have been published. Presumably, all modes are stable or almost stable. None of the numerous dynamic difficulties of the previous feathering feedback system were encountered, which must be attributed, in part, to the advantages of the flapping feedback system and to the experience gained in the development process. Since the AMCS has not been placed in production, the reliability of a floating swashplate positioned merely by the balance of various spring moments is questionable. However, the principle of emasculating the lifting rotor with respect to low-frequency pitching and rolling moments has been successfully demonstrated. This emasculation removes the flight dynamics problems of hingeless rotors associated with angle-of-attack instability, control oversensitivity, pitch-roll coupling, gust sensitivity, stick reversal, and pitch-up divergence and allows the designer to achieve desirable flight dynamics characteristics without knowledge of the rotor tilting dynamics. The equality of pitch and roll damping in hover, combined with a usually small roll/pitch inertia ratio, provides a shorter response time constant in roll than in pitch, which is desirable. Control power is substantial on the ground where the fuselage attitude is controlled more by ground contact than by the rotor, so that careful taxiing is required, as is the case with all hingeless rotorcraft. Autorotational landings with the AMCS have been studied analytically but not experimentally.

6.2 Lagged Rotor Tilting Moment Feedback

A design with almost all the flight dynamics characteristics of the Lockheed AMCS but which avoids the floating gyroswashplate is described in reference 2.88. The design can be explained with the help of figure 6.1. For small $1/\tau$, the dynamic system remains almost the same if the body attitude feedback loop (solid lines) is replaced by a body attitude rate feedback loop (dashed lines). The gyroswashplate can be omitted if the cyclic actuator is designed with lag τ. As described in reference 2.88, this system can be built with purely mechanical components. As in the Lockheed AMCS system, undesirable rotor tilt is removed to improve flying qualities. Control sensitivity does not depend on the rotor but only on the cyclic actuator, on the aerodynamic fuselage damping, and on the body attitude rate feedback gain. As flight speed increases, fuselage damping increases and control sensitivity in terms of asymptotic pitch or roll rate per unit control input decreases. For flight conditions with adequate fuselage damping, the attitude rate feedback is not required. However, in hover, the fuselage damping is almost zero and the desired control sensitivity must be obtained with body pitch and roll rate feedback since the rotor damping is removed by the rotor feedback.

Although it is not difficult to design an essentially rate-responsive cyclic actuator to replace the gyroswashplate in figure 6.1, a more conventional control system with a proportional cyclic servo is possible with the same characteristics as the Lockheed AMCS. The system in figure 6.1 with dashed feedback loop remains the same if the gyro dynamics are removed from the central signal path and substituted in three places: in the rotor feedback loop, in the body feedback loop, and as a feedforward system for pilot input. The system shown in figure 6.2 is obtained (see ref. 2.44). This electronic system can be used in parallel with a direct mechanical control system and can be disconnected if the system fails. Thus, there are purely mechanical or electromechanical feedback systems that use a conventional nonfloating swashplate to provide almost the same control dynamics as the Lockheed AMCS. If either essentially rate-responsive actuators or feedback and feedforward lags are used, such systems can effectively emasculate the rotor with respect to tilt and remove all the low-frequency, flight-dynamic problems of hingeless rotors. Similarly for the AMCS, the rotor dynamics need not be known to design for the desired flying qualities. It is sufficient to know the body dynamics. The horizontal tail does not have to compensate the rotor angle-of-attack instability but merely has to stabilize the fuselage.
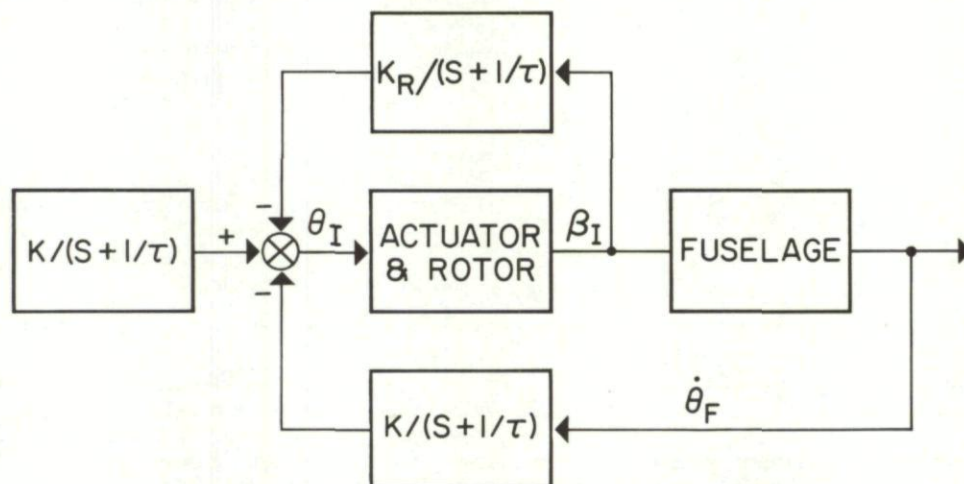

Fig. 6.2 Electromechanical control system equivalent to the Lockheed AMCS.

Although low-frequency flight dynamics can be determined for these feedback systems without knowledge of rotor tilt dynamics, lagged rotor tilting moment feedback does destabilize some high-frequency rotor modes. This problem was studied in references 2.85, 2.88, and in the review of reference 2.88. In figure 6.3 (taken from ref. 2.85), the solid lines are based on a linear Floquet type of analysis with periodic coefficients in the system equations and the dashed lines indicate a constant coefficient approximation. The advance ratio is 0.8, the blade number is 4, the blade Lock number is 8, the blade flapping frequency is 1.15Ω, and the constant chord rigid blades are flexibly hinged at the rotor center. The feedback equations with dimensionless time (time unit $1/\Omega$) are the same for
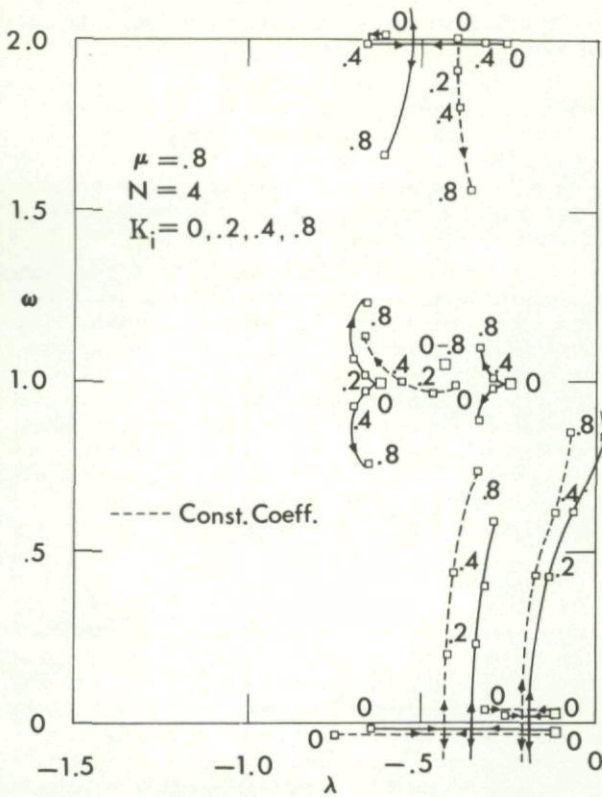
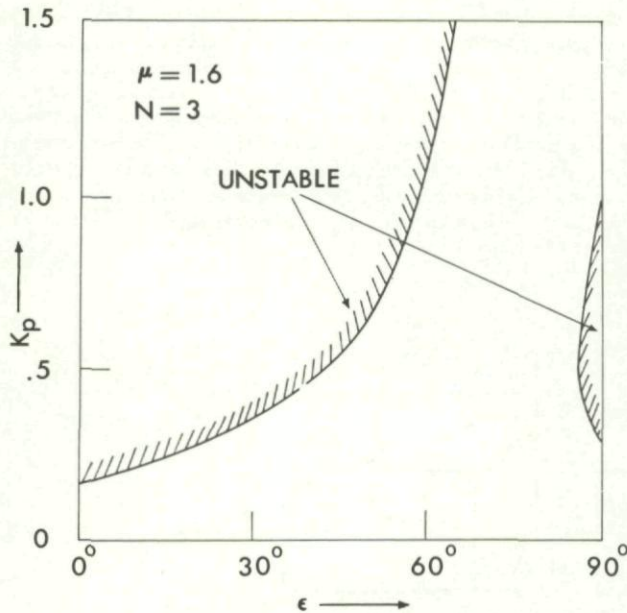Fig. 6.3 Effect of lagged rotor tilting moment feedback gain on characteristic values.

Fig. 6.4 Effect of cross-feedback phase angle on limiting gain for proportional rotor tilting feedback.

pitch and roll without cross-feedback:

$$\dot{\theta}_I + 0.1\theta_I = -K_i\beta_I$$
$$\dot{\theta}_{II} + 0.1\theta_{II} = -K_i\beta_{II}$$

(6.5)

where θ_I, θ_{II}, β_I, and β_{II} are forward and left cyclic pitch and cyclic flapping, respectively. The lag τ is 10 — the time for 1.6 rotor revolutions. The stability limit is reached for a feedback gain of K_i = 0.7. The unstable mode with frequency 0.8Ω has large coning and differential coning components. For three blades with the same characteristics, the maximum gain at the stability limit is somewhat smaller; however, the unstable mode is quite different and consists of a progressing flapping mode with a frequency of 1.5Ω and little coning. At a higher advance ratio, the gain limit becomes smaller and at an advance ratio of 1.6, it is only 0.17 for four blades and 0.28 for three blades. As shown in the review of reference 2.88, the gain limit drops rapidly with increasing blade Lock number when rotor damping is decreased, and it rises with increasing blade flapping stiffness. If coupled rotor/body dynamics are used rather than the fixed hub case of figure 6.3, some of the lower-frequency modes are changed in damping and frequency, while the higher-frequency modes remain approximately unchanged. Blade flexibility reduces the stability as shown in reference 2.82.

6.3 Proportional Rotor Tilting Moment Feedback

While the Lockheed floating gyroswashplate and the equivalent combination of lagged rotor tilting moment plus lagged pitch rate feedback essentially remove the effect of rotor characteristics on flight dynamics — except for the high-frequency response — proportional rotor tilting moment feedback merely modifies the rotor characteristics to make them more acceptable. If proportional cyclic flapping feedback is used without cross-feedback — fore and aft cyclic flapping is fed only into the longitudinal control and not into the lateral control and vice versa — the review of reference 2.88 (based on ref. 6.3) indicates that flapping instability occurs at low feedback gains. However, high gains can be reached with cross-feedback (ref. 2.85).

The following feedback equations are assumed:

$$\tau\dot{\theta}_I + \theta_I = -\beta_I K_p \cos \epsilon + \beta_{II} K_p \sin \epsilon$$
$$\tau\dot{\theta}_{II} + \theta_{II} = -\beta_I K_p \sin \epsilon - \beta_{II} K_p \cos \epsilon$$

(6.6)

Figure 6.4 (taken from ref. 2.85) refers to a three-bladed rotor with rigid blades flexibly hinged at the root having a natural flap frequency of 1.15Ω and a Lock number of 8 operating at an advance ratio of 1.6. For $\tau = 0$, the gain K_p at the stability limit is shown as a function of the feedback phase angle ϵ. For $\epsilon = 0$, the gain limit is low; the gain limit is high for $\epsilon = 60°$ to $80°$. Lag values τ typical of high-speed hydraulic servos have no substantial effect on the stability limit. Proportional rotor tilting moment feedback can alleviate the undesirable hingeless rotor characteristics such as angle-of-attack instability, control oversensitivity, pitch-up divergence, gust sensitivity, etc. Unlike the lagged tilting moment feedback, it does not require a body attitude rate feedback since rotor damping, though reduced, is still available. The hingeless rotor is merely conditioned and not completely emasculated as for the gyroswashplate or its equivalent lagged tilting moment system.

6.4 Coning or Normal Acceleration Feedback into Collective Pitch

Normal acceleration feedback into cyclic pitch was found to excessively destabilize the rotor coning mode (ref. 2.44). Coning feedback, which is almost identical to normal acceleration feedback into collective pitch, was proposed and studied in reference 6.4 and later applied to the McDonnell XV-1 compound helicopter. A very large gain of over 2 was used without encountering coning mode difficulties at conventional advance ratios. The feedback equations are

$$\tau\dot{\theta}_0 + \theta_0 = -K_0\beta_0 \qquad \text{coning feedback}$$
$$\tau\dot{\theta}_0 + \theta_0 = K_a(\dot{w} - q\mu) \qquad \text{acceleration feedback}$$

(6.7)

where w is the downward velocity; q, the nose-up pitch rate; and μ, the advance ratio. A body-fixed reference system is used. Both feedback systems substantially alleviate rotor angle-of-attack instability. However, high gains are possible only at moderate advance ratio. The coning feedback case shown in figure 6.5 (taken from ref. 2.85) is valid for the same hingeless rotor as in figure 6.4 for $\tau = 0$. The limiting gain is much smaller than for proportional rotor tilting feedback. For a four-bladed rotor, the limiting gain drops still

further. The conclusion is then that coning or normal accelera-tion feedback into collective pitch is feasible at high gains for moderate advance ratios but only small gains can be used at high advance ratios.

The Westland Lynx helicopter has a normal acceleration feedback into collective pitch of about $2.7°$ per g with a lag time of about 0.1 second which increases the speed for acceptable operational pilot workload in turbulent conditions from 120 to 165 knots (ref. 2.3). As mentioned previously, this feedback system is considered to be an integral part of the controls. Combining coning feedback into collective pitch and proportional rotor cyclic flapping feedback into cyclic pitch is equivalent to delta three pitch-flap coupling for $\epsilon = 90°$, $K_p = K_0$, $\tau = 0$ [Eqs. (6.6) and (6.7)]. This will provide good flapping stability even at high advance ratio unless the blade is too soft in torsion and too near the reverse-flow torsional divergence limit (ref. 2.84). When this type of combined feedback is used, a phase angle somewhat less than $90°$ provides even better stability, as was the case for proportional tilting feedback shown in figure 6.4.

6.5 Conventional Stability Augmentation Applied to Hingeless Rotorcraft

Tests with Bell Model 583 with a four-bladed hingeless rotor have shown that a conventional SAS can improve the flying qualities of hingeless rotorcraft. Similar observations were made with the Westland Lynx helicopter. However, no quantitative, analytical, or flight-test results of the effectiveness of an SAS have been published for either of these hingeless helicopters. The Lockheed hingeless rotorcraft were always flown with the gyroswashplate system — considered to be an improvement over SAS. Analytical results for the effects of stability augmentation on the AH-56A without the gyroswashplate system are given in reference 2.44 and are

Fig. 6.5 Effect of coning feedback gain on characteristic values.

reviewed briefly here. The analysis included the effects of the regressing, progressing, and coning modes of the rotor. A linear constant coefficient analysis was performed, including a variety of body feedback laws and parameters. The speed range from zero to 200 knots was covered. The results are given in terms of root locus plots for the various flight dynamics modes.

As explained in section 5.4, a fully coupled analysis using the three basic rotor modes yields a complex conjugate pair of roots for the advancing blade flapping mode and one pair for the collective flapping mode. The regressing blade flapping mode combines with the body modes to yield a complex conjugate pair for the short-period pitch mode, and another for the short-period roll mode. Three more roots remain for the longitudinal modes — one complex conjugate pair for the phugoid and one real root — and three more roots for the lateral-directional modes — one complex conjugate pair for the dutch roll mode and one real root for the spiral mode (a total of 14 roots). In the upper speed range, the AH-56A without feedback would have (according to ref. 2.44) a pitch divergence, a stable phugoid, and a short-period pitch mode.

For pitch response, the main problem the feedback system must solve is to remove the pitch divergence at high flight speed without destablizing the phugoid and short-period pitch modes. At 200 knots, rate feedback alone cannot remove the pitch divergence. Attitude feedback alone can stabilize the pitch divergence but it destabilizes the phugoid. Therefore, a combination of rate and attitude feedback is required to obtain a stable real root and stable phugoid. The values selected are an attitude feedback of 12 in. stick/rad and a rate feedback of 6 in. stick/rad/sec, which results, at 200 knots, in a pitch convergence, a highly damped phugoid with a damping ratio of 0.68 (increased from 0.4), and a short-period pitch mode for which the damping ratio is reduced from 0.9 to 0.6. If a lagged pitch rate feedback is used instead of the attitude feedback, the pitch divergence cannot be completely removed; however, a lag time of 10 seconds gave a time to double amplitude of about 24 seconds.

While the selected feedback gave satisfactory roots, an excessive g response at high speed occurred, which would require, for example, airspeed scheduling of the pitch rate feedback. If the pitch rate feedback is replaced by lagged cyclic flapping feedback in accordance with figure 6.2, the control sensitivity is automatically reduced with increasing flight speed bacause of the increasing body damping (as explained earlier). No excessive g response at high speed is then obtained. Note that this characteristic is peculiar to the AH-56 where the fixed wing generates most of the lift at high speed. Except for the excessive g response and some control problems after ground contact, a pitch rate plus pitch attitude or lagged rate feedback appears to achieve satisfactory handling characteristics of a hingeless helicopter up to high flight speeds. The development of a simple automatic flight-control system for the BO-105 helicopter is discussed in reference 6.5.

7 ANALYTICAL MODELING TECHNIQUES

In chapter 3, a hierarchy of dynamics concepts was discussed, beginning with the isolated blade and ending with the complete rotor-body dynamic system. In this chapter, additional details of the analytical modeling of hingeless rotorcraft are presented, encompassing both structural and aerodynamic modeling. The term "analytical modeling" refers to the process of establishing the system equations. The solutions of these system equations are discussed in chapter 8.

7.1 Structural Modeling with Rigid Blades

The following equations are the basis of the air resonance analysis for the Bolkow BO-105 hingeless rotor helicopter, results of which are presented in reference 2.15. The analysis was originally limited to zero forward velocity, but was extended to include forward flight conditions.* In the Vertol C-56 form presented here, the elastic blades are represented by rigid blades hinged sequentially hub
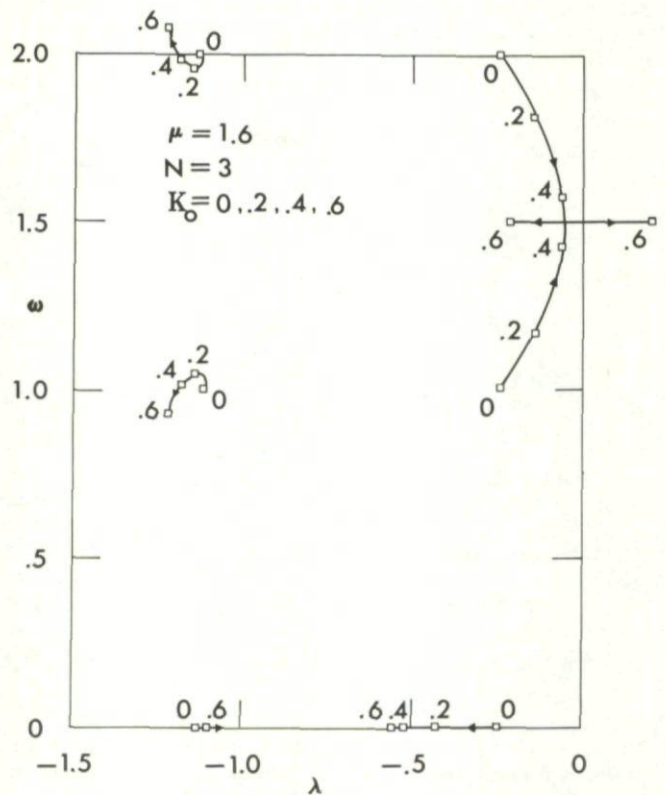
---

*The author is indebted both to the Boeing Vertol Company and to Messerschmitt-Boklow-Blohm, GmbH, for the basic equations for the Vertol C-56 and the MBB Blama programs, respectively.

outward by a feathering hinge, a flapping hinge, and a lead-lag hinge, all elastically restrained. The analysis at MBB (ref. 2.10) assumes an additional outboard torsional hinge, also elastically restrained, to approximate the torsional blade deflections (see fig. 4.3). The system used at MBB is shown in figure 7.1 (taken from ref. 2.10). The rotor support is considered elastically attached to the body. The MBB program, called "Blama" (blade-mast program), accepts up to 35 degrees of freedom: 6 for the body, 5 for the mast (excluding yaw), and 4 per blade for up to 6 blades. The model includes precone, prelead, pitch-lead, pitch-flap, and flap-lead couplings. Reference 2.15 also considered empennage degrees of freedom, which did not produce air resonance in the operational rotor speed range. Elastic pylon modes were not important for the air resonance problem of the BO-105 helicopter and are omitted.

An inertial reference system has been used, although a body-fixed reference system is more practical, since it reduces the number of degrees of freedom and allows a more direct application of wind-tunnel test results. The analytical model in its nonlinear form can be used for time history programs; in its linear form, it can be used for eigenvalue determination. Although originally developed for air resonance computations, in its extended form it is also applicable to general flight dynamic analyses. At MBB, the linear flight dynamic analysis was performed by extracting aerodynamic derivatives from the Blama model, which were then used in a conventional derivative analysis. A more accurate procedure presently being pursued is to use the complete linearized Blama program for the flight dynamic analysis without first computing the derivatives. A similar linearized program of this form has been successfully applied to hingeless rotor flight dynamic studies at Lockheed (ref. 2.37).

Fig. 7.1 System used for MBB "Blama" program.

The rigid blade is represented by mass elements dm_b with the deflection vector:

$$x_b = x + \Phi_x \Phi_y \left(x_R + \Psi \left| x_\theta + \Theta [x_\beta + B(x_\zeta + Zr)] \right| \right) \quad (7.1)$$

The vector x is the deflection of the total aircraft c.g. The vector x_R positions the rotor center with respect to the aircraft c.g, vector x_θ positions the feathering hinge with respect to the rotor center, vector x_β positions the flapping hinge with respect to the feathering hinge, vector x_ζ positions the lead-lag hinge with respect to the flapping hinge, and vector r positions the blade mass element with respect to the lead-lag hinge. The deflection of the fuselage c.g. is

$$x_f = x + \Phi_x \Phi_y x_o \quad (7.2)$$

Vector x_o positions the fuselage c.g. with respect to the total aircraft c.g. The transformations in equation (7.1) before linearization are

Fuselage roll and pitch:

$$\Phi_x = \begin{bmatrix} 1 & 0 & 0 \\ 0 & \cos\phi_x & -\sin\phi_x \\ 0 & \sin\phi_x & \cos\phi_x \end{bmatrix}, \Phi_y = \begin{bmatrix} \cos\phi_y & 0 & \sin\phi_y \\ 0 & 1 & 0 \\ -\sin\phi_y & 0 & \cos\phi_y \end{bmatrix} \quad (7.3)$$

Rotor rotation:

$$\Psi = \begin{bmatrix} -\sin\psi & -\cos\psi & 0 \\ \cos\psi & -\sin\psi & 0 \\ 0 & 0 & 1 \end{bmatrix} \quad (7.4)$$

Feathering:

$$\Theta = \begin{bmatrix} \cos\theta & 0 & -\sin\theta \\ 0 & 1 & 0 \\ \sin\theta & 0 & \cos\theta \end{bmatrix} \quad (7.5)$$

Flapping:

$$B = \begin{bmatrix} 1 & 0 & 0 \\ 0 & \cos\beta & \sin\beta \\ 0 & -\sin\beta & \cos\beta \end{bmatrix} \quad (7.6)$$

Lead-lag:

$$Z = \begin{bmatrix} \cos\zeta & \sin\zeta & 0 \\ -\sin\zeta & \cos\zeta & 0 \\ 0 & 0 & 1 \end{bmatrix} \quad (7.7)$$

With the fuselage angular velocity A_f, the system kinetic energy T is

$$2T = \int dm_b \, \dot{x}_b^T \dot{x}_b + \dot{x}_f^T M_f \dot{x}_f + A_f^T I_f A_f \quad (7.8)$$

which is to be integrated over all blades; M_f and I_f are the fuselage mass and moment of inertia matrices. The system potential energy is

$$2V = \Sigma (K_\zeta \zeta^2 + K_\beta \beta^2 + K_\theta \theta^2) \quad (7.9)$$

to be summed over all blades; K_ζ, K_β, and K_ϕ are the spring rates for the lead-lag, flapping, and feathering hinges, respectively. The equations of motion can now be derived from the Lagrange equations:

$$\frac{d}{dt}\left(\frac{\partial T}{\partial \dot{q}_i}\right) - \frac{\partial T}{\partial q_i} + \frac{\partial V}{\partial q_i} = Q_i \quad (7.10)$$

where q_i represents one of the blade coordinates ϕ, β, or ζ for each blade or one of the body coordinates described by the linear and angular deflection vectors of the rigid body. The rates $\dot{x}_b$ and $\dot{x}_f$ in equation (7.8) are obtained by differentiating equations (7.1) and (7.2) with respect to time, which introduces (through to eqs. (7.3) to (7.7)) the rates $\dot{q}_i$ of the blade and fuselage coordinates for which equation (7.8) must be differentiated. The generalized forces Q_i are obtained by first establishing the aerodynamic forces ΔF on a blade element, then transforming to the inertial system by

$$\Delta F_{in} = \Phi_x \Phi_y \ \Psi \Theta BZ(\Delta F) \tag{7.11}$$

from which

$$\Delta Q_i = \Delta F_{in} \frac{\partial x_b}{\partial q_i} \tag{7.12}$$

which must be summed over the blade elements. In addition, the body aerodynamic contributions must be considered for forward flight. If individual blade coordinates for all blades are used, the analysis covers also the reactionless modes. If multiblade coordinates are used for only the regressing, advancing, and collective modes, as in the Vertol C-56 program, the analytical effort is reduced, but reactionless modes are excluded. Some additional comments on multiblade coordinates are made later.

7.2 Structural Modeling with Elastic Blades

Compared to the rigid blade analysis discussed in the previous section, the structural blade representation can be improved by introducing along the blade span further spring-restrained feathering, flapping, and lead-lag hinges with interconnecting rigid blade portions. The deflection of the rigid inboard blade section is given by equation (7.1). The deflection of the next blade section would include new transformations Θ_1, B_1, and Z_1 with new coordinates θ_1, β_1, and ζ_1, which would also appear in equation (7.9). The time rates of the new coordinates would appear in equation (7.8). Thus, in an N-bladed rotor, each additional rigid blade section would require 3N additional coordinates and their rates and associated transformations given by equations (7.5), (7.6), and (7.7). Such a finite-element representation of rotor-body dynamics has not been developed to date.

At zero forward speed where the aerodynamic blade damping is constant, one could extract from a linearized finite-element analysis the eigenvalues and natural modes characterized not only by the amplitudes but also by the phase angles at each blade station. One could then perform a modal type of rotor-body dynamic analysis with damped blade modes. However, the usual method is to perform a modal analysis with the blade natural modes in a vacuum, that is, without aerodynamic damping. For undamped natural modes, all portions of the blade oscillate with the same phase. While actual phase differences along the span are small for the modes with low damping (such as the lead-lag modes), the torsion mode, and the higher flap-bending modes have considerable damping and will show some phase differences between the oscillations of the inner and outer blade portions. When undamped modes are used in a modal analysis, the aerodynamic effects produce not only damping of each mode, but also intermode coupling that results in new damped modes with phase shifts along the blade span.

The advantage of the modal type of analysis is that, for forcing functions of mainly low-frequency content, as they occur in flight mechanics, the higher modes can be neglected and only the first few modes retained. If only flap bending is considered, the deflection mode $y(x,t)$ is represented by the infinite series:

$$y(x,t) = \sum_{j=1}^{\infty} \eta_j(x)\beta_j(t) \tag{7.13}$$

where $\eta_j(x)$ is the deflection of the jth undamped mode and $\beta_j(t)$ is the corresponding generalized coordinate. Because of the orthogonality relation,

$$\int \eta_i \eta_j \ dm = 0 \tag{7.14}$$

one obtains, from equation (7.13),

$$\beta_i(t) = \int y(x,t)\eta_i dm / \int \eta_i^2 \ dm \tag{7.15}$$

The $y(x,t)$ are relative deflections in a rotating frame and must be transformed into absolute deflections by a series of transformations such as in equation (7.1). The generalized coordinates $\beta_j(t)$ now replace the flapping angle β of the preceding section. Kinetic energy, potential energy, and the generalized forces contain spanwise intergrals where the modal deflections $\eta_j(x)$ and their slopes occur as factors.

The question of how many modes are required in an adequate structural elastic blade representation is a difficult one. The number will be smaller when more of the structural details are considered in the determination of the mode shapes. It was found in reference 2.82 that using mode shapes of the nonrotating blade leads to larger truncation errors of the series equation (7.13) than using mode shapes of the rotating blade. The experience at Lockheed shows that a very exact structural representation of the blade root is important so that the natural modes include the proper couplings between feathering, lead-lag, and flap elastic deflections (ref. 2.37 and 2.40). Usually, two flap-bending modes, two lead-lag-bending modes, and one torsional elastic blade mode are used, including the effects of rotation and all elastic and inertial coupling effects. For flight dynamics analyses, one elastic flap-bending mode may be adequate in many cases (ref. 2.82), where several hingeless rotor hub moment derivatives computed with one and two flap-bending modes are compared for two types of blades and for advance ratios of 0.8 and 1.6.

When two flap-bending modes are used, reference 2.82 shows that neglecting the aerodynamic intermode coupling (as in ref. 2.80) can lead to substantial errors in the rotor derivatives, particularly with respect to trim. Such errors can be larger than those which occurred when the entire second mode was omitted. With normal modes, it is important to truncate the mathematically infinite series so that only the aerodynamic terms associated with the neglected higher-mode deflections are omitted, but not any other aerodynamic terms. For example, the truncation of the series for the elastic hub moment leads to unnecessary errors. (see refs. 2.80 and 2.82). In the computation of the undamped blade modes, a finite-element method is used with a large number of elements — typically 20 to 30 per blade — whereby the transfer matrix method for proceeding from one element to the next is a useful tool (see, e.g., ref. 3.2). As indicated in references 2.75 and 2.82, the rigid-blade flight dynamic analysis is adequate up to an advance ratio of about 0.4. For advance ratios up to 0.8, the elastic first mode should be used. Beyond an advance ratio of 0.8, the second elastic blade mode becomes increasingly important. These conclusions were drawn for the substall region. In the partial rotor stall regions, the elastic blade modes probably should be considered earlier.

7.3 Aerodynamic Airfoil Modeling

As for articulated and teetering rotors, hingeless rotor flight dynamics are usually based on quasisteady airfoil data. Compressibility and stall effeccs are also considered. While unsteady aerodynamics is not important for flight dynamics studies in the

unstalled regime, the use of steady-state airfoil stall data leads to a considerable error in underpredicting the lifting capability of the rotor. When the angle of attack increases rapidly, airfoils generate substantially higher maximum lift than during slow changes in angle of attack. There is also the phenomenon of so-called "moment stall," which consists of changes in airfoil aerodynamic moments that precede "lift stall." The literature on unsteady airfoil stall is growing rapidly. A complete theory of this phenomenon does not yet exist, but there are empirical methods, based on oscillating airfoil measurements which attempt to account for dynamic stall in the aerodynamic analysis of lifting rotors. Reference 7.1 is a recent example of this type of work; reference 7.2 attempts to establish the causes for dynamic stall in the boundary layer; and reference 7.3 summarizes the work on dynamic airfoil stall.

In testing the validity of the assumptions, the rotor wake downwash problem discussed in the following section adds to the unknowns and a high degree of sophistication is required in the experimental methods to even attempt to separate airfoil phenomena from wake phenomena. The hingeless rotor shares all these problems with articulated and teetering rotors and it is beyond the scope of this report to more than mention these problems. In practice, not only good data on the characteristics of the selected airfoil are needed, but an airfoil design must represent a good overall compromise of conflicting requirements. Reference 7.4 reviews the airfoil design methods presently available. Reference 7.5 reports on the development of a cambered airfoil for the Westland Lynx helicopter.

While there are still considerable gaps in the aerodynamic airfoil modeling of lifting rotors for high lift operating conditions, the high advance ratio, low-lift flapping dynamics typical of winged or compound helicopter rotors can be accurately modeled with only a linear aerodynamic representation. The only airfoil data necessary are the lift-curve slopes for normal and reversed-flow conditions. Although this concept has been used earlier (ref. 7.6), it has been formalized and prepared for easy application in reference 2.55, based on an elastically restrained, centrally hinged rigid-blade model. The concept has been extended to include blade torsion in reference 2.52 and blade flexibility in reference 2.82. The approximate validity of the concept not only for steady flight conditions but also for responses to harmonic control inputs with and without hub tilting moment feedback has been demonstrated in low-lift, wind-tunnel tests with a 7.5-ft hingeless rotor model (refs. 2.43, 2.45, 2.46 and 2.48). Wake downwash and blade elastic effects were omitted in the comparisons with tests and according to reference 2.75, these effects were not always negligible. Nevertheless, the simple aerodynamic modeling with a linear airfoil lift slope, both in normal and reversed flow, appears to be quite adequate for flapping dynamics up to the highest advance ratios if stall in major disk areas is absent and if some corrections for wake and blade elasticity effects are made. Compressibility effects could be included by modifying the linear lift slopes in the affected regions without destroying the linear character of the analysis. The theory of reference 2.55 (as extended in refs. 2.52 and 2.82) yields only rotor lift and hub moments, but yields no rotor horizontal forces which are needed for a complete flight dynamics analysis including phugoid and dutch roll modes.

The simple relations that can be obtained even at a high advance ratio with linear lift-slope airfoil modeling are based on the blade flapping equation in a rotating reference system (time unit $1/\Omega$):

$$(2/\gamma)\ddot{\beta} + C(\psi)\dot{\beta} + [2P^2/\gamma + K(\psi)]\,\beta = \lambda m_\lambda(\psi) + \Theta m_\Theta(\psi) \qquad (7.16)$$

where γ is the blade Lock number; P, the fundamental blade flapping frequency; λ, the inflow velocity, positive up (velocity unit ΩR); and θ, the blade pitch angle. The four functions of azimuth angle ψ in equation (7.16) are given in reference 2.55. The hub moment coefficient (positive down) in the rotating reference system is

$$C_M/a\sigma_1 = -(1/\gamma)(P^2 - 1)\beta \qquad (7.17)$$

The pitching and rolling moment coefficients are

$$\begin{aligned} C_m/a\sigma &= C_{Mc}/2a\sigma_1 \\ C_\ell/a\sigma &= C_{Ms}/2a\sigma_1 \end{aligned} \qquad (7.18)$$

where a is the airfoil lift slope; σ_1, the solidity ratio of one blade; σ, that of all blades; and C_{Mc} and C_{Ms}, the cosine and sine components of C_M. While this simple airfoil modeling, preferably with wake and blade elasticity corrections, is adequate for coupled rotor-body dynamics, the inclusion of inplane blade dynamics requires airfoil drag data. The importance of stall for the stability of the coupled flap-lag blade motions was mentioned previously.

7.4 Aerodynamic Wake Modeling

Aerodynamic wake modeling is a problem that articulated and teetering rotors have in common with hingeless rotors, although the hingeless rotor is more sensitive to errors in inflow modeling.

For articulated rotors, uniform downwash from momentum theory was usually adequate in flight dynamics studies except for the low-speed regime when it led to sizeable errors in lateral flapping. Nonuniform downwash was mainly of interest as a contributing source of rotor vibrations. For hingeless rotors, however, wake nonuniformity contributes substantially to flight dynamic problems. It affects control and other derivatives and can influence the stability of the blade inplane motion. It is beyond the scope of this report to review the large and rapidly growing literature on rotor wake investigations, and only a few comments are made. There are four sources for wake modeling: momentum theory, vortex or potential theory, wake measurements, and indirect determination of wake characteristics from rotor responses. For teetering or articulated rotors with zero or small hub moments, axial momentum balance is of prime importance. For uniform disk loading and steady forward flight, a proportional relation between uniform inflow and rotor lift increments is obtained. Extending this concept to hingeless rotors requires an additional angular momentum balance about the longitudinal and lateral axes. If a first harmonic inflow distribution is assumed,

$$\lambda_i = \lambda_o + \lambda_s \sin\psi + \lambda_c \cos\psi \qquad (7.19)$$

one obtains, after linearization, the following relations between inflow coefficient increments and rotor thrust and moment coefficient increments in hover (ref. 2.75):

$$\left. \begin{aligned} \Delta\lambda_o &= \Delta C_T/4\lambda_o \\ \Delta\lambda_s &= -\Delta C_\ell\,3/4\,\lambda_o \\ \Delta\lambda_c &= -\Delta C_m\,3/4\,\lambda_o \end{aligned} \right\} \qquad (7.20)$$

For forward flight, one obtains

$$\left. \begin{aligned} \Delta\lambda_o &= \Delta C_T/2\mu \\ \Delta\lambda_s &= -\Delta C_\ell\,3/2\mu \\ \Delta\lambda_c &= -\Delta C_m\,3/2\mu \end{aligned} \right\} \qquad (7.21)$$

In a more refined, steady-state momentum theory, the momentum balance is written for a small portion of the rotor disk and is combined with the blade element lift expression. Then a nonuniform inflow distribution associated with nonuniform disk loading is obtained over both the rotor radius and the azimuth angle. For hover, the inflow is zero in the center of the rotor and maximum at the blade tip. The theoretical inflow distribution compares well with measured time averages of inflow.

A combined momentum and blade element theory, that yields both the blade loads and the nonuniform inflow distribution was developed in reference 2.37 for high advance ratios. The theory is based on the linear lift-slope assumption both for normal and reversed flow. The participating air volume is that of the sphere with radius BR. This volume is uniformly distributed over the disk which results in the height of the participating air cylinder of (4/3)BR (B is the tip loss factor). The theory has not yet been checked against tests but the mean inflow is the same as for the classical momentum theory.

Most of the recent rotor wake analyses use discrete vortex element representations. For determining low-frequency blade response, the older models are not necessarily less accurate than the newer ones. In Reference 7.7, lateral flapping of articulated rotors at low advance ratios was best represented by use of the wake data of reference 7.8. In reference 7.9, this type of early vortex theory is extended and compared with tests for a teetering rotor at advance ratios of 0.09 to 0.23. The Lockheed Rexor program uses an inflow model based on these data (ref. 2.37). A review of modern work on rotor wakes is given in reference 7.10. A free wake analysis for hover is described in reference 7.11. Such an analysis is oversophisticated for use in flight dynamics. A rather simple vortex wake analysis for which all shed and trailed vorticity is located in the horizontal plane behind the rotor is developed in reference 7.12,

Flight dynamics analyses are often performed with an inflow distribution that is uniform in the lateral direction and trapezoidal in the longitudinal direction, the rear portion of the rotor disk experiencing the larger downwash. The mean value of the inflow is determined from axial momentum balance. The MBB Blama program uses this inflow model. Lockheed experience shows that the stability of the regressing inplane blade mode is substantially affected by the fore and aft nonuniformity of the inflow distribution. Boeing-Vertol also found that air resonance stability limits for the BO-105 helicopter varied substantially with nonuniform inflow.

The rotor wake is very complex and is not yet fully understood even for steady flight conditions. In flight dynamics, however, the wake for unsteady conditions is required, and very little information is available on this subject. A distinction should be made between unsteady wake effects or transient downwash dynamics and unsteady airfoil aerodynamics, as developed for a lifting rotor in reference 7.13. In reference 7.13, the vorticity shed from the oscillating blade is assumed to be embedded in a uniform wake of the hovering rotor. The theory predicts (and has been confirmed experimentally) blade flutter at low lift, which usually disappears with increasing collective pitch. The theory has been extended to forward flight conditions. Reference 7.14 is a recent review of rotor unsteady aerodynamics; however, most of this work is limited to high-frequency flutter phenomena and is not applicable to flight-dynamic problems.

An early nonsteady rotor wake model for hover, based on apparent mass momentum theory, is given in reference 7.15; this theory correlates well with measured full-scale rotor responses to rapid collective pitch inputs. The air volume participating in the acceleration is assumed to be a cylinder of 0.85 radius height — the theoretical value obtained for an impermeable, axially accelerated, circular disk. A similar concept has been applied to hingeless rotor tilting motions in reference 7.16 and correlated with the model test results presented in reference 2.83. The nonsteady inflow is described by adding rate terms to equation 7.20:

$$\left.\begin{aligned} \Delta\lambda_o + \tau_o\Delta\dot{\lambda}_o &= \Delta C_T/4\lambda_o \\ \Delta\lambda_s + \tau\Delta\dot{\lambda}_s &= -\Delta C_\ell \, 3/4 \, \lambda_o \\ \Delta\lambda_c + \tau\Delta\dot{\lambda}_c &= -\Delta C_m \, 3/4 \, \lambda_o \end{aligned}\right\} \qquad (7.22)$$

This process is equivalent to passing the quasisteady wake components through a low-pass filter, a procedure used in such global programs as the Bell C-81 and the Lockheed Rexor (as noted, e.g., in ref. 2.40). The filter time constants τ_o and τ should be determined either from theory or test results. Such results are available for a hingeless rotor model in references 2.43 and 2.45, although only for low-lift conditions. The time constants change substantially with rotor lift.

Hingeless rotor flapping amplitudes in response to cyclic pitch inputs are strongly influenced by the wake (as shown in fig. 7.2 taken from ref. 2.83). The absolute value of the flapping amplitude per unit cyclic pitch amplitude is plotted versus the progressing or regressing cyclic pitch excitation frequency. The solid line represents flapping without inflow; the dashed line represents the measured flapping amplitude. The advance ratio is zero, collective pitch is 5°, the blade flapping natural frequency is 1.2Ω, and the blade Lock number is $\gamma = 4.0$. For a steady cyclic pitch input, the inflow reduces flapping and thereby the control power to 63%. This reduction was predicted, for example, in references 5.7 and 2.80, and it was shown that it can be analytically represented by a reduction in blade Lock number. Not previously recognized was the amplification of the flapping response by the inflow at a low cyclic pitch regressing frequency. This phenomenon gradually disappears as the flapwise blade stiffness is reduced.

Both steady and unsteady rotor wake phenomena exert a substantial influence on hingeless rotorcraft, particularly in low-speed flight, and wake effects are not yet completely understood.

Fig. 7.2 Effect of aerodynamic wake on hingeless rotor flapping amplitude in hover.

8 MATHEMATICAL ANALYSIS TECHNIQUES

Because of their novelty and their greater potential for instabilities, hingeless rotors have stimulated the development of certain analysis techniques.

8.1 Nonlinear Modeling

Nonlinearities in the equations of motion originate in aerodynamic, inertial, and structural effects. Especially for hingeless rotors, the structural nonlinearities are significant and can cause instabilities of the coupled flap-lag-torsion blade motions. If nonlinear terms are retained, the system of nonlinear equations must be solved by numerical integration. The analysis is accomplished in three steps: (1) trim analysis, (2) time history after a disturbance, and (3) data processing to evaluate damping of critical modes. For trim analysis, the system is usually simplified by omitting individual blade degrees of freedom and by assuming that all blades perform the same motion as a function of azimuth angle.
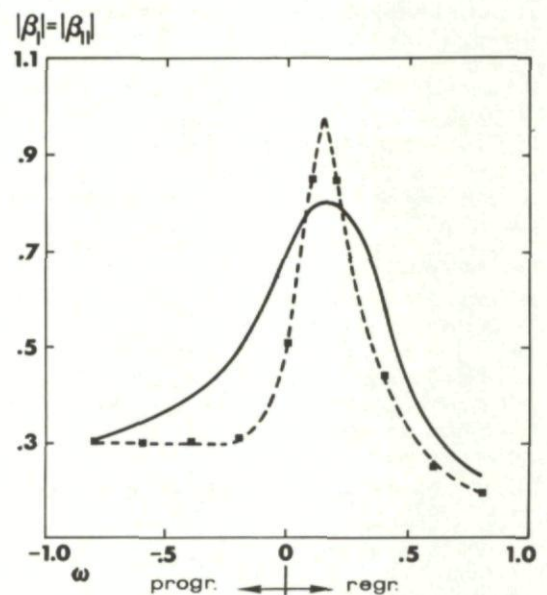
The blade motion is periodic with a frequency equal to the rotor rotational frequency. When the desired trim state is achieved, the response to a certain input is computed, usually with a Runge-Kutta routine applied to a state variable form of the equations (containing only first-order time derivatives).

Success in interpreting the time history depends on the selection of the input. To determine the damping of a certain mode, if the natural frequency of this mode is known, a good input would excite this mode for several oscillations. Observation of the decay of the oscillations, after discontinuing the input, would provide the desired damping information. Figure 8.1 (taken from ref. 2.10) shows the computed time history of the BO-105 helicopter after periodic roll excitation at the frequency of the air resonance mode. As explained in section 5.1, at the operational rotor speed of the BO-105 helicopter, there are two modes with approximately the same natural frequency: the highly damped roll mode with lightly coupled blade inplane motion and the lightly damped regressing inplane mode with lightly coupled body roll motion. Figure 8.1 shows the rapid decay of the body roll mode (second curve from the top) and the slow decay of the inplane mode (fourth curve) taken in the rotating reference system. Total flapping and total blade pitch amplitude are little affected by roll excitation or its discontinuation. Figure 8.1 also shows the rapid buildup of both body roll and lead-lag motion after the periodic lateral cyclic pitch input begins. The responses of figure 8.1 do not exhibit recognizeable nonlinear behavior, although they are the results of a nonlinear analysis. The responses would be quite similar for a linearized analysis that treated perturbations from a trim condition.
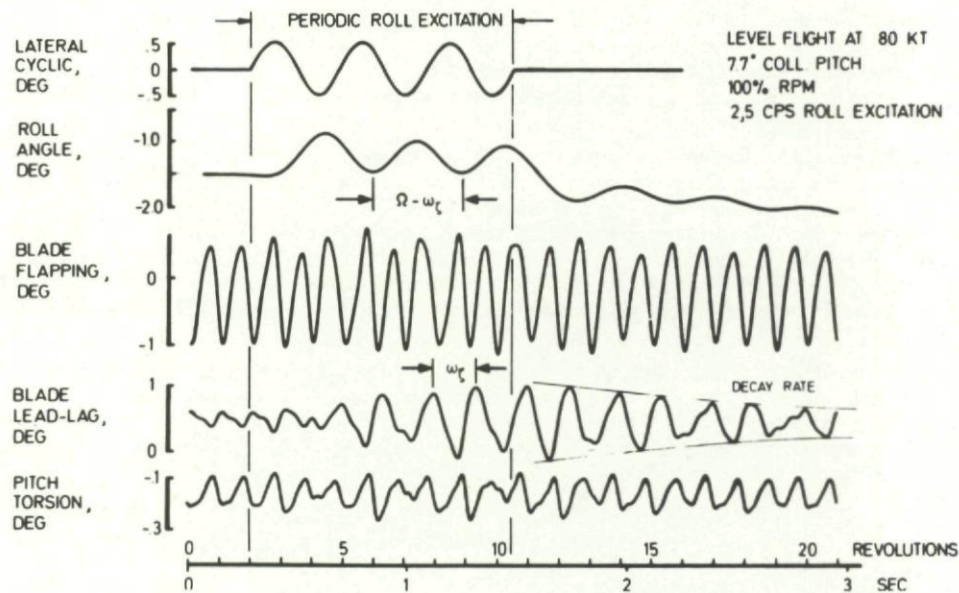
Fig. 8.1 Time history after periodic roll excitation with frequency of air resonance mode.

Usually, time histories from nonlinear models are not as easy to interpret as those in Figure 8.1, where only two quite different modes were properly excited near their natural frequency. The regressing inplane mode was also easily detectable because of its low damping. Identifying other modes and their frequencies and damping from time histories is often difficult. A method used to separate the transient of the reactionless inplane mode from the general blade response is described in reference 2.38. The response is first subjected to a fast Fourier transform that allows the determination of the frequency of the mode under study. The response is then Fourier analyzed with this frequency as base frequency, with the higher Fourier series terms omitted. The time block for this Fourier analysis is shifted several steps along the time axis, resulting in an amplitude decay with time from which the damping of the mode can be determined. The method called "moving block peak plot" is applicable to time histories of transients obtained either with a mathematical model or from experimental measurements.

Another approach to this problem is to linearize the nonlinear system at a given trim condition and determine frequencies, damping, and mode shapes from the linear perturbation equations. For example, the Lockheed Rexor program in its "fly" mode, that is, after trim is established, has an option available to perturb all 30 dynamic degrees of freedom at any azimuth position to obtain periodic coefficients for a linear system of equations, (see ref. 2.37). Mathematical analysis techniques for linear models are discussed in section 8.3.

8.2 Multiblade Coordinates

Most global programs, such as the Lockheed Rexor, the Bell C-81, and the MBB Blama, use individual blade coordinates. An exception is the Boeing-Vertol C-56 program (Sec. 7.1) that introduces (for a four-bladed rotor) the three multiblade coordinates of longitudinal and lateral rotor tilt and coning. If only time histories are required, from numerical step-by-step integration, multiblade coordinates would probably offer no particular advantage except possibly to reduce the computation effort. However, in a linearized system of equations which allows the determination of natural frequencies, damping, and mode shapes, the use of multiblade coordinates can substantially simplify the mathematical model. Multiblade coordinates also make it easier to identify the multiblade modes described in section 3.2.

The transformations between individual blade coordinates, β_k, and multiblade coordinates β_0, β_I, β_{II}, ... are given by (see ref. 2.85)

$$\beta_k = \beta_0 + \beta_I \cos \psi_k + \beta_{II} \sin \psi_k + \beta_{III} \cos 2 \psi_k + \beta_{IV} \sin 2 \psi_k + \ldots, k = 1, 2, \ldots, N \tag{8.1}$$

with the inverse,

$$\left.\begin{array}{l} \beta_0 = (1/N) \sum_{k=1}^{N} \beta_k, \quad \beta_I = (2/N) \sum_{k=1}^{N} \beta_k \cos \psi_k, \quad \beta_{II} = (2/N) \sum_{k=1}^{N} \beta_k \sin \psi_k \\[2mm] \beta_{III} = (2/N) \sum_{k=1}^{N} \beta_k \cos 2 \psi_k, \quad \beta_{IV} = (2/N) \sum_{k=1}^{N} \sin 2 \psi_k \end{array}\right\} \tag{8.2}$$

Of course, there must be as many multiblade coordinates as there are blades. When the number of blades N is even, equation (8.1) contains N+1 multiblade coordinates; however, two coordinates can be combined. For example, for four blades, the last two terms of equation (8.1) are for consecutive blades:

$$\left. \begin{array}{l} \beta_k \quad = \ldots + \beta_{III} \cos 2\psi_k + \beta_{IV} \sin 2\psi_k \\ \beta_{k+1} = \ldots + \beta_{III} \cos 2\left(\psi_k + \frac{2\pi}{4}\right) + \beta_{IV} \sin 2\left(\psi_k + \frac{2\pi}{4}\right) \end{array} \right\} \tag{8.3}$$

For consecutive blades, these terms are the same with opposite sign. For the third blade, the expression is the same as for the first blade. Therefore, the last two terms can be replaced by

$$\beta_{III} \cos 2\psi_k + \beta_{IV} \sin 2\psi_k = \beta_d(-1)^k \tag{8.4}$$

For a six-bladed rotor, the last two terms of equation (8.1) can be replaced by

$$\beta_V \cos 3\psi_k + \beta_{VI} \sin 3\psi_k = \beta_d(-1)^k \tag{8.5}$$

and so on. The inverse of equatnions (8.4) and (8.5) is

$$\beta_d = (1/N) \sum_{k=1}^{N} \beta_k(-1)^k \tag{8.6}$$

Equation (8.6) is valid only for even N. The remaining multiblade coordinates and all multiblade coordinates for odd N are defined by equation (8.2). If β_k is the blade flapping angle, β_o represents coning, β_I represents forward tilting, β_{II} represents left tilting, the higher multiblade coordinates represent warping, and β_d represents differential coning where subsequent blades have opposite amplitudes — possible only for an even number of blades. Multiblade coordinates can be defined similarly for other blade motions such as lead-lag and feathering, and also for elastic blade modes.

Without aerodynamic forces, the multiblade coordinates can be easily related to normal multiblade modes. For β_o and β_d the coordinates directly represent two multiblade normal modes in a vacuum (which can be termed collective and differential collective, or reactionless, modes), the latter occurring only for even-bladed rotors. The remaining multiblade coordinates can be paired so that each pair represents an advancing and a regressing normal mode. This will be shown for a rotor with three or more blades with the tilting coordinates β_I and β_{II}. In a vacuum, the individual blade flapping equation (assuming a rigid blade elastically hinged at the rotor center) for the kth blade is, in a rotating reference system,

$$\ddot{\beta}_k + P^2\beta_k = 0 \tag{8.7}$$

where P is the natural flapping frequency. For soft flapwise hingeless rotors, the value P is between 1.05 and 1.15. Inserting into equation (8.7), for each of the three blades

$$\beta_k = \beta_I \cos \psi_k + \beta_{II} \sin \psi_k$$

The resulting equation is denoted by $F_\beta(\psi_k) = 0$, and after forming $\sum_{k=1}^{3} F_\beta(\psi_k) \cos \psi_k = 0$ and $\sum_{k=1}^{3} F_\beta(\psi_k) \sin \psi_k = 0$, a set of two equations is obtained for the multiblade coordinates β_I and β_{II}:

$$\left. \begin{array}{l} \ddot{\beta}_I + (P^2-1)\beta_I + 2\dot{\beta}_{II} = 0 \\ \ddot{\beta}_{II} + (P^2-1)\beta_{II} - 2\dot{\beta}_I = 0 \end{array} \right\} \tag{8.8}$$

These equations are satisfied for

$$\beta_I = e^{i\omega t}, \beta_{II} = ie^{i\omega t}, \omega = 1 \pm P \tag{8.9}$$

which describe advancing and regressing normal modes. Similarly, every other pair of cyclic multiblade coordinates defines two normal modes in vacuum — an advancing mode and a regressing mode. In hover, these modes are damped; in forward flight, they become aerodynamically coupled.

Elastic rotor hub forces and moments are easily expressed in terms of the multiblade coordinates. The main computational advantage of using them in a linear analysis is that the variability of the coefficients in the equations of motion is much smaller than in the equations for individual blades. The individual blade equations, both in rotating and nonrotating reference systems have periodic coefficients that vary with first, second, third, etc., harmonics of the rotor rotational frequency. In a multiblade representation of an N-bladed rotor, the lowest harmonic of the coefficients is the Nth for N odd, and the (N/2)th for N even (ref. 2.85). For advance ratios up to 0.4 and for rotors with three or more blades, all terms in the multiblade flapping equations with periodic coefficients can usually be omitted in a flight dynamics analysis without appreciable errors, except rotorcraft with high-gain feedback systems. Up to $\mu = 0.8$, a multiblade constant coefficient system of equations can be used as a first approximation to establish the correct trends as indicated by the dashed root curves in figure 6.3. With individual blade coordinates, a constant coefficient approximation is not possible even for low advance ratio.

For near hover conditions, a more compact formulation for multiblade coordinates is obtained by use of complex notation (see ref. 2.79). In this notation, equations (8.8) are written as

$$\ddot{\beta} + (P^2-1)\beta - 2i\dot{\beta} = 0 \tag{8.10}$$

This can be seen by multiplying the second of equations (8.8) by i, adding it to the first, and substituting

$$\beta = \beta_I + i\beta_{II} \tag{8.11}$$

Except for low advance ratio, this substitution into the multiblade equations is not suitable since the complex amplitudes β_I and β_{II} are not generally perpendicular to each other in the complex plane as they are in equation (8.9).

8.3 Linear Constant and Periodic Coefficient Modeling

For advance ratios up to about 0.4, the linear flight dynamics equations can usually be approximated by constant coefficient equations if multiblade coordinates are used. The equations are written in state variable form with only the first time derivatives. The complex eigenvalues and eigenvectors can then be determined directly from

$$\dot{x} = Fx \tag{8.12}$$

where x is the state vector and F is the constant coefficient state matrix. For a flight dynamics analysis with a flapping rotor with three or more blades and a rigid body with a body-fixed reference system, there are 14 state variables, 8 for the body and 6 for the rotor. A cost effective computer method of obtaining the complex eigenvalues and eigenvectors is as follows: First generate the coefficients p_1, p_2, ..., p_n of the characteristic polynomial

$$\lambda^n + p_1\lambda^{n-1} + p_2\lambda^{n-2} + \ldots + p_n = 0 \tag{8.13}$$

by the Leverrier-Faddev method (see, e.g., ref. 8.1). Then extract the real and complex conjugate roots by a subroutine also given in reference 8.1. Finally, the eigenvectors are found with a simultaneous equations subroutine. The alternative root squaring or iteration method was less cost effective for problems of this size (see ref. 8.2).

The characteristic polynomial equation (8.13) has only real or complex conjugate pairs of roots. For real eigenvalues, the eigenvectors are also real. For complex conjugate eigenvalues the iegenvectors are also complex conjugates. The real mode for an eigenvalue pair $\lambda_j \pm i\omega_j$ is found by

$$x_j(t) = A_j\, e^{(\lambda_j+i\omega_j)t} + A_j^*\, e^{(\lambda_j-i\omega_j)t} \tag{8.14}$$

where A_j and A_j^* are the complex conjugate pair of eigenvectors that indicate amplitude and phase relations between the state variables for the jth mode. If A is the modal matrix whose columns are the eigenvectors A_j, an initial value problem can be written in the form:

$$x(t) = Aa\, e^{(\lambda+i\omega)t} \tag{8.15}$$

from which

$$a = A^{-1}x(0) \tag{8.16}$$

Differentiating equation (8.15) and inserting x(t) from equation (8.15) into (8.12) yields

$$A^{-1}FA = \lambda + i\omega \tag{8.17}$$

which shows that $\lambda+i\omega$ is the diagonal matrix of eigenvalues and A, the modal matrix of the state matrix F.

For advance ratios above 0.4, the periodic terms, even if multiblade coordinates are used, become increasingly more important and can lead to instabilities that are not predicted by the constant coefficient system of equations. Extending the preceding relations to periodic linear systems is rather simple if the state transition matrix is used (see, e.g., ref. 8.3). The state transition matrix concept is applied to helicopter dynamics in references 2.86, 2.47 and 2.85. Alternative, though less practical, solutions for the periodic linear system equations are applied to helicopter dynamics in references 8.4 and 8.5. (Reference 2.85 is followed here.)

Equations (8.12), (8.14), and (8.15) for constant coefficient linear systems remain the same for periodic linear systems, except that the state and modal matrices F and A are now periodic functions with period T. The state transition matrix $\phi(t,\tau)$ is defined by

$$\dot{\phi}(t,\tau) = F(t)\phi(t,\tau)\ , \ldots \phi(\tau,\tau) = I \tag{8.18}$$

This matrix can easily be generated by solving the initial value problem for each column with one state variable being one at time $t = \tau$ and the others being zero. Set $\tau = 0$ and simply write $\phi(t)$ instead of $\phi(t,0)$. By superposition, the general initial value problem can be expressed with the state transition matrix by

$$x(t) = \phi(t)x(0) \tag{8.19}$$

The initial value problem is also expressed with matrix A(t) by equation (8.15). After inserting equation (8.16) into (8.15) and comparing the factors of x(0) on the right-hand sides of equations (8.15) and (8.19), one obtains

$$\phi(t) = A(t)e^{(\lambda+i\omega)t} A^{-1}(0) \tag{8.20}$$

from which

$$A(t) = \phi(t)A(0)e^{-(\lambda+i\omega)t} \tag{8.21}$$

If equation (8.20) is written for t = T and if A(0) = A(T), one obtains (after rearranging)

$$A^{-1}(0)\phi(T)A(0) = e^{(\lambda+i\omega)T} = \Lambda \tag{8.22}$$

In comparison with equation (8.17), Λ is the diagonal matrix of eigenvalues of $\phi(T)$ and A(0) is the associated modal matrix. Solving for λ and ω by

$$(\lambda + i\omega)T = \ln \Lambda \tag{8.23}$$

one finds that ωT is not uniquely determined since $\pm n2\pi$ can be added with an arbitrary integer n. Accordingly, the time-varying periodic modal matrix A(t) from equation (8.21) is also not unique. However, the normal modes defined by

$$x_j(t) = A_j(t)\, e^{(\lambda_j+i\omega_j)t} \tag{8.24}$$

are unique since, according to equation (8.21), they are the columns of the matrix $\phi(t)A(0)$.

While the characteristic polynomial equation (8.13) has only real and complex conjugate roots for the time invariant state matrix F, the characteristic polynomial for $\phi(T)$ can also have single complex roots. Since $x_j(t)$ in equation (8.24) is real, the modal column $A_j(t)$ associated with a real root is also real. The modal column associated with a single complex root is complex so that $x_j(t)$ from equation (8.24) is real. Finally, for a pair of complex conjugate roots, the associated modal columns are complex conjugates so that

$$x_j(t) = A_j(t)\, e^{(\lambda_j+i\omega_j)t} + A_j^*(t)\, e^{(\lambda_j-i\omega_j)t} \tag{8.25}$$

is again real. When computing the values $\lambda_j + i\omega_j$ from equation (8.23) for a complex conjugate pair Λ_j and Λ_j^*, one must select from the many possible values of ω_j a pair that is also complex conjugate to ensure that $x_j(t)$ from equation (8.25) is real.

For plots of the time-variable normal modes, it is convenient to omit the exponential decay or amplification factor $e^{\lambda_j t}$. This was done for the two examples of a normal mode of a periodic system in figure 8.2 (taken from ref. 2.85). The figure refers to a hingeless rotor with fixed hub and tilting moment feedback defined by equations (6.5). The blade Lock number is 8, the advance ratio is 0.8, the blade flapping frequency is 1.15Ω, and the feedback gain is $K_i = 0.8$. The modes are unstable since both values of λ_j are positive. The upper graph for a three-bladed rotor presents the three multiblade coordinates β_0, β_I, and β_{II}. The figure shows an advancing mode of frequency 1.5Ω with some coning participation. The lower graph for a four-bladed rotor therefore includes the differential coning

coordinate β_d. The advancing mode frequency is now 0.84Ω and all four multiblade coordinates strongly participate. Note that the unstable mode for the three-bladed rotor is associated with a single complex eigenvalue of $\phi(T)$, while the unstable mode for the four-bladed rotor is associated with a complex conjugate eigenvalue of $\phi(T)$. The first type of instability could not occur for a constant coefficient system. Reference 2.85 shows that, for N = 3, this type of instability can also occur at an advance ratio of 0.4 if $K_i > 1.2$. Near the stability limit, the periodic terms can be important even at a low advance ratio, although for an adequate stability margin the constant coefficient approach usually is sufficient.

While the natural modes of the periodic system (fig. 8.2) are uniquely determined, the eigenvalues $\lambda_j + i\omega_j$ are not, and if the root plots are to be presented as in figures 6.3 and 6.5, a selection principle must be applied. The procedure used in these figures was to compare the lower frequencies with those obtained with the constant coefficient system, but to omit the negative region of $i\omega$ and move the curves into the positive half-plane. Curves corresponding to complex conjugate Λ_j pairs are recognized by their symmetry about the $\omega = 0$ and 1.5 lines for three blades and about the $\omega = 1$ and 2 lines for four blades.

8.4 Linear Stochastic Modeling

Hingeless rotorcraft without feedback systems or without large horizontal tails are sensitive to turbulence in the upper speed range. It is of interest to determine the response to atmospheric turbulence and its variation with basic rotor parameters as well as feedback system parameters. Unlike fixed-wing aircraft for which an extensive literature on analysis and testing of turbulence responses exists, very little information is available on the responses of rotorcraft to turbulence. If the derivative approach to rotorcraft flight dynamics is used, the analytical methods are the same as those used for airplanes. The von Kármán-Taylor atmospheric turbulence model is usually assumed according to which the horizontal and vertical turbulence velocity components relative to the aircraft can be stochastically described by a continuous linear Gauss-Markov process. The covariance or power spectral density functions depend only on one physical parameter: the turbulence scale length L that varies from a few hundred feet at low altitude to a few thousand feet at high altitude. The aircraft turbulence response then depends on the ratio of the turbulence scale length to a suitable aircraft length. For rotorcraft, the rotor radius R is used as the reference length so L/R is the parameter that determines the turbulence response at a given advance ratio μ.

Fig. 8.2 Unstable modes of hingeless rotors with lagged rotor tilting feedback at advance ratio of 0.8.

As discussed previously, the derivative approach to rotorcraft flight dynamics gives erroneous results for the short-time responses important in determining rotorcraft response to turbulence. In a rotorcraft turbulence analysis, the first three multiblade flapping coordinates β_0, β_I, and β_{II} should be included. For a higher advance ratio the periodic terms must be retained in the system equations. The problem then is to compute the random response of a linear, periodic, time-varying system to random Gaussian inputs with given power spectral density or given autocorrelation function. According to a general theorem on random processes, the response of a linear system to Gaussian input is also Gaussian. A Gaussian process is uniquely determined by mean and covariance functions of time.

Problems can often be solved without assuming the Gaussian character of the stochastic processes. If one is interested only in covariances or power spectral densities, the weaker assumptions of the so-called mean-square calculus are sufficient. If one is interested in obtaining threshold crossing statistics necessary for structural reliability considerations, the stronger assumption of Gaussian processes must be made. From the point of view of mean-square calculus, one considers weakly stationary random processes, for which the covariances and power spectral densities are time-invariant. This concept has been extended in reference 8.6 to weakly periodic random processes for which the covariances are periodic functions of time. It can easily be shown that a linear stable periodic system steadily excited by a weakly periodic random process with the same period has responses that are also weakly periodic random processes. This occurs when a rotorcraft flies with constant speed through a region of constant atmospheric turbulence.

There are several methods of computing the random response of a time-varying linear system to random inputs. Reference 2.87 uses a frequency domain approach (outlined in ref. 8.7) to compute random rotor blade vibrations. This method is practical for given input power spectral density. If the input can be represented as filtered white noise, a time-domain method used in automatic control theory, (ref. 8.8) can be more computer cost effective (ref. 2.84). The filter method was also applied to rotor random response analyses in references 8.9, 8.10, and 6.2. A correct stochastic lifting rotor analysis with the proper correlations of the blade loads both spanwise and azimuthwise has not yet been performed. Partial solutions for restrictive conditions are presented in references 8.11 and 8.12. The usual assumption is that the entire rotor experiences the turbulence velocities that occur at the center of the rotor. The adequacy of this "point" assumption has been checked in reference 8.13 by accounting for the correlations between vertical turbulence velocities across the rotor disk in the longitudinal direction. Only the 0.7R station was considered and lateral correlations were omitted. It was found that for a turbulence scale length/rotor radius ratio of 4, the correlation across the rotor disk had little effect on the random blade response compared to the "point" approximation. Usually, L/R is much larger than 4.0. For a low-altitude turbulence scale length of L = 400 ft and a rotor diameter of 66 ft, L/R = 12. The point approximation therefore appears to be well justified for current rotorcraft, at least so far as the first blade flapping mode is concerned.

No turbulence response analysis has been performed with the complete rotor-body system, and no tests are available with which to compare the results of such an analysis. However, data are available for fixed-hub and tilting moment feedback. Figure 8.3 (taken from ref. 2.85) shows the standard deviation of the flapping amplitude over one rotor rotation period for the same case as shown in figure 6.3 for an advance ratio of $\mu = 1.6$ and a turbulence scale/rotor radius ratio of 12. The response shown is for a unit standard deviation of the dimensionless vertical turbulence velocity. It is seen that feedback with a gain of $K_i = 0.1$ in equation (6.5) results in some reduction
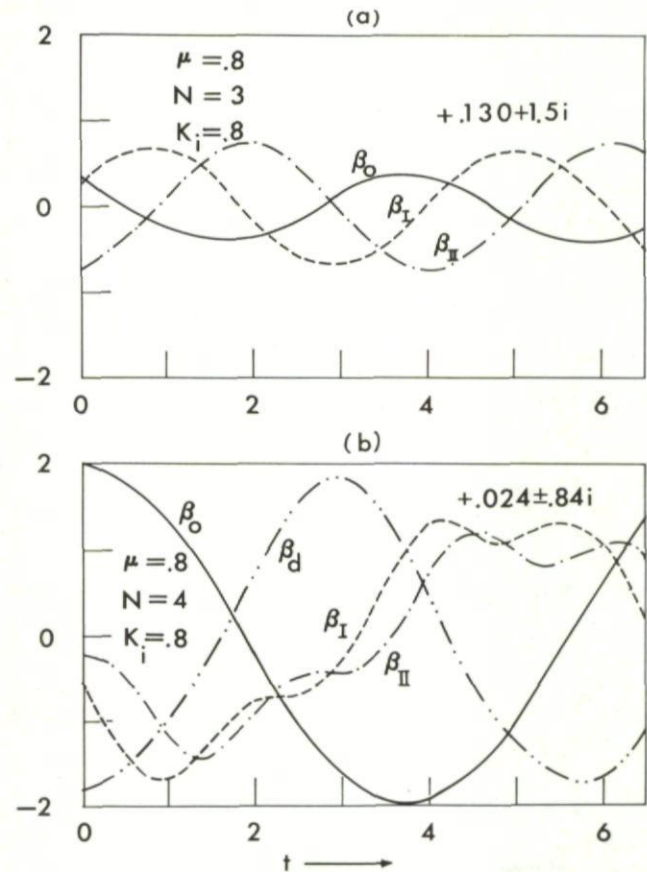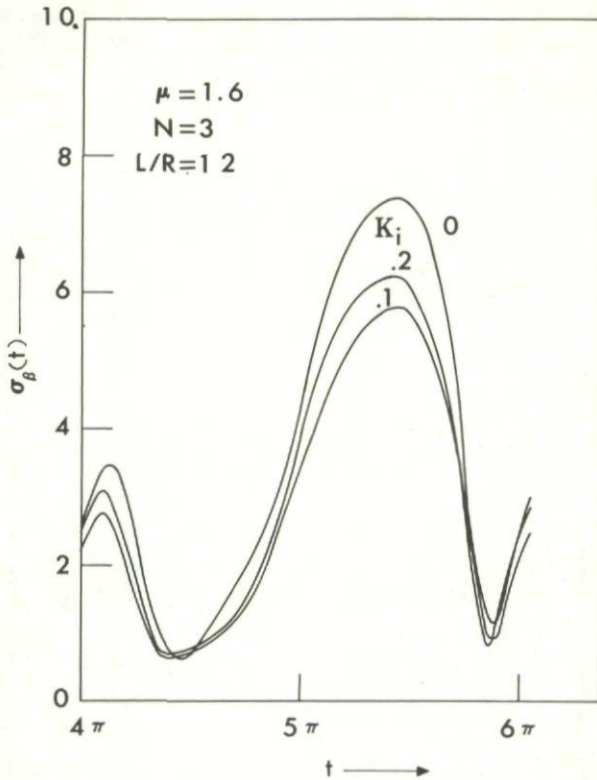
Fig. 8.3 Effect of lagged tilting moment feedback gain on flapping standard deviation from atmospheric turbulence.

in $\sigma_\beta(t)$, but feedback with a gain of $K_i = 0.2$ reverses the trend. This results from a reduction in the damping of certain rotor modes as the flapping stability limit is approached.

It can be said that the analysis techniques for linear stochastic modeling of rotorcraft flight dynamics are available but have not yet been applied except to restricted cases.

9 MODEL AND FLIGHT-TESTING TECHNIQUES AND RESULTS

The special problems of hingeless rotors have stimulated an interest in dynamic model and flight testing. A survey of modern test methods and some selected test results is therefore appropriate. Some aspects of testing hingeless rotor models are included in reference 9.1.

9.1 Model Testing for Derivatives

A derivative flight dynamics analysis assumes that the rotor adjusts itself instantaneously to changes in the body linear and angular velocity components. The rotor state variables — tilt and rate of tilt, coning and rate of coning — are neglected. Cyclic and collective controls are also assumed to have instantaneous responses. A 6 X 6 matrix of rotor aerodynamic derivatives relates the three forces and three moments about the aircraft center of gravity to the three linear and three angular velocity components. Furthermore, a 6 X 3 matrix of control derivatives relates the body forces and moments to the cyclic and collective pitch inputs, resulting in a total of 54 derivatives. Some of the derivatives are small and can be neglected, but many should be measured in a proper wind-tunnel model program. Because of the nonlinearity of the rotor characteristics, the derivatives depend on the trim condition and they also change strongly with advance ratio. The set of pertinent derivatives must therefore be measured for many flight conditions. Usually, there are strong interference effects between rotor and body which need to be measured. An example would be to determine the tail effectiveness or fixed-wing contributions by measuring the rotor forces and moments separately from the body forces and moments. To gain some insight into the interference phenomenon, it is also desirable to measure the flow-field near the tail surfaces or the fixed wing.

A complete derivative model test program for a rotorcraft is a vast enterprise and is undertaken rarely if at all. The usual argument against the effort is that the Reynolds or Mach number scaling effects are so great that the results cannot be applied accurately to the full-scale vehicle. While this is true if the measured derivatives are applied directly, the test data can be correlated with analytical data and can contribute to the substantiation of analytical models. Unless the test data are evaluated properly, including corrections for Reynolds or Mach number effects or other inadequacies of the model, the raw test data should be applied with reservations.

Some aircraft derivatives and a comparison with analysis are shown in figures 9.1 and 9.2 for the Froude Scale model of the ABC vehicle (ref. 2.63). The fifth-scale model was tested to an advance ratio of 0.1 on the Princeton Dynamic Model Track facility. The
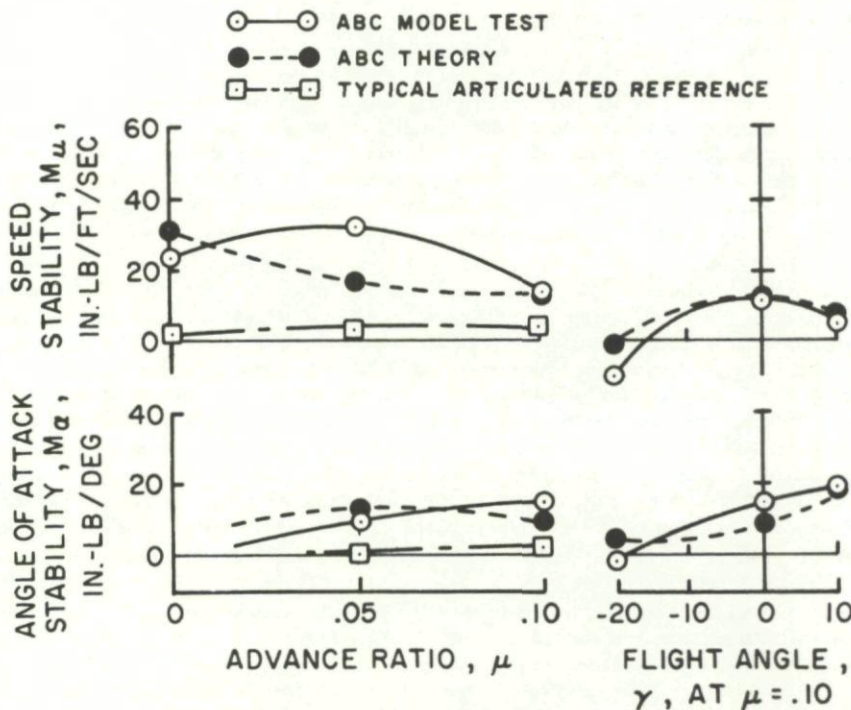
Fig. 9.1 Pitching moment derivative with angle of attack and with speed for ABC fifth-scale model.
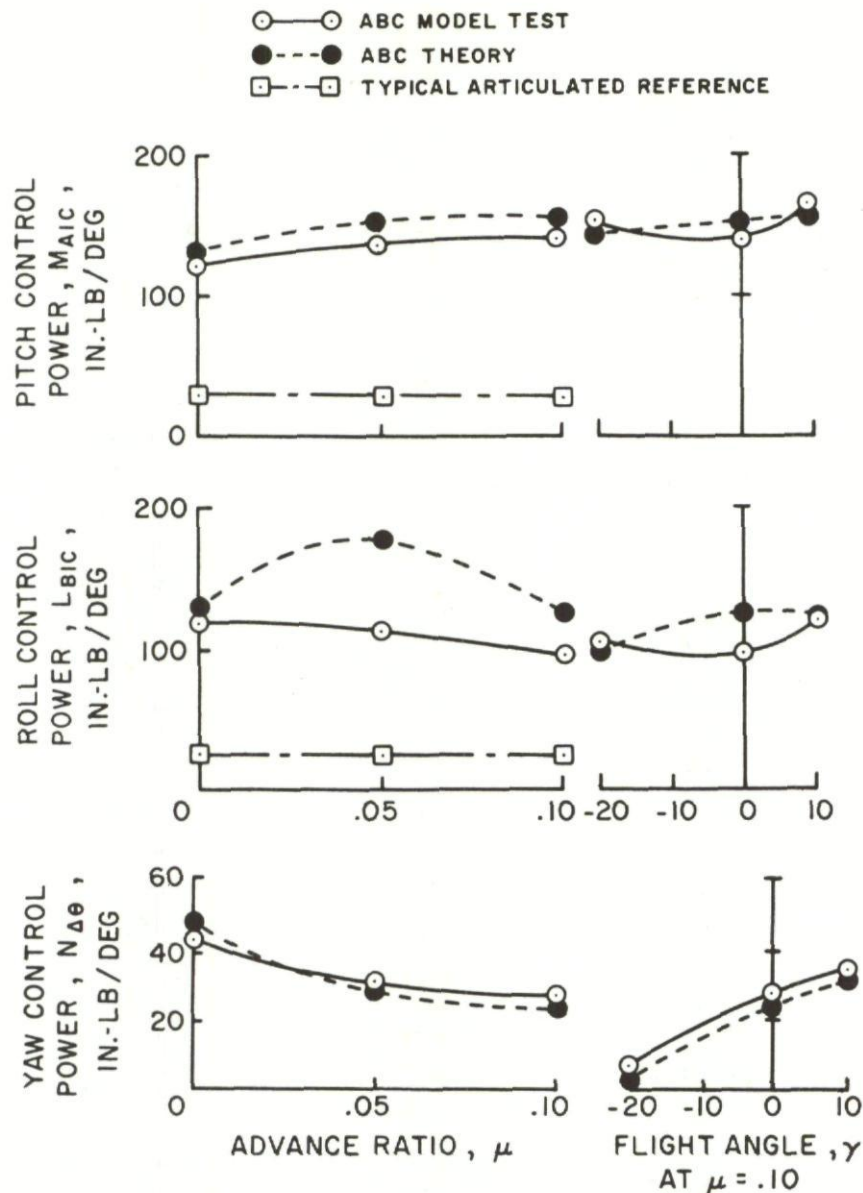
Fig. 9.2 Pitch, roll, and yaw control derivatives for the ABC fifth-scale model.

model/full-scale rotor tip speed ratio is 0.44. The Reynolds number ratio is 0.085. Blade mass and elasticity and body mass and moments of inertia are properly scaled. The blade rotating flapwise frequency is 1.45Ω, the blade frequency of the full-scale rotor. There are three blades per rotor. The model disk loading was 1.54 psf compared to 7.85 psf for the full-scale vehicle. The moments given (in in.-lb) are for the model scale.

Figure 9.1 compares the measured speed stability and angle-of-attack stability derivatives versus advance ratio μ with analytical values and values for a typical articulated rotorcraft. The right-hand graphs give the effect of flight-path angle γ on the derivatives at $\mu =$ 0.10. Negative γ represents descent. Both speed stability and angle-of-attack instability are greater by an order of magnitude than for an articulated rotorcraft despite a large horizontal tail surface. The analytical values are considerably in error at $\mu = 0.05$, presumably because of an inadequate rotor wake representation. Speed and angle-of-attack derivatives become zero in a descent. The horizontal tail is apparently outside the rotor wake downwash area in this descent condition, and the tail more effectively compensates the rotor angle-of-attack instability.

The pitch, roll, and yaw control derivatives shown in figure 9.2 are several times greater than for an articulated rotor. Pitch control power increases with speed and roll control power decreases with speed. The analytical prediction is again in error at $\mu = 0.05$, probably because of the rotor wake representation. Yaw control power decreases with advance ratio, especially in a descent at $\mu = 0.1$. The lack of yaw control power from differential collective pitch in a descent is typical of coaxial or synchropter configurations and is not related to the high blade flapping stiffness of the ABC.

Another set of hingeless rotor derivatives (taken from ref. 2.75) is shown in figure 9.3. Eleven derivatives are plotted versus advance ratio. The flap frequency is 1.17Ω and the blade Lock number is 4.2. The test data were obtained with a four-bladed, 7.5-ft rotor model in the USAAMRDL-Ames 7-by 10-foot Wind Tunnel at approximately zero lift (see ref. 2.46). The solid lines are from a linear analysis that includes blade bending flexibility but not downwash effects. The dashed lines are from the same linear analysis and include an empirical downwash model developed in reference 2.75. For some derivatives, the downwash is not important. Others are affected substantially by downwash, particularly at low advance ratio.

9.2 Model Frequency Response Testing

Frequency response testing is practical only for wind-tunnel models. Extensive frequency response measurements with a 7.5-ft hingeless rotor model, using harmonic inputs to the cyclic and collective controls, are presented in reference 2.46 and summarized in reference 2.45. Responses to harmonic hub pitch and roll angular rotations are presented in reference 2.43. Only low lift conditions
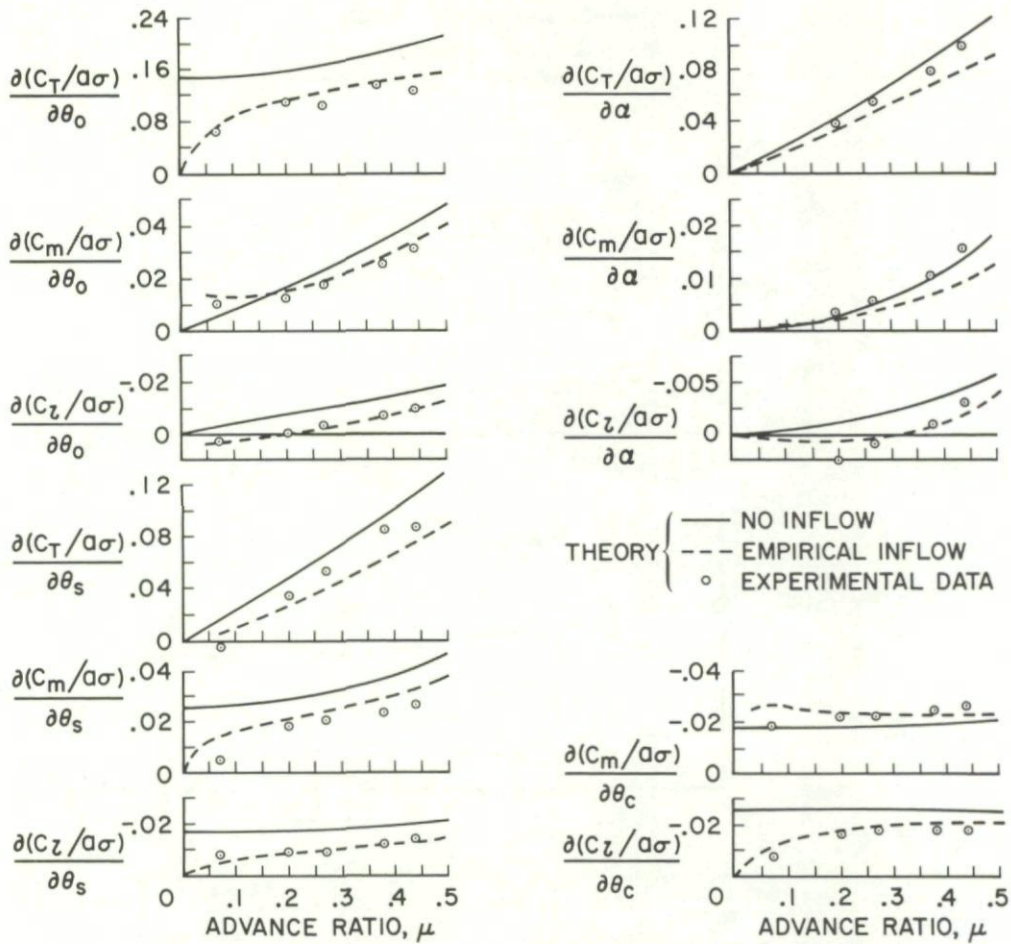
Fig. 9.3 Comparison of eleven analytical and experimental hingeless rotor derivatives for a Lockheed 7.5-ft hingeless rotor model in the USAAMRDL Ames 7-by-10-Foot Wind Tunnel, P = 1.17, γ = 4.2.

were tested and the blades were quite stiff flapwise with rotating flap frequencies of 1.33, 1.56, and 2.32Ω. The advance ratio range was 0.29 to 1.44, and the forcing frequency range was 0.04 to 4Ω. This frequency range covers the regressing, coning, and advancing rotor mode frequencies.

Figure 9.4 compares analytical and experimental longitudinal tilting responses to longitudinal cyclic control input for a flapping frequency of 1.56Ω at an advance ratio of 0.79. The solid line represents the analytical result using the linear theory of reference 2.55, which includes reversed-flow effects, assumes a rigid blade flexibly hinged at the rotor center, and neglects the rotor downwash. Generally, this analytical model correlates quite well with the tests, although the logarithmic scale for the amplitude ratio tends to obscure discrepancies between the analysis and test results. An increase of 6 dB corresponds to a doubling of the amplitude ratio. The two response peaks at the regressing and advancing flapping mode frequencies are clearly predicted by the analysis. The measured phase angles also correlate well with the analytical results. The agreement between analysis and test results is not as good for lower blade flapping frequencies.
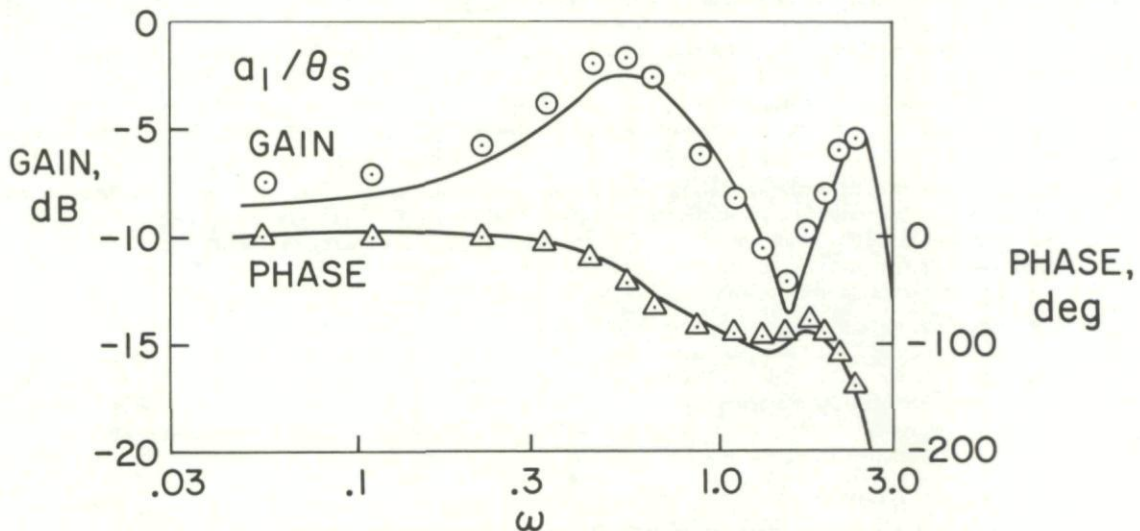
Fig. 9.4 Comparison of analytical and experimental longitudinal tilt frequency response to longitudinal cyclic pitch; μ = 0.79, P = 1.56.

Figure 9.5 (taken from ref. 2.43) compares analytical and test results for the longitudinal tilt response to harmonic hub pitching. The flap frequency is 1.56Ω and the advance ratio is 0.41. Compared to figure 9.4, the gain (in dB) is much larger. The deviations between analytical and test results are now substantial, most likely because of resonance of the model fuselage. The actual motion at the hub was not measured and may have been affected by model fuselage vibration modes. Since none of the test conditions were near a flapping stability limit, the constant coefficient multiblade representation was adequate for predicting the frequency response (as expected from fig. 6.3 and confirmed in ref. 2.45). The savings in computer effort with the multiblade constant coefficient approximation are considerable since time histories and the associated Fourier analysis are avoided.
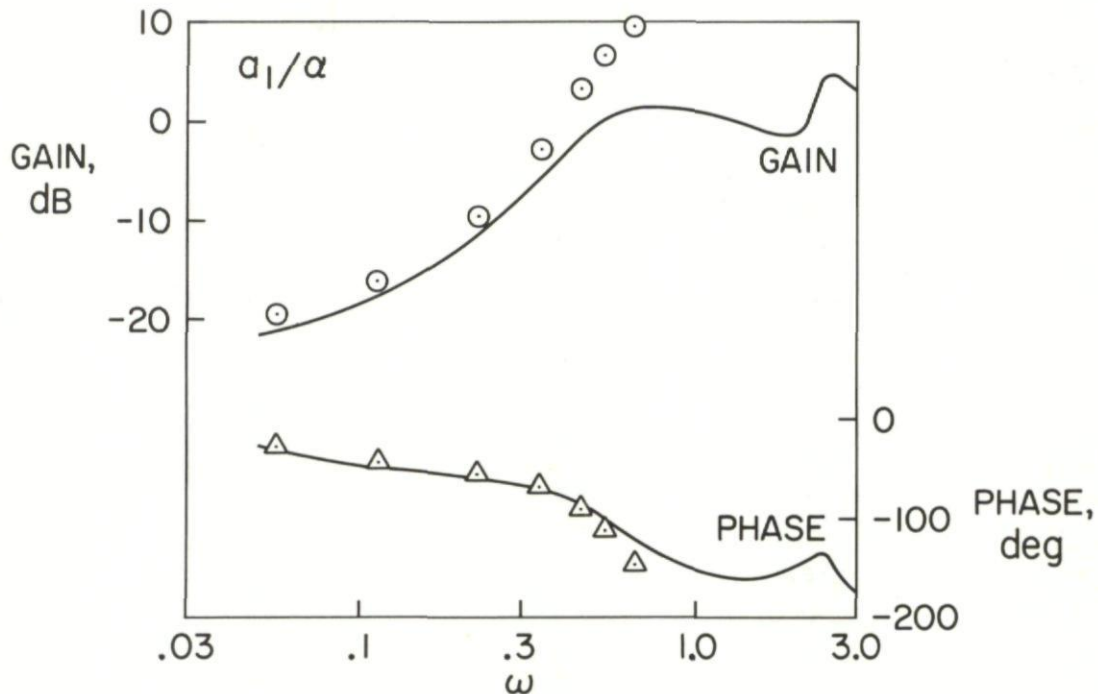
Fig. 9.5 Comparison of analytical and experimental longitudinal tilt frequency response to hub pitch; $\mu = 0.41$, P = 1.56.

The frequency response tests reported in references 2.45 and 2.46 were also extended to include lagged rotor tilting moment feedback (described in Sec. 6.2). Figures 9.6 and 9.7 compare the longitudinal tilting response to harmonic collective pitch input, open loop, and closed loop, respectively. The advance ratio is 0.54 and the flapping frequency is 1.33Ω. Below a frequency of 0.2Ω, the closed-loop system shows a much lower response than the open-loop system. However, the regressing mode at 0.33Ω shows a higher response with the closed-loop system. In the low-frequency range, the phase changes from zero for the open-loop system to 90° for the closed-loop system. It is thus evident that improved flight dynamics of the lagged tilting moment feedback system would be offset by a greater flapping response to gusts at the regressing flapping mode frequency.
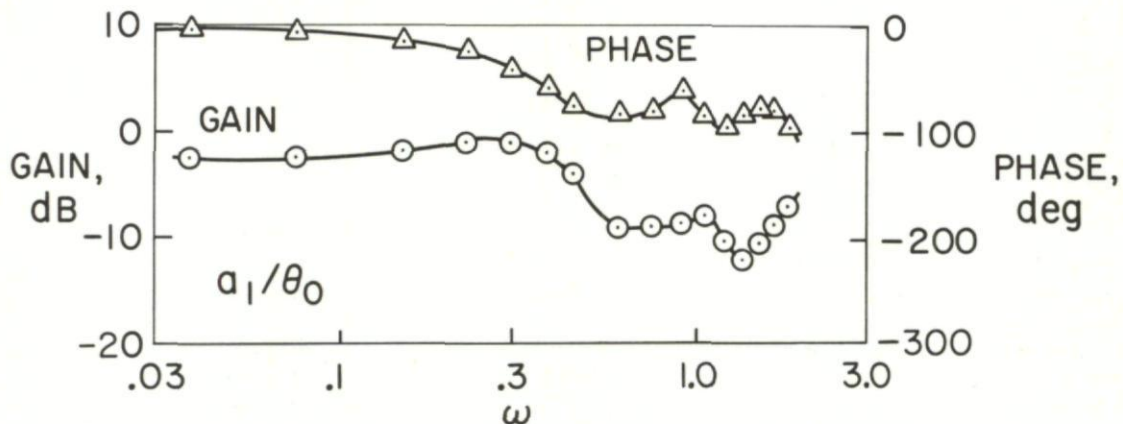
Fig. 9.6 Experimental longitudinal tilt frequency response to collective pitch; $\mu = 0.54$, P = 1.33.

9.3 Transient Testing for Lightly Damped Modes

Transient testing, that is, the recording of transients after a pulse excitation, is widely used in flight testing. Unavoidably, several modes are excited simultaneously and it is difficult to separate them except when all modes but one are well damped. The lightly damped or amplified mode persists longer than the well-damped modes, and the frequency and damping of this mode can be measured. Of the flight dynamics modes, the phugoid usually has the least damping and the longest period and can be conveniently studied in flight. Figure 9.8 compares analytical and test data for the period and time to double amplitude of the phugoid for the BO-105 helicopter (ref. 2.20). The test data were evaluated from pitch attitude and pitch rate measurements after a collective pitch pulse. Coupling with lateral and yawing motions was small at the lower speeds and all controls were held fixed after the collective pitch pulse. At high speeds, coupled lateral and yawing motions are minimized by appropriate control inputs. The shortest time to double amplitude that could be measured with this technique was about 3 seconds. As shown in figure 9.8, this occured at 100 knots.
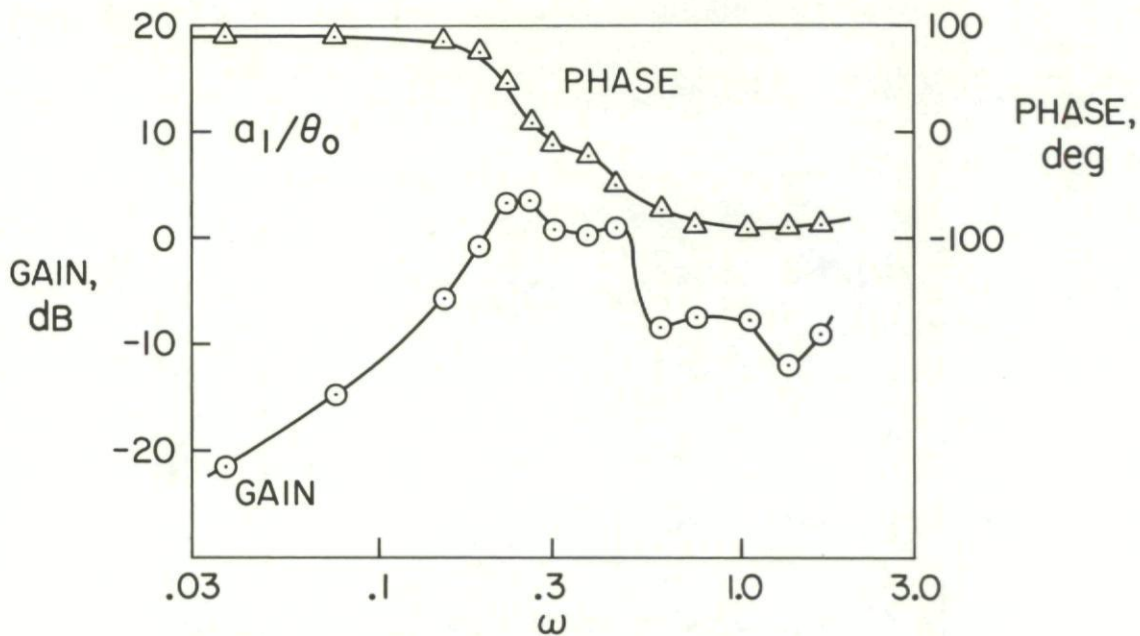
Fig. 9.7   Experimental longitudinal tilt frequency response to collective pitch including rotor lagged tilting feedback; $\mu = 0.54$, P = 1.33.
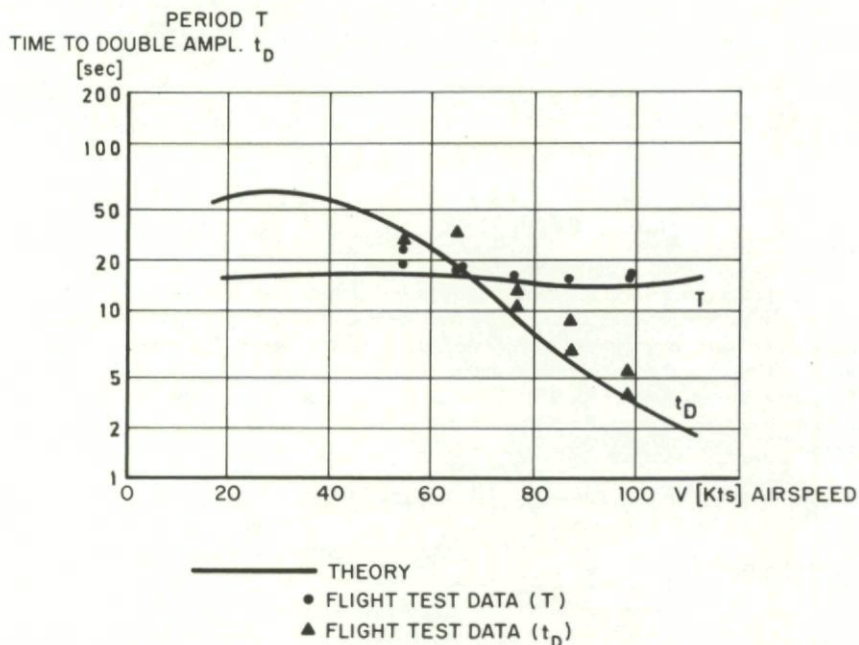

Fig. 9.8   Phugoid period and doubling time for BO-105 helicopter — comparison of analytical and test data.

Another lightly damped mode for hingeless rotorcraft is the regressing inplane or air resonance mode. Its frequency is very close to the difference of rotor rotational speed and blade inplane frequency. This mode is excited in flight with a brief lateral stick oscillation at roughly the air resonance frequency. A response similar to the computed response shown in figure 8.1 is then superimposed on the steady-state or trim forced response of the blade inplane deflection. Since the frequency of the desired mode is known, it is necessary only to filter out the trim response, either with an on-line filter or during subsequent data processing. The former is preferable so that the telemetered response can be directly observed on an oscilloscope or on oscillograph records.

The excitation of the air resonance mode in flight is not without danger. The damping ratio is at best only a few percent and may be amplitude-dependent if friction is the main source of damping. The mode may be stable for small excitation and unstable for large excitation. The nonlinearity of the phenomena that sometimes extend beyond the linear stability limit to a limit cycle does not necessarily provide a practical protection, as can be seen from an example in reference 2.78, which shows large limit cycle amplitudes beyond the linear stability limit. Other types of nonlinearity, for example, in structural damping, may be beneficial. Because of the dangers involved, it is not advisable to approach the air resonance stability limit in transient flight testing. The tests should be used merely to substantiate and refine an analytical model that can then be used to predict the conditions for actual instability, which, of course, should be well outside the flight envelope.

In testing scaled models of rotorcraft, one usually relies on natural disturbances to excite a potentially unstable mode and snubbers are used as soon as the divergence of the mode is apparent. An on-line filter that allows one to better recognize the potentially unstable mode on the oscilloscope is also desirable for model transient testing. The technique of fast Fourier transform spectral anslysis and moving block peak plots (discussed in Sec. 8.1) is also suitable for on-line application. Figure 9.9 (taken from ref. 2.12) shows the body roll, body pitch, and blade chordwise moment traces for a hingeless rotorcraft model representative of the BO-105 helicopter. The air

Ω = 1,300 rpm, COLLECTIVE PITCH = 13 deg
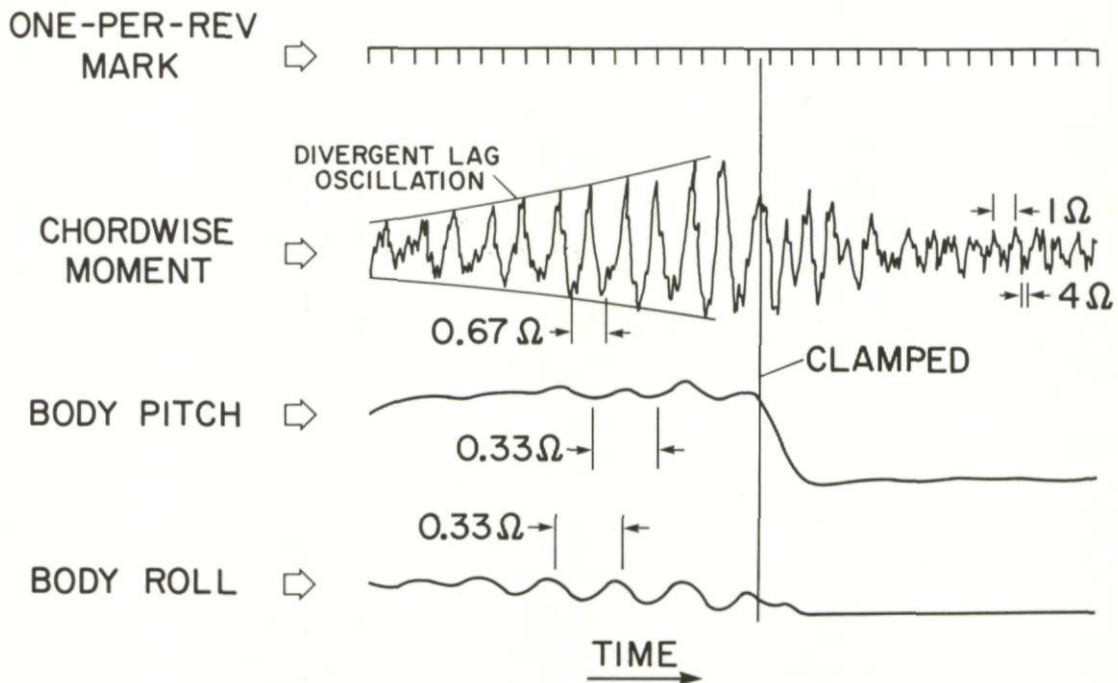
Fig. 9.9 Air resonance mode divergence measured for a Boeing-Vertol hingeless rotorcraft model, representative of the BO-105 helicopter.

resonance stability limit in terms of collective pitch setting (13°) was slightly exceeded and the resulting oscillatory divergence was terminated by snubbing the body. In some cases, it is safer to excite the mode of interest well below the stability limit where natural disturbances are ineffective. This method was used successfully in a hover condition for the tests reported in references 2.71 and 2.74.

9.4 System Identification from Transients

The method of system identification outlined below has not yet been applied to hingeless rotorcraft or to rotorcraft models, but may become an important tool in the future. The method uses transient test data to determine the state matrix F in equation (8.12). After the state matrix is obtained, mode shapes, frequencies, and dampings can be determined using the methods outlined in section 8.3. Therefore, the strongly damped modes as well as the weakly damped modes, can be obtained from the test data. Furthermore, forced response analyses can be performed on the basis of a state matrix extracted, either in part or entirely, from transient tests.

To be successful, the transients used in this method must involve all modes of the system. Also, the analytical description of the system (Eq. 8.12) must be adequate. If essential state variables are omitted (e.g., rotor flapping), one could not expect a system identification that is valid in all respects. The identification method is flexible, for example, a priori knowledge of some of the state matrix components can be used while identifying those components that are not known or are not well known. System identification methods can be based on the extended Kalman filter given, for example, in reference 8.8. A rather simple parameter estimation is possible with a linear estimator derived from the Kalman filter equations if the state variables and their rates have been measured. The method allows for wide variations in the initial estimate of the parameters and in the variance of the initial estimate. For example, the initial estimate can be zero and its variance arbitrarily large. A transient record with adequate excitation of all essential modes will then provide — after numerical integration of a set of ordinary differential equations — final values for the parameter estimates and their variances. If the variance of the estimate approaches zero, no further information is obtained by processing the transient data.

This method of parameter estimation does not allow for measurement noise in the state variables, and it lumps both measurement noise for the accelerations and process noise into one noise vector. If measurement errors are present in the state vector measurements, the estimation is biased by an amount approximately inversely proportional to the signal/noise ratio in the state vector measurements (ref. 9.2). The estimate is also biased if the system is nonlinear. If the state variable measurements are polluted by high-frequency noise, the data should be smoothed by a low-pass filter that does not produce phase shifts in the signal. Such a digital filter was developed by Graham (ref. 9.3). Care must be taken that the filter does not exclude frequencies that are significant for the system. The response data can also be improved by making use of relationships among the various response signals. These relations can be used as process equations in a Kalman filter along with measurement equations that contain the smoothed measurements.

If the state variable rates are not known, and if the state variable measurements include large errors, a nonlinear algorithm must be used where state variables and parameters are estimated simultaneously. The nonlinear identification schemes require a much greater computation effort and can easily become unstable unless rather good initial estimates are used for the parameters. A linear identification scheme that uses measurements of the state variables and their rates has been used in references 3.4 and 3.5 to initiate a nonlinear identification scheme of the flight dynamics state matrix of the CH-53A articulated rotor helicopter. The measured transients were first smoothed with the help of a digital Graham-type filter, then further treated with a Kalman filter based on mathematical relations between the test variables (not the system equations). The third step was the parameter estimate with a linear identification scheme in the form of a least-squares algorithm. The fourth step was the nonlinear identification scheme based on the results of the linear estimation scheme. The estimates from the linear method were not much different from the final values of the nonlinear scheme and appear to be adequate in many cases.

As mentioned previously, the two main requirements for successful identification are excitation of all modes in the transients and an adequate mathematical model for the system. To satisfy the first requirement, reference 3.5 uses the records from several different

flight maneuvers simultaneously. The importance of the second requirement is shown in figure 9.10 (taken from ref. 3.4). It refers to the CH-53A helicopter (100 knots flight speed, 33,500 lb weight, and an aft c.g. location). The transients on which the identifications are based have been obtained from an elaborate nonlinear analytical model. The 6 D. O. F. quasi-static response from a conventional
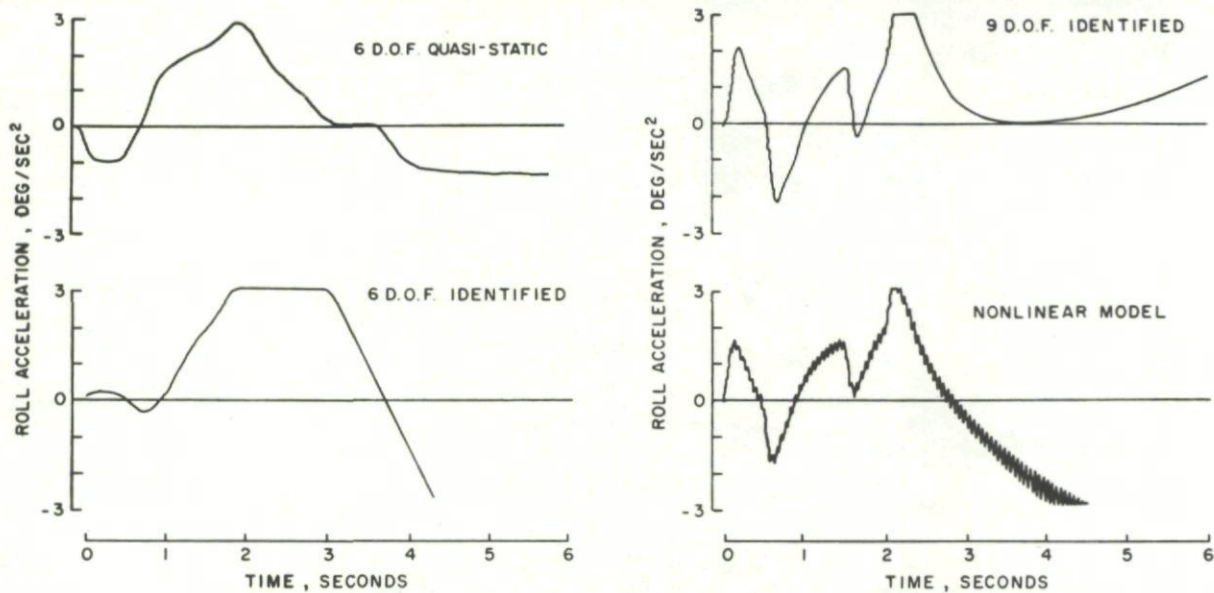

Fig. 9.10   Roll acceleration time history comparisons of three different linear models with that of a nonlinear model for the CH-53A helicopter at 100 knots.

derivative analysis shows a response quite different from the "true" response obtained with the nonlinear analytical model. After the state matrix is identified, the responses to control pulses were computed; the roll acceleration is shown in figure 9.10. Identifying the state matrix (from the "true" response) for a linear 6 D. O. F. system results in a response similar to that for the derivative approach. Identifying the state matrix for a linear 9 D. O. F. system, including rotor states, results in a response quite similar to the "true" response up to 3 seconds from the control pulse. This illustrates the fact that the identification scheme needs the correct system equations and that the conventional derivative approach is inadequate for the short-term response within a few seconds after a control pulse. Long-term responses such as the phugoid can, however, be correctly predicted with the conventional derivative approach so that the 6 D. O. F. identification is useful in this respect.

10   REFERENCES

1.1   Coleman, R. P., "Theory of Self-Excited Mechanical Oscillations of Hinged Rotor Blades," NACA Advanced Restricted Rept. 3G29, 1943; republished as NACA Rept. 1351.

1.2   Gabel, R. and Capurso, V., "Exact Mechanical Instability Boundaries as Determined from the Coleman Equation," J. Am. Hel. Soc., Vol. 7, No. 1, Jan. 1962, pp. 17-23.

1.3   Cheney, M. C., Jr., "Results of Preliminary Studies of a Bearingless Helicopter Rotor Concept," J. Am. Hel. Soc., Vol. 17, No. 4, Oct. 1972, pp. 16-26.

2.1   Anon., J. Am. Hel. Soc., Vol. 1, No. 1, History and Development Issue, Jan. 1956.

2.2   Hohenemser, K. H. and Perisho, C. H., "Analysis of the Vertical Flight Dynamic Characteristics of the Lifting Rotor with Floating Hub and Off-Set Coning Hinges," J. Am. Hel. Soc., Vol. 3, No. 4, Oct. 1958, pp. 20-34.

2.3   Berrington, D. K., "Design and Development of the Westland Sea Lynx," 29th Annual National Forum, American Helicopter Society, Preprint 711, May 1973.

2.4   McKenzie, K. T. and Howell, D. A. S., "The Prediction of Loading Actions on High Speed Semi-Rigid Rotor Helicopters," AGARD Specialists Meeting on Helicopter Rotor Loads Prediction Methods, Milan, Italy, March 1973, AGARD-CP-122.

2.5   Balmford, D. E. H., "Ground and Flight Test Experience with the Westland Scout Hingeless Rotor Helicopter," 39th Meeting of Flight Mechanics Panel, Langley Research Center, Hampton, Va., Sept. 1971, AGARD-CP-121.

2.6   Ellis, D. V., "The Ground and Air Resonance of Semi-Rigid Rotor Helicopters," ARC 33254, LD 266, Nov. 1971.

2.7   Jones, J. P., "The Helicopter Rotor," The Aeronaut. J. Roy. Aeronant Soc., Vol. 74, No. 719, Nov. 1970, pp. 861-872.

2.8   Speechley, J., "A Review of Engineering Developments in Helicopter Design," The Aeronaut J. Roy. Aeronaut Soc., Vol. 73, No. 705, Sept. 1969, pp. 759-768.

2.9   Alexander, H. R. and Leone, P. F., "V/STOL Dynamics and Aeroelastic Rotor-Airframe Technology, Vol. I, State of the Art Review of V/STOL Rotor Technology," AFFDL-TR-72-40, Jan. 1973.

2.10   Huber H. B., "Effect of Torsion-Flap-Lag Coupling on Hingeless Rotor Stability," 29th Annual National Forum, American Helicopter Society, Washington D.C. May 1973, Preprint 731.

2.11   Huber, H. B., "Some Objectives in Applying Hingeless Rotors to Helicopters and V/STOL Aircraft," AGARD Fluid Mechanics Panel Specialist Meeting, Aerodynamics of Rotary Wings, Marseille, France, Sept. 1972, AGARD-CP-111.

2.12   Burkam, J. E. and Miao W. L., "Exploration of Aeroelastic Stability Boundaries with a Soft-in-Plane Hingeless Rotor Model," J. Am. Hel. Soc., Vol. 17, No. 4, Oct. 1972, pp. 27-35.

2.13   Reichert G. and Huber, H., "Influence of Elastic Coupling Effects on the Handling Qualities of a Hingeless Rotor Helicopter," 39th AGARD Flight Mechanics Panel Meeting, Hampton, Va., Sept. 1971, AGARD-CP-121.

2.14   Richardson, D. A., "The Application of Hingeless Rotors to Tilting Prop/Rotor Aircraft," J. Am. Hel. Soc., Vol. 16, No. 3, July 1971, pp. 34-38.

2.15 Lytwyn, R. T., Miao, W. L. and Woitsch, W., "Airborne and Ground Resonance of Hingeless Rotors," J. Am. Hel. Soc., Vol. 16, No. 2, April 1971, pp. 2-9.

2.16 Reichert, G., "The Influence of Aeroelasticity on Stability and Control of a Helicopter with a Hingeless Rotor," AGARD 34th Flight Mechanics Panel Meeting, Marseille, France, April 1969, AGARD-CP-46.

2.17 Gallot, J., "Effets Aeroelastique sur les Qualités de Vol d'un Rotor Rigide," AGARD 34th Flight Mechanics Panel Meeting, Marseille, France, April 1969, AGARD-CP-46.

2.18 Woitsch, W. and Weiss, H., "Dynamic Behavior of a Hingeless Fiberglass Rotor," VTOL Research, Design and Operations Meeting, Atlanta, Georgia, Feb. 1969, AIAA Paper 69-204.

2.19 Weiland, E. F., "Development and Test of the BO-105 Rigid Rotor Helicopter," J. Am. Hel. Soc., Vol. 14, No. 1, Jan. 1969, pp. 22-37.

2.20 Reichert, G. and Oelker, P., "Handling Qualities with the Bolkow Rigid Rotor System," 24th Annual National Forum, American Helicopter Society, Washington D.C., May 1968, Preprint 218.

2.21 Young, M. I. and Lytwyn, R. T., "The Influence of Blade Flapping Restraint on the Dynamic Stability of Low Disk Loading Propeller Rotors," J. Am. Hel. Soc., Vol. 12, No. 4, Oct. 1967, pp. 38-60.

2.22 Reichert, G., "Flugmechanische Besondertheiten des gelenklosen Hubschrauberrotors", Jahrbuch 1965 der WGLR, pp. 176-184. English Translation: NASA-TTF-11373, December 1967.

2.23 Reichert, G., "Flugeigenschaften bei Hubschraubern mit elastisch angeschlossenen Rotorblättern," Jahrbuch 1963 der WGLR, pp. 136-149; also NASA TTF-11374, July 1968.

2.24 Hughes, C. and Wernicke, R., "Flight Evaluation of a Hingeless Flexbeam Rotor System," BHC Rept. 299-099-575, Oct. 1973 (to appear as USAAMRDL report).

2.25 Livingston, C. L., "Prediction of Stability and Control Characteristics of Rotorcraft," Mideast Region American Helicopter Society Symposium on Status of Testing and Modeling Techniques for V/STOL Aircraft, Phildelphia, Pa., Oct. 1972.

2.26 Sonneborn, W. G. O., "High Mach Number/High Advance Ratio Flight Test Program with the High-Performance UH-1 Compound Helicopter," USAAVLABS TR 71-2, Feb. 1971.

2.27 Sonneborn, W. G. O. and Hartwig, L. W., "Results of High Speed Flight Research With the High-Performance UH-1 Compound Helicopter," 27th Annual National Forum, American Helicopter Society, Washington D.C., May 1971, Preprint 570.

2.28 Drees, J. M. and Harvey, K. W., "Helicopter Gust Response at High Forward Speed," J. Aircraft, Vol. 7, No. 3, May-June 1970, pp. 225-230.

2.29 Cresap, W. L. and Darlington, E. C., "Rigid Rotor Research Summary 1957-1969," Bell Helicopter Co. Rept. 599-025-900, Rev. A, Sept. 1970.

2.30 Gaffey, T. M., "The Effect of Positive Pitch-Flap Coupling on Rotor Blade Motion Stability," J. Am. Hel. Soc., Vol. 14, No. 2, April 1969, pp. 49-67.

2.31 Ward, J. F., "Exploratory Flight Investigation and Analysis of Structural Loads Encountered by a Helicopter Hingeless Rotor System," NASA TN D-3676, 1966.

2.32 Huston, R. J., "An Exploratory Investigation of Factors Affecting the Handling Qualities of a Rudimentary Hingeless Rotor Helicopter," NASA TN D-3418, 1966.

2.33 Ward, J. F. and Huston, R. J., "A Summary of Hingeless Rotor Research at NASA-Langley," 20th Annual National Forum, American Helicopter Society, Washington D.C., May 1964.

2.34 Huston, R. J. and Tapscott, R. J., "The Results of Some Wind Tunnel and Flight Studies with Helicopters at NASA," New York Academy of Sciences Conference on VTOL Aircraft, New York, Dec. 1962.

2.35 Cresap, W. C., "Rigid Rotor Development and Flight Tests," 30th IAS Annual Meeting, New York, Jan. 1962, IAS Paper 62-17.

2.36 Cresap, W. L., "Development and Tests of Multibladed Semirigid Rotor Systems," J. Am. Hel. Soc., Vol. 5, No. 2, April 1960, pp. 3-12.

2.37 Potthast, A. J., "Lockheed Hingeless Rotor Technology Summary-Flight Dynamics," Lockheed Rept. LR 25987, June 1973.

2.38 Anderson, W. D., "Investigation of Reactionless Mode Stability Characteristics of a Stiff Inplane Hingeless Rotor System," 29th Annual National Forum, American Helicopter Society, May 1973, Preprint 734.

2.39 Potthast, A. J. and Blaha, J. T., "Handling Qualities Comparison of Two Hingeless Rotor Control System Designs," 29th Annual National Forum, American Helicopter Society, May 1973, Preprint 741.

2.40 Carlson, R. M. and Kerr, A. W., "Integrated Rotor/Body Loads Prediction," AGARD Specialists Meeting on Rotor Loads Prediction Methods, Milan, Italy, March 1973, AGARD-CP-122.

2.41 Kerr, A. W., Potthast, A. J. and Anderson, W. D., "An Interdisciplinary Approach to Integrated Rotor/Body Mathematical Modeling," Symposium on Status of Testing and Modeling for V/STOL Aircraft, American Helicopter Society, Philadelphia, Pa., Oct. 1972.

2.42 Watts, G. A. and Biggers, J. C., "Hingeless Rotor Vibration and Loads at High Advance Ratio," Symposium on Status of Testing and Modeling for V/STOL Aircraft, American Helicopter Society, Philadelphia, Pa., Oct. 1972.

2.43 Kuczynski, W. A., "Experimental Hingeless Rotor Characteristics at Full Scale First Flap Mode Frequencies," Lockheed LR 25491 (AMRDL contract NAS2-5419, phase III), Oct. 1972; also NASA CR-114519.

2.44 Heimbold, R. C. and Griffith, D. C., "Synthesis of an Electromechanical Control System for a Compound Hingeless Rotor Helicopter," J. Am. Hel. Soc., Vol. 17, No. 2, April 1972, pp. 55-65.

2.45 Kuczynski, W. A., Sharpe, D. L. and Sissingh, G. J., "Hingeless Rotor Experimental Frequency Response and Dynamic Characteristics with Hub Moment Feedback Control," 28th Annual National Forum, American Helicopter Society, May 1972, Preprint 612.

2.46 Kuczynski, W. A. and Sissingh, G. J., "Characteristics of Hingeless Rotors with Hub Moment Feedback Controls Including Experimental Rotor Frequency Response," Lockheed LR 25048 (AMRDL contract NAS2-5419, phase II), Jan. 1972; also

NASA CR-114427/28 (Phase I report to AMRDL contract NAS2-5419 by the same authors appeared as Lockheed LR 24122, Feb. 1971; also NASA CR-114290).

2.47   Gockel, M. A., "Practical Solution of Linear Equations with Periodic Coefficients," J. Am. Hel. Soc., Vol. 17, No. 1, Jan. 1972, pp. 2-10.

2.48   Kuczynski, W. A. and Sharpe, D. L., "Hingeless Rotor Characteristics at High Advance Ratio," AIAA 4th Fluid and Plasma Dynamics Conference, Palo Alto, Calif., June 1971, AIAA Paper 71-580.

2.49   Watts, G. A. and Biggers, J. C., "Horizontal Stoppable Rotor Conversion," 27th Annual National Forum, American Helicopter Society, Washington D.C., May 1971, Preprint 502.

2.50   Johnston, J. F. and Cook, J. R., "AH-56A Vehicle Development," 27th Annual National Forum, American Helicopter Society, May 1971, Preprint 574.

2.51   Gorenberg, N. B. and Harvick, W. P., "Analysis of Maneuverability Effects on Rotor/Wing Design Characteristics," Lockheed LR 24051 (USAAVLABS contract DAA502-70-0032), March 1971.

2.52   Sissingh, G. J. and Kuczynski, W. A., "Investigations on the Effect of Blade Torsion on the Dynamics of the Flapping Motion," J. Am. Hel. Soc., Vol. 15, No. 2, April 1970, pp. 2-9.

2.53   Cardinale, S. V., "Soft Inplane Matched Stiffness/Flexure-Root-Blade Rotor System, Summary Report," USAAVLABS TR 68-72, Aug. 1969.

2.54   Donham, R. E., Cardinale, S. V. and Sachs, I. B., "Ground and Air Resonance Characteristics of a Soft In-Plane Rigid Rotor System," AIAA/AHS VTOL Research Design and Operations Meeting, Atlanta, Georgia, Feb. 1969, AIAA Paper 69-205.

2.55   Sissingh, G. J., "Dynamics of Rotors Operating at High Advance Ratios," J. Am. Hel. Soc., Vol. 13, No. 3, July 1968, pp. 56-63.

2.56   Spreuer, W. E., "Experimental Flight Tests of the XH-51A Compound Helicopter," J. Am. Hel. Soc., Vol. 13, No. 3, July 1968, pp. 64-69.

2.57   Lentine, F. P., Groth, W. P. and Oglesby, T. H., "Research in Maneuverability of the XH-51A Compound Helicopter," USAAVLABS TR 68-23, June 1968.

2.58   Culver, I. H., "Progress of the Rigid Rotor Concept," Aeronaut. J. Roy. Aeronaut. Soc., Vol. 72, No. 686, Feb. 1968.

2.59   Sissingh, G. J., "Response Characteristics of the Gyro-Controlled Lockheed Rotor System," J. Am. Hel. Soc., Vol. 12, No. 4, Oct. 1967, pp. 61-75.

2.60   McCloud, J. L., III, and Biggers, J. C., "Full-Scale Wind-Tunnel Tests of Nonarticulated Helicopter Rotor," NASA TN D-2392, 1964.

2.61   Statler, W. H., Heppe, R. R. and Cruz, E. S., "Results of the XH-51A Rigid Rotor Research Helicopter Program," 19th Annual National Forum, American Helicopter Society, May 1963.

2.62   Culver, I. H. and Rhodes, J. E., "Structural Coupling in Blades of Rotating Wing Aircraft," IAS 30th Annual Meeting, New York, Jan. 1962, IAS Paper 62-33.

2.63   Halley, D. H., "ABC Helicopter Stability, Control and Vibration Evaluation on the Princeton Dynamic Model Track," 29th Annual National Forum, American Helicopter Society, Washington D.C., May 1973, Preprint 744.

2.64   Paglino, V. M. and Beno, E. A., "Full Scale Wind Tunnel Investigation of the Advancing Blade Concept Rotor System," USAAMRDL TR 71-25, 1971.

2.65   Burgess, R. K., "Development of the ABC Rotor," 27th Annual National Forum, American Helicopter Society, Washington D.C., May 1971, Preprint 504; also AGARD-CP-121.

2.66   Paglino, V. M., "Forward Flight Performance of a Coaxial Rigid Rotor," 27th Annual National Forum, American Helicopter Society, Washington D.C., May 1971, Preprint 524.

2.67   Cheney, M. C., Jr., "The ABC Helicopter," J. Am. Hel. Soc., Vol. 14, No. 4, Oct. 1969, pp. 10-19.

2.68   Baldock, B. A., "Some Calculations for Air Resonance of a Helicopter with Nonarticulated Rotor Blades," RAE TR 72083, Aug. 1972.

2.69   Cansdale, R., Gaukroger, D. R. and Skingle, C. W., "A Technique for Measuring Impedances of a Spinning Model Rotor," RAE TR 71092, May 1971.

2.70   Brotherhood, P. and James, C. A., "Some Flight Experiments on the XH-51 N Helicopter," RAE TM Aero. 1342, Aug. 1971.

2.71   Ormiston, R. A. and Bousman, W. G., "A Study of Stall-Induced Flap-Lag Instability of Hingeless Rotors," 29th Annual National Forum, American Helicopter Society, Washington D.C., May 1973, Preprint 730.

2.72   Hodges, D. H. and Ormiston, R. A., "Stability of Elastic Bending and Torsion of Uniform Cantilevered Rotor Blades in Hover," AIAA/ASME/SAE 14th Structures, Structural Dynamics, and Materials Conference, Williamsburg, Va., March 1973, AIAA Paper 73-405

2.73   Johnson, W., "A Perturbation Solution of Rotor Flapping Stability," AIAA 2nd Atmospheric Flight Mechanics Conference, Palo Alto, Calif., Sept. 1972, AIAA Paper 72-955.

2.74   Ormiston, R. A. and Bousman, W. G., "A Theoretical and Experimental Investigation of Flap-Lag Stability of Hingeless Helicopter Rotor Blades," NASA TM X-62, 179, Aug. 1972.

2.75   Ormiston, R. A. and Peters, D. A., "Hingeless Helicopter Rotor Response with Non-Uniform Inflow and Elastic Blade Bending," J. Aircraft, Vol. 9, No. 10, Oct. 1972, pp. 730-736.

2.76   Ormiston, R. A. and Hodges, D. H., "Linear Flap-Lag Dynamics of Hingeless Helicopter Rotor Blades in Hover," J. Am. Hel. Soc., Vol. 17, No. 2, April 1972, pp. 2-14.

2.77   Friedmann, P., "Aeroelastic Instabilities of Hingeless Helicopter Blades," AIAA 11th Aerospace Science Meeting, Washington, D.C., Jan. 1973, AIAA Paper 73-193.

2.78   Tong, P., "Non-linear Instability of a Helicopter Blade," AIAA 2nd Atmospheric Flight Mechanics Conference, Palo Alto, Calif., Sept. 1972, AIAA Paper 72-956.

2.79   Curtiss, H. C., Jr., "Complex Coordinates in Near Hovering Rotor Dynamics," J. Aircraft, Vol. 10, No. 5, May 1973, pp. 289-295.

2.80   Curtiss, H. C., Jr. and Shupe, N. K., "A Stability and Control Theory for Hingeless Rotors," 27th Annual National Forum, American Helicopter Society, Washington D.C., May 1971, Preprint 541.

2.81   Young, M. I., "The Influence of Pitch and Twist on Blade Vibrations," J. Aircraft, Vol. 10, No. 6, June 1973, pp. 383-384.

2.82   Hohenemser, K. H. and Yin, S. K., "On the Question of Adequate Hingeless Rotor Modeling in Flight Dynamics," 29th Annual National Forum, American Helicopter Society, Washington D.C., May 1973, Preprint 732.

2.83   Hohenemser, K. H. and Crews, S. T., "Model Tests on Unsteady Rotor Wake Effects," J. Aircraft, Vol. 10, No. 1, Jan. 1973, pp. 58-60.

2.84   Gaonkar, G. H., Hohenemser, K. H. and Yin, S. K., "Random Gust Response Statistics for Coupled Torsion-Flapping Rotor Blade Vibrations," J. Aircraft, Vol. 9, No. 10, Oct. 1972, pp. 726-229.

2.85   Hohenemser, K. H. and Yin, S. K., "Some Applications of the Method of Multiblade Coordinates," J. Am. Hel. Soc., Vol. 17, No. 3, July 1972, pp. 3-12.

2.86   Peters, D. A. and Hohenemser, K. H., "Application of the Floquet Transition Matrix to Problems of Lifting Rotor Stability," J. Am. Hel. Soc., Vol. 16, No. 2, April 1971, pp. 25-33.

2.87   Gaonkar, G. H. and Hohenemser, K. H., "Stochastic Properties of Turbulence Excited Rotor Blade Vibrations," AIAA J. Vol. 9, No. 3, March 1971, pp. 419-424.

2.88   Johnson, R. L. and Hohenemser, K. H., "On the Dynamics of Lifting Rotors with Thrust and Tilting Moment Feedback Controls," J. Am. Hel. Soc., Vol. 15, No. 1, Jan. 1970, pp. 42-58 (Review and discussion by Sissingh).

2.89   Bramwell, A. R. S., "An Introduction to Helicopter Air Resonance," The City University, London, RM Aero 72/4.

2.90   Bramwell, A. R. S., "A Method for Calculating the Stability and Control Derivatives of Helicopters with Hingeless Rotors," The City University, London, RM Aero 69/4, 1969.

2.91   Putman, W. F. and Traybar, J. J., "An Experimental Investigation of Compound Helicopter Aerodynamics in Level and Descending Forward Flight and Ground Proximity," USAAMRDL TR 71-19, July 1971.

3.1   Niebanck, C. F., Astill, C. J., Carta, F. O. and Elman, H. L., "Prediction of Rotor Instability at High Forward Speeds," USAAVLABS TR 68-18, Feb. 1969.

3.2   Myklestad, N. O., Fundamentals of Vibration Analysis, McGraw Hill Book Co., New York, 1956.

3.3   Blankenship, B. L. and Harvey, K. W., "A Digital Analysis for Helicopter Performance and Rotor Blade Bending Moments," J. Am. Hel. Soc., Vol. 7, No. 4, Oct. 1962, pp. 55-68.

3.4   Molusis, J. A., "Helicopter Derivative Identification from Analytic Models and Flight Test Data," NASA Parameter Estimation Symposium, Edwards Air Force Base, April 1973.

3.5   Molusis, J. A., "Helicopter Stability Derivative Extraction from Flight Data Using the Bayesian Approach to Estimation," J. Am. Hel. Soc., Vol. 18, No. 2, April 1973, pp. 12-23.

4.1   Pei Chi Chou, "Pitch-Lag Instability of Helicopter Rotors", J. Am. Hel. Soc., Vol. 3, No. 3, July 1958, pp. 30-39.

4.2   Miller, R. H., "A Method of Improving the Inherent Stability of Helicopters," J. Aeronaut. Sci., Vol. 17, No. 6, June 1950, pp. 363-374.

5.1   Anon., V/STOL Handling, II, Documentation, AGARD Rept. 577, Part II, June 1973.

5.2   Anon., V/STOL Handling, I, Criteria and Discussion, AGARD Rept. 577, Dec. 1970.

5.3   Anon., Flying Qualities of V/STOL Aircraft, MIL-F-83300, Dec. 1970.

5.4   Anon., Recommendations for V/STOL Handling Qualities, AGARD Rept. 408A, Oct. 1964.

5.5   Anon., Helicopter Flying and Ground Handling Qualities, MIL-H-8501A, April 1962.

5.6   Edenborough, H. K. and Wernicke, K. G., "Control and Maneuver Requirements for Armed Helicopters," 20th Annual National Forum, American Helicopter Society, May 1964.

5.7   Miller, R. H., "Rotor Blade Harmonic Air Loading," AIAA J., Vol. 2, No. 7, July 1964, p. 1260.

5.8   Head, R. E., "Evaluation of Some Flight Safety Aspects of the Single-Engine Unloaded Rotor Winged Helicopter," J. Am. Hel. Soc., Vol. 4, No. 4, Oct. 1959, pp. 4-10.

6.1   Kilmer, F. G. and Sklaroff, J. R., "Redundant System Design and Flight Test Evaluation for the TAGS Digital Control System," 29th Annual Forum, American Helicopter Society, Washington D.C., May 1973, Preprint 721.

6.2   Hall, W. E., Jr. and Bryson, A. E., Jr., "Inclusion of Rotor Dynamics in Controller Design for Helicopters," J. Aircraft, Vol. 10, No. 4, April 1973, pp. 200-206.

6.3   Sissingh, G. J., "Variation of Rotor Dynamic Response by Self-Contained Mechanical Feedback," IAS Preprint 61-25, 1961.

6.4   Hohenemser, K., "A Type of Rotor with Inherent Stability," J. Aeronaut Sci., Vol. 17, No. 9, Sept. 1950, pp. 555-564.

6.5   Konig, H. and Schmitt, H., "Optimization of Automatic Flight Control Concepts for Light Helicopters with All-Weather Capability, 12th AGARD Guidance and Control Panel Meeting, Konstanz, June 1971, AGARD-CP-86.

7.1   Carta, F. O., Cammerford, G. L. and Carlson, R. G., "Determination of Airfoil and Rotor Blade Dynamic Stall Response," J. Am. Hel. Soc., Vol. 18, No. 2, April 1973, pp. 31-39.

7.2   Johnson, W. and Ham, N. D., "On the Mechanism of Dynamic Stall," J. Am. Hel. Soc., Vol. 17, No. 4, Oct. 1972, pp. 36-45.

7.3   McCroskey, W. J., "Recent Developments in Rotor Blade Stall," AGARD-CP-111, Paper 15, Feb. 1973.

7.4   Reichert, G. and Wagner, S. N., "Some Aspects of the Design of Rotor Airfoil Shapes," AGARD-CP-111, Paper 14, Feb. 1973.

7.5   Pearcey, H. H., Wilby, P. G., Riley, M. J. and Brotherhood, P., "The Derivation and Verification of a New Rotor Profile on the Basis of Flow Phenomena, Airfoil Research and Flight Tests," AGARD-CP-111, Paper 16, Feb. 1973.

7.6   Hohenemser, K. H., "Some Aerodynamic and Dynamic Problems of the Compound Rotor-Fixed Wing Aircraft," Proceedings 8th Annual Forum, American Helicopter Society, Washington D.C., May 1952, pp. 147-173.

7.7   Harris, F. D., "Articulated Rotor Blade Flapping Motion at Low Advance Ratio," J. Am. Hel. Soc., Vol. 17, No. 1, Jan. 1972, pp. 41-48.

44

7.8   Castles, W. and deLeeuw, J. H., "The Normal Component of the Induced Velocity in the Vicinity of Lifting Rotors and Some Examples of Its Application," NACA TN 2912, 1953.

7.9   Heyson, H. H. and Katzoff, S., "Induced Velocities Near a Lifting Rotor with Non-uniform Disk Loading," NACA Rept. 1319, 1957.

7.10 Landgrebe, A. J. and Cheney, M. C., Jr., "Rotor Wakes — Key to Performance Prediction," AGARD-CP-111, Paper 1, Feb. 1973.

7.11 Clark, D. R. and Leiper, A. C., "The Free Wake Analysis, A Method for the Prediction of Helicopter Rotor Hovering Performance," J. Am. Hel. Soc., Vol. 15, No. 1, Jan. 1970, pp. 3-11.

7.12 Ormiston, R. A., "An Actuator Disc Theory for Rotor Wake Induced Velocities," AGARD-CP-111, Paper 2, Feb. 1973.

7.13 Loewy, R. G., "A Two-Dimensional Approach to the Unsteady Aerodynamics of Rotary Wings," J. Aerosp. Sci., Vol. 24, 1957, pp. 82-98.

7.14 Ward, J. F. and Young, W. H., Jr., "A Summary of Current Research in Rotor Unsteady Aerodynamics With Emphasis on Work at Langley Research Center," AGARD-CP-111, Paper 10, Feb. 1973.

7.15 Carpenter, P. J. and Fridovich, B., "Effect of a Rapid Blade Pitch Increase on the Thrust and Induced Velocity Response of a Full Scale Helicopter Rotor," NACA TN 3044, 1953.

7.16 Crews, S. T., Hohenemser, K. H. and Ormiston, R. A., "An Unsteady Wake Model for a Hingeless Rotor," J. Aircraft, Vol. 10, No. 12, Dec. 1973.

8.1   Pennington, R. G., Introductory Computer Methods and Numerical Analysis, The MacMillan Co., New York, 1966, p. 355.

8.2   Yin, S. K., "The Method of Multiblade Coordinates in the Linear Analysis of Lifting Rotor Stability and Gust Response," Doctor of Science Dissertation, Washington Univ., St. Louis, Missouri, June 1971.

8.3   De Russo, P. M., Roy, R. J. and Close, C. M., State Variables for Engineers, John Wiley and Sons, Inc., New York, 1967.

8.4   Crimi, P., "A Method for Analyzing the Aeroelastic Stability of a Helicopter Rotor in Forward Flight," NASA CR-1332, Aug. 1969.

8.5   Piarulli, V. and White, R. A., "A Method for Determining the Characteristic Functions Associated with the Aeroelastic Instabilities of Helicopter Rotors in Forward Flight," NASA CR-1577, June 1970.

8.6   Prelewicz, D. A., "Response of Linear Time Varying Systems to Random Excitation," AIAA J. Vol. 10, No. 8, Aug. 1972, pp. 1124-1125.

8.7   Sveshnikov, A. A., Applied Methods of the Theory of Random Functions," Pergamon Press, New York, 1966, p. 135.

8.8   Bryson, A. E., Jr. and Ho, Y. C., Applied Optimal Control, Ginn and Co., Waltham, Mass., 1969, Ch. 12.

8.9   Wan, F. Y. M. and Lakshmikantham, C., "Rotor Blade Response to Random Loading: A Direct Time Domain Approach," AIAA J., Vol. 11, No. 1, Jan. 1973, pp. 24-28.

8.10 Gaonkar, G. H., "A General Method with Shaping Filters to Study Random Vibration Statistics of Lifting Rotors with Feedback Controls," J. Sound and Vibration, Vol. 21, No. 2, 1972, pp. 213-225.

8.11 Barlow, J. B., "On the Force and Moments of a Propeller Moving Axially Through Homogeneous Turbulence," VTOL Research, Design and Operations Meeting, Atlanta, Georgia, Feb. 1970, AIAA Paper 70-549.

8.12 Wan, F. Y. M. and Lakshmikantham, C., "The Spacial Correlation Method and a Time Varying Flexible Structure," AIAA/ASME/SAE 14th Structures, Structural Dynamics, and Materials Conference, Williamsburg, Va., March 1973, AIAA Paper 73-406.

8.13 Gaonkar, G. H. and Hohenemser, K. H., "An Advanced Stochastic Model for Threshold Crossing Studies of Rotor Blade Vibrations," AIAA J., Vol. 10, No. 8, Aug. 1972, pp. 1100-11-1.

9.1   Ormiston, R. A., "Helicopter Modelling," The Aeronaut. J. Roy. Aeronaut. Soc., Vol. 77, No. 755, Nov. 1973.

9.2   Chen, R. T. N., Eulrich, B. J. and Lebacqz, J. V., "Development of Advanced Techniques for the Identification of V/STOL Aircraft Stability and Control Parameters," Cornell Aeronaut. Lab. Rept. BM-2820-F-1, Aug. 1971.

9.3   Graham, R. J., "Determination and Analysis of Numerical Smoothing Weights," NASA TR R-179, 1963.

Appendix to List of References

Some pertinent publications that appeared after the manuscript was completed in 1973 are listed below.

References A1-A9 from the Proceedings of the Specialists Meeting on Rotorcraft Dynamics, AHS/NASA-Ames Research Center, Moffett Field, Calif., Feb. 1974.

A-1   Paper 1, Peters, D. A., "Hingeless Rotor Frequency Response with Unsteady Inflow."

A-2   Paper 3, Hohenemser, K. H., and Prelewicz, D. H., "Computer Experiments on Periodic Systems Identification Using Rotor Blade Transient Flapping-Torsion Responses At High Advance Ratio.

A-3   Paper 4, Bielawa, R. L., "Dynamic Analysis of Multi-Degree-of-Freedom Systems Using Phasing Matrices."

A-4   Paper 5, Biggers, J. C., "Some Approximations to the Flapping Stability of Helicopter Rotors."

A-5   Paper 6, Friedman, P. and Silverthorn, L. J., "Flap-Lag Dynamics of Hingeless Helicopter Blades of Moderate and High Advance Ratios."

A-6   Paper 14, Miao, W. L. and Huber, H. B., "Rotor Aeroelastic Stability Coupled with Helicopter Body Motion."

A-7   Paper 18, Anderson, W. D. and Johnston, J. F., "Comparison of Flight Data and Analysis for Hingeless Rotor Regressive Inplane Mode Stability."

A-8   Paper 19, Sonneborn, W. G. O., and Yen, J., "Hub Moment Springs on Two-Bladed Teetering Rotors."

A-9   Paper 20, Young, M. I., Bailey, D. J. and Hirschbein, M. J., "Open and Closed Loop Stability of Hingeless Rotor Helicopter Air and Ground Resonance."

A-10 Anderson, W. D. and Watts, G. A., "Rotor Blade Wake Flutter," Lockheed Rept. LR 26213, Dec. 1973.

A-11 Johnston, J. F. and Conner, F., "The Reactionless Inplane Mode of Stiff Inplane Hingeless Rotors," Lockheed Rept. LR 26214, Dec. 1973.
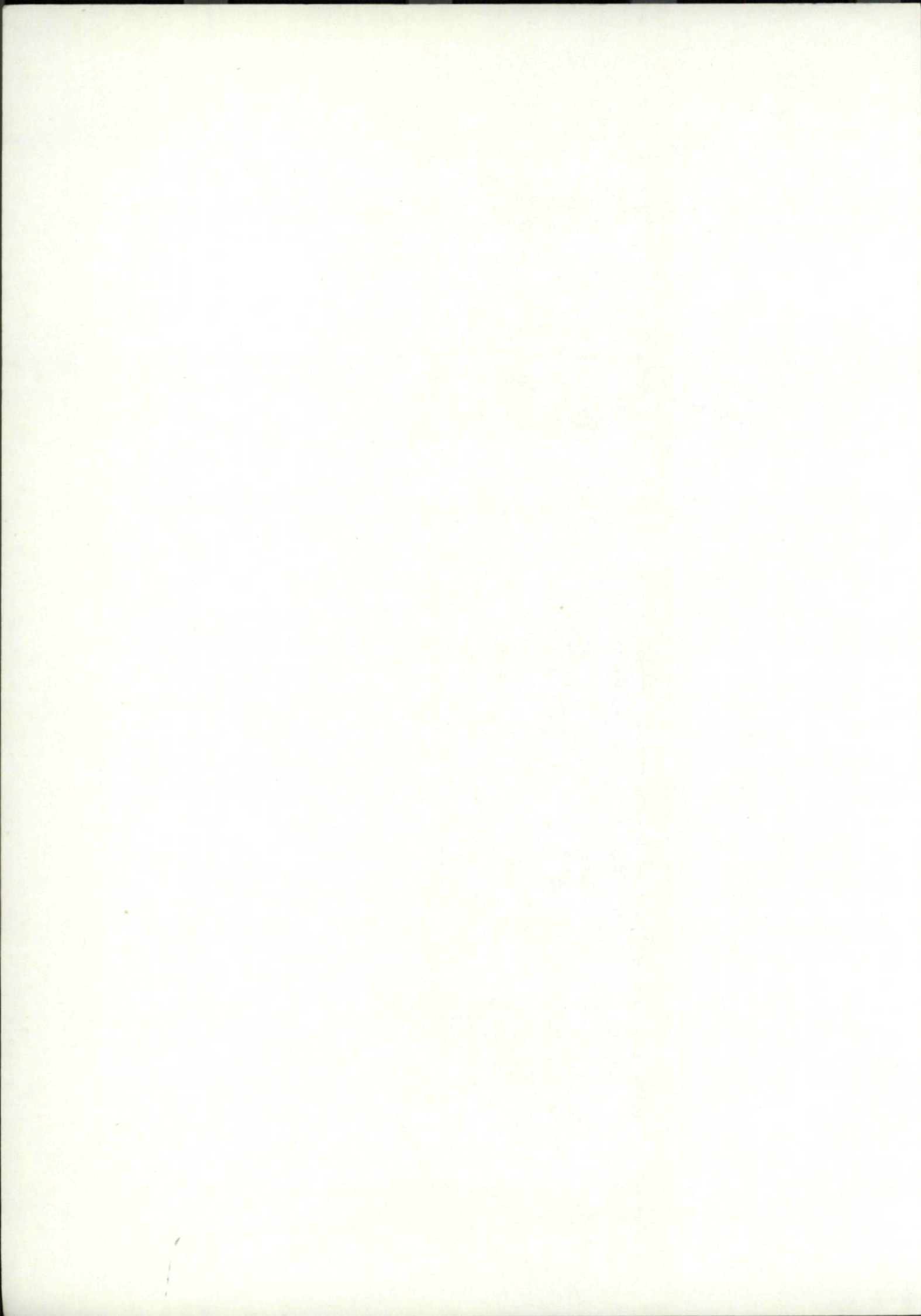
A-12   Donham, R. E. and Cardinale, S. V., "Flight Test and Analytical Data for Dynamics and Loads in a Hingeless Rotor," Lockheed Rept. LR 26215, Dec. 1973.

A-13   Potthast, A. J. and Kerr, A. W., "Flying Qualities of a Gyro-Controlled Hingeless-Rotor Compound Helicopter" Lockheed Rept. LR 26216, Dec. 1973.

A-14   London, R. J., Watts, G. A. and Sissingh G. J. "Experimental Hingeless Rotor Characteristics at Low Advance Rotor with Thrust," NASA CR-114684, Dec. 1973.

11 ACKNOWLEDGMENTS

AGARDograph No.197 Advisory Group for Aerospace Research and Development, NATO HINGELESS ROTORCRAFT FLIGHT DYNAMICS Kurt H.Hohenemser Published September 1974 52 pages incl. references and figures The state of hingeless rotorcraft research and development in the NATO countries as of 1973 is described. In the Introduction, the special place of the hingeless rotorcraft within the family of rotorcraft is considered. The chapter on the history of hingeless rotorcraft describes the hingeless rotor research and development of the various rotorcraft manufacturers and the P.T.O.	AGARD-AG-197 533.662.6:533.661: 629.735.55.017.2 Rotary wing aircraft Airfoils Rotary wings Aerodynamics Design Research projects Feedback controls Flight tests Mathematical models	AGARDograph No.197 Advisory Group for Aerospace Research and Development, NATO HINGELESS ROTORCRAFT FLIGHT DYNAMICS Kurt H.Hohenemser Published September 1974 52 pages incl. references and figures The state of hingeless rotorcraft research and development in the NATO countries as of 1973 is described. In the Introduction, the special place of the hingeless rotorcraft within the family of rotorcraft is considered. The chapter on the history of hingeless rotorcraft describes the hingeless rotor research and development of the various rotorcraft manufacturers and the P.T.O.	AGARD-AG-197 533.662.6:533.661: 629.735.55.017.2 Rotary wing aircraft Airfoils Rotary wings Aerodynamics Design Research projects Feedback controls Flight tests Mathematical models
AGARDograph No.197 Advisory Group for Aerospace Research and Development, NATO HINGELESS ROTORCRAFT FLIGHT DYNAMICS Kurt H.Hohenemser Published September 1974 52 pages incl. references and figures The state of hingeless rotorcraft research and development in the NATO countries as of 1973 is described. In the Introduction, the special place of the hingeless rotorcraft within the family of rotorcraft is considered. The chapter on the history of hingeless rotorcraft describes the hingeless rotor research and development of the various rotorcraft manufacturers and the P.T.O.	AGARD-AG-197 533.662.6:533.661: 629.735.55.017.2 Rotary wing aircraft Airfoils Rotary wings Aerodynamics Design Research projects Feedback controls Flight tests Mathematical models	AGARDograph No.197 Advisory Group for Aerospace Research and Development, NATO HINGELESS ROTORCRAFT FLIGHT DYNAMICS Kurt H.Hohenemser Published September 1974 52 pages incl. references and figures The state of hingeless rotorcraft research and development in the NATO countries as of 1973 is described. In the Introduction, the special place of the hingeless rotorcraft within the family of rotorcraft is considered. The chapter on the history of hingeless rotorcraft describes the hingeless rotor research and development of the various rotorcraft manufacturers and the P.T.O.	AGARD-AG-197 533.662.6:533.661: 629.735.55.017.2 Rotary wing aircraft Airfoils Rotary wings Aerodynamics Design Research projects Feedback controls Flight tests Mathematical models

hingeless rotor research at government laboratories and universities. A hierarchy of dynamic concepts from isolated blade dynamics to complete rotor/body dynamics is introduced. The effects of the basic rotor design parameters on flight dynamics are traced and certain hingeless rotorcraft problems are treated in some detail. A special chapter is devoted to the alleviation of hingeless rotor flight-dynamics problems by feedback control systems. Finally, analytical modeling techniques, mathematical analysis techniques, and model and flight testing techniques for hingeless rotorcraft are discussed.
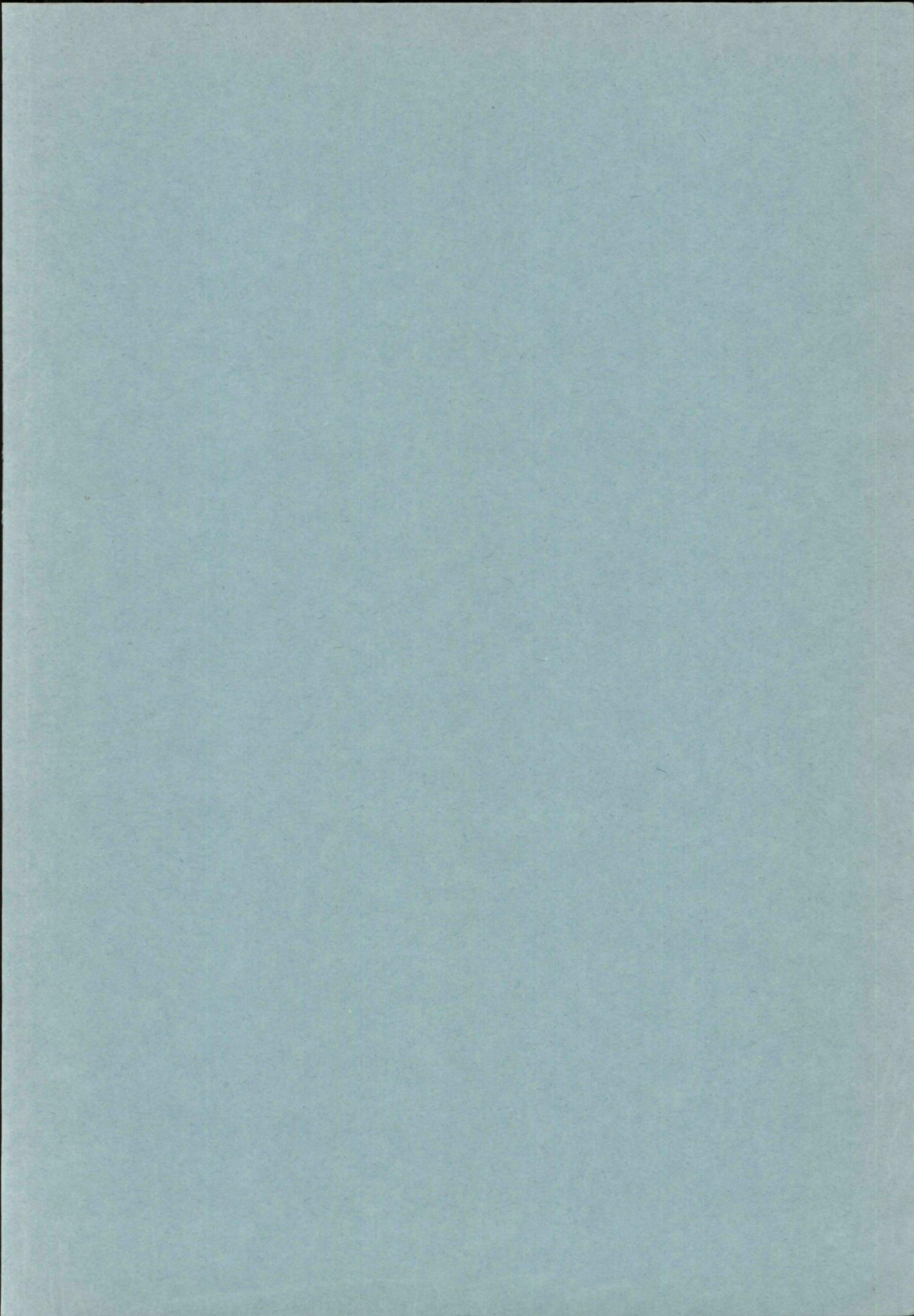
This AGARDograph has been sponsored by the Flight Mechanics Panel of AGARD.

AGARDograph No.197 Advisory Group for Aerospace Research and Development, NATO HINGELESS ROTORCRAFT FLIGHT DYNAMICS Kurt H.Hohenemser Published September 1974 52 pages incl. references and figures The state of hingeless rotorcraft research and development in the NATO countries as of 1973 is described. In the Introduction, the special place of the hingeless rotorcraft within the family of rotorcraft is considered. The chapter on the history of hingeless rotorcraft describes the hingeless rotor research and development of the various rotorcraft manufacturers and the P.T.O.	AGARD-AG-197 533.662.6:533.661: 629.735.55.017.2 Rotary wing aircraft Airfoils Rotary wings Aerodynamics Design Research projects Feedback controls Flight tests Mathematical models	AGARDograph No.197 Advisory Group for Aerospace Research and Development, NATO HINGELESS ROTORCRAFT FLIGHT DYNAMICS Kurt H.Hohenemser Published September 1974 52 pages incl. references and figures The state of hingeless rotorcraft research and development in the NATO countries as of 1973 is described. In the Introduction, the special place of the hingeless rotorcraft within the family of rotorcraft is considered. The chapter on the history of hingeless rotorcraft describes the hingeless rotor research and development of the various rotorcraft manufacturers and the P.T.O.	AGARD-AG-197 533.662.6:533.661: 629.735.55.017.2 Rotary wing aircraft Airfoils Rotary wings Aerodynamics Design Research projects Feedback controls Flight tests Mathematical models
AGARDograph No.197 Advisory Group for Aerospace Research and Development, NATO HINGELESS ROTORCRAFT FLIGHT DYNAMICS Kurt H.Hohenemser Published September 1974 52 pages incl. references and figures The state of hingeless rotorcraft research and development in the NATO countries as of 1973 is described. In the Introduction, the special place of the hingeless rotorcraft within the family of rotorcraft is considered. The chapter on the history of hingeless rotorcraft describes the hingeless rotor research and development of the various rotorcraft manufacturers and the P.T.O.	AGARD-AG-197 533.662.6:533.661: 629.735.55.017.2 Rotary wing aircraft Airfoils Rotary wings Aerodynamics Design Research projects Feedback controls Flight tests Mathematical models	AGARDograph No.197 Advisory Group for Aerospace Research and Development, NATO HINGELESS ROTORCRAFT FLIGHT DYNAMICS Kurt H.Hohenemser Published September 1974 52 pages incl. references and figures The state of hingeless rotorcraft research and development in the NATO countries as of 1973 is described. In the Introduction, the special place of the hingeless rotorcraft within the family of rotorcraft is considered. The chapter on the history of hingeless rotorcraft describes the hingeless rotor research and development of the various rotorcraft manufacturers and the P.T.O.	AGARD-AG-197 533.662.6:533.661: 629.735.55.017.2 Rotary wing aircraft Airfoils Rotary wings Aerodynamics Design Research projects Feedback controls Flight tests Mathematical models

hingeless rotor research at government laboratories and universities. A hierarchy of dynamic concepts from isolated blade dynamics to complete rotor/body dynamics is introduced. The effects of the basic rotor design parameters on flight dynamics are traced and certain hingeless rotorcraft problems are treated in some detail. A special chapter is devoted to the alleviation of hingeless rotor flight-dynamics problems by feedback control systems. Finally, analytical modeling techniques, mathematical analysis techniques, and model and flight testing techniques for hingeless rotorcraft are discussed.

This AGARDograph has been sponsored by the Flight Mechanics Panel of AGARD.

DISTRIBUTION OF UNCLASSIFIED AGARD PUBLICATIONS

NOTE: Initial distributions of AGARD unclassified publications are made to NATO Member Nations through the following National Distribution Centres. Further copies are sometimes available from these Centres, but if not may be purchased in Microfiche or photocopy form from the Purchase Agencies listed below. THE UNITED STATES NATIONAL DISTRIBUTION CENTRE (NASA) DOES NOT HOLD STOCKS OF AGARD PUBLICATIONS, AND APPLICATIONS FOR FURTHER COPIES SHOULD BE MADE DIRECT TO THE APPROPRIATE PURCHASE AGENCY (NTIS).

NATIONAL DISTRIBUTION CENTRES

BELGIUM
Coordonnateur AGARD – VSL
Etat-Major de la Force Aérienne
Caserne Prince Baudouin
Place Dailly, 1030 Bruxelles

CANADA
Defence Scientific Information Service
Department of National Defence
Ottawa, Ontario K1A OZ3

DENMARK
Danish Defence Research Board
Østerbrogades Kaserne
Copenhagen Ø

FRANCE
O.N.E.R.A. (Direction)
29, Avenue de la Division Leclerc
92, Châtillon sous Bagneux

GERMANY
Zentralstelle für Luftfahrtdokumentation
und Information
8 München 86
Postfach 860881

GREECE
Hellenic Armed Forces Command
D Branch, Athens

ICELAND
Director of Aviation
c/o Flugrad
Reykjavik

ITALY
Aeronautica Militare
Ufficio del Delegato Nazionale all'AGARD
3, Piazzale Adenauer
Roma/EUR

LUXEMBOURG
See Belgium

NETHERLANDS
Netherlands Delegation to AGARD
National Aerospace Laboratory, NLR
P.O. Box 126
Delft

NORWAY
Norwegian Defence Research Establishment
Main Library
P.O. Box 25
N-2007 Kjeller

PORTUGAL
Direccao do Servico de Material
da Forca Aerea
Rua de Escola Politecnica 42
Lisboa
Attn: AGARD National Delegate

TURKEY
Turkish General Staff (ARGE)
Ankara

UNITED KINGDOM
Defence Research Information Centre
Station Square House
St. Mary Cray
Orpington, Kent BR5 3RE

UNITED STATES
National Aeronautics and Space Administration (NASA)
Langley Field, Virginia 23365
Attn: Report Distribution and Storage Unit
(See Note above)

PURCHASE AGENCIES

Microfiche or Photocopy	*Microfiche*	*Microfiche*
National Technical Information Service (NTIS) 5285 Port Royal Road Springfield Virginia 22151, USA	ESRO/ELDO Space Documentation Service European Space Research Organization 114, Avenue Charles de Gaulle 92200 Neuilly sur Seine, France	Technology Reports Centre (DTI) Station Square House St. Mary Cray Orpington, Kent BR5 3RF England

Requests for microfiche or photocopies of AGARD documents should include the AGARD serial number, title, author or editor, and publication date. Requests to NTIS should include the NASA accession report number.

* * *

Full bibliographical references and abstracts of AGARD publications are given in the following bi-monthly abstract journals:

Scientific and Technical Aerospace Reports (STAR),
published by NASA,
Scientific and Technical Information Facility
P.O. Box 33, College Park
Maryland 20740, USA

Government Reports Announcements (GRA),
published by the National Technical
Information Services, Springfield
Virginia 22151, USA